3-D Description and Reservoir Modeling of Channel-Levee and Lobe Sandstones in the Permian Bell Canyon Formation, West Texas

by

Mark D. Barton
Joseph S. Yeh
Christopher D. White

January 1998

CONTENTS

Figures

Tables

Appendix Figures

Appendix Tables

EXECUTIVE SUMMARY

The Bureau of Economic Geology, The University of Texas at Austin, has conducted an integrated outcrop characterization and reservoir modeling study on deep-water sandstones of the Permian Bell Canyon Formation, West Texas. The study was funded by Statoil.

The primary objective of this study was to construct a deterministic three-dimensional reservoir model of facies architecture within a submarine channel-levee and lobe system on the basis of data collected from well-exposed outcrops.

The Permian-age Delaware Mountain Group (the Brushy Canyon, Cherry Canyon, and Bell Canyon Formations) was deposited in a deep-water setting by a system of submarine channel levees with attached lobes. Facies and stratigraphic relationships were described on the basis of laterally continuous outcrops of the Bell Canyon Formation and were placed in a well-defined cyclic stratigraphic framework. Sequence-stratigraphic concepts were used to define depositionally based rock bodies that were mapped in three dimensions.

In the Willow Mountain case study, eight lithosomes were mapped, and facies distributions were documented within each lithosome using facies isopach or proportion maps. The mapped volume was 20 m thick, 2,000 m in length parallel to depositional strike, and 1,000 m in length perpendicular to depositional strike. The surface and facies maps were edited and reconciled using three-dimensional geocellular modeling software, and the resulting areal grids of rock-body thickness were stacked to construct a reservoir model, using a cornerpoint geometry description that is compatible with current reservoir simulation software.

In addition to the text of this report, extensive data and figures are included on accompanying CD-ROM volumes.

SCOPE

This report summarizes an integrated outcrop characterization and reservoir modeling study of deep-water sandstones of the Permian Bell Canyon Formation, West Texas. A deterministic three-dimensional reservoir model of facies architecture within a submarine channel-levee and lobe system was constructed on the basis of data collected from well-exposed outcrops in the Willow Mountain area. The main body of this report is divided into three sections. Section 1 documents facies and bedding architecture of a well-exposed channel-levee and lobe system. Section 2 focuses on the organization and structure of geologic data collected from the outcrop used to map the rock bodies. Section 3 discusses the gridding methods used to construct the reservoir model. Relevant data and images are included on CD-ROM's transmitted with this report.

SECTION 1: OUTCROP CHARACTERIZATION OF BELL CANYON SANDSTONES

Introduction

The objective of this section is to describe the architecture of upper Bell Canyon sandstones as seen in outcrop exposures. The outcrops were examined to address two primary issues: (1) to determine by what process the sandstone and siltstones were deposited, and (2) to identify fundamental architectural elements and document their geometry, dimensions, and internal facies composition.

Regional Setting and Stratigraphic Framework

The Bell Canyon Formation is a deep-water siliciclastic unit that accumulated in the Delaware Basin during the Late Permian. The Delaware Basin, located in West Texas and southeast New Mexico, is a circular basin about 150 km in diameter (fig. 1). The basin was semirestricted with its southern end partially open to a seaway and its northern end surrounded
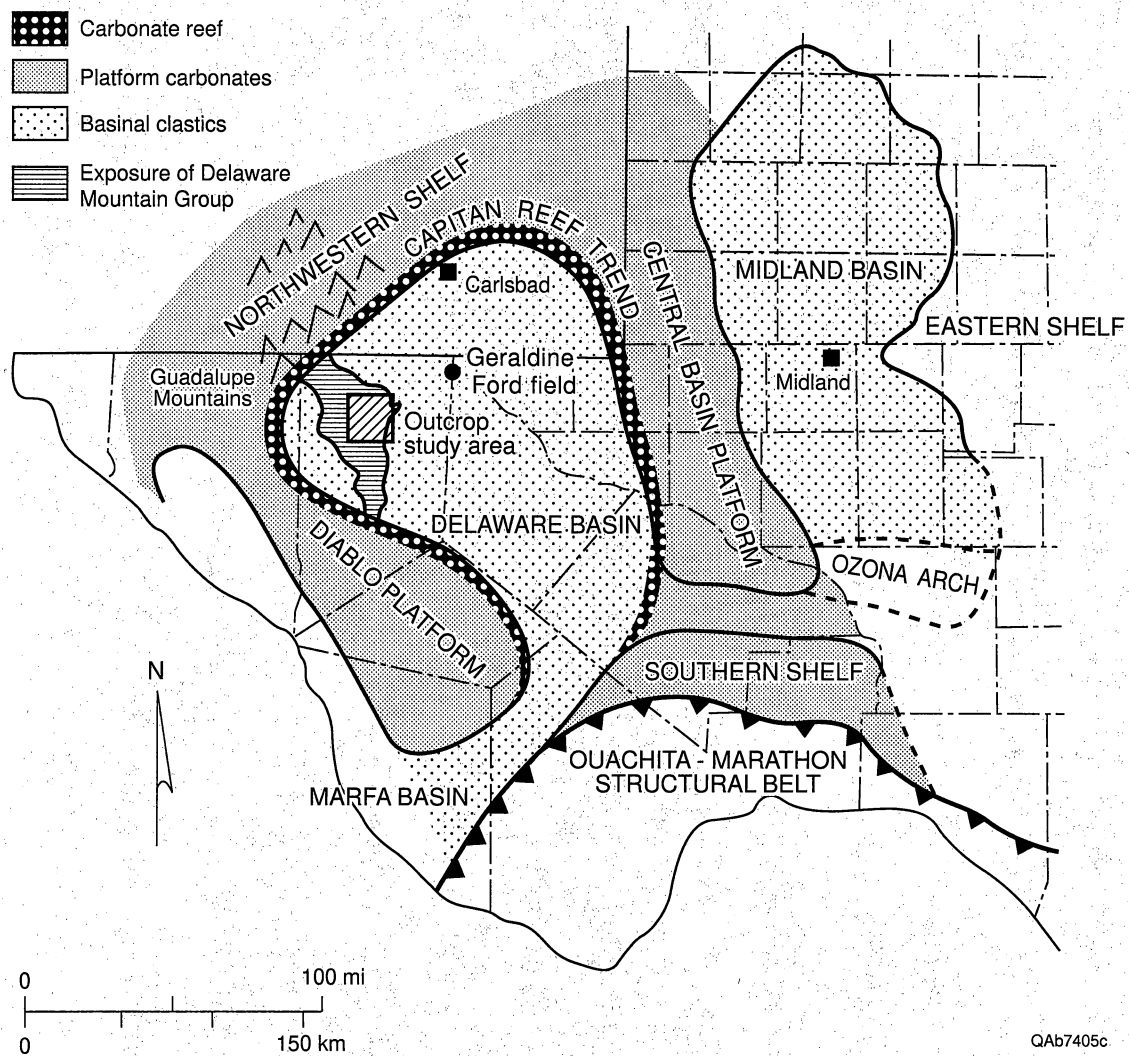
Figure 1. Map showing location and paleogeographic setting of Delaware Basin during the Late Permian.

by a broad, shallow carbonate shelf and a narrow, steeply dipping carbonate slope. Shelf-to-basin correlations of time-equivalent strata indicate that water depths were between 300 and 600 m during deposition of the Bell Canyon Formation (Kerans and others, 1992). Bedding surfaces within the carbonate reef and slope dip steeply basinward, dropping as much as 600 m over the distance of several kilometers.

The Bell Canyon Formation is the youngest formation in the Delaware Mountain Group. The Delaware Mountain Group includes (in ascending stratigraphic order) the Brushy Canyon, Cherry Canyon, and Bell Canyon Formations (fig. 2). Maximum thickness of the Bell Canyon Formation is about 360 m near the center of the basin. Near the margins of the basin it interfingers with and onlaps adjacent carbonate reef and slope deposits of the Capitan Formation. Time-equivalent shelf strata include (in ascending stratigraphic order) the Seven Rivers, Yates, and Tansill Formations. The Bell Canyon Formation is overlain by gypsum deposits of the Castille Formation.

The Delaware Mountain Group is composed largely of siltstone and fine sandstone with minor amounts of carbonate mudstone and pelagic organic matter. Clay-sized siliciclastic material is almost entirely absent. Based on Folk's classification (1974), petrographic analysis of the sandstone and siltstones indicates they are arkoses with an average composition of $Q_{65} F_{31} R_4$ (Dutton and others, 1997a).

The sandstones, siltstones, and carbonates of the Bell Canyon Formation are organized into cyclic successions (Jacka and others, 1969; Meissner, 1972; Jacka, 1979; Gardner, 1992). At least three scales of cyclicity have been recognized; these are referred to as low-, intermediate-, and high-frequency cycles (fig. 3). At the largest scale (low-frequency), thick limestones and/or organic-rich siltstones divide the Delaware Mountain Group into three clastic wedges that are 300 to 450 m thick and that roughly correspond to the Brushy Canyon, Cherry Canyon, and Bell Canyon Formations. The clastic wedges thin and pinch out near the margin of the basin as they onlap or interfinger with carbonate slope deposits.
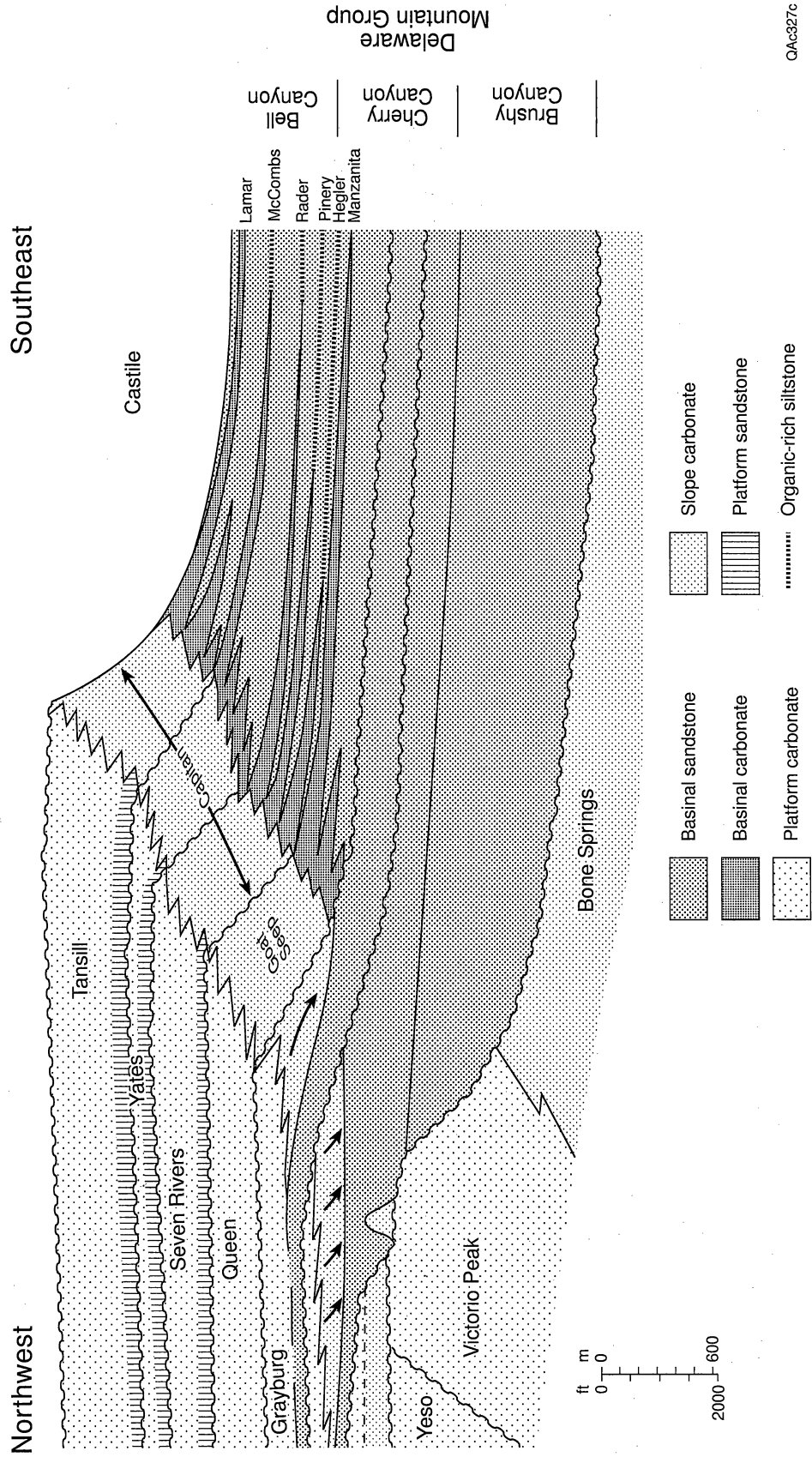
Figure 2. Northwest to southeast cross section illustrating Late Permian stratigraphy in northwestern part of the Delaware Basin.

5
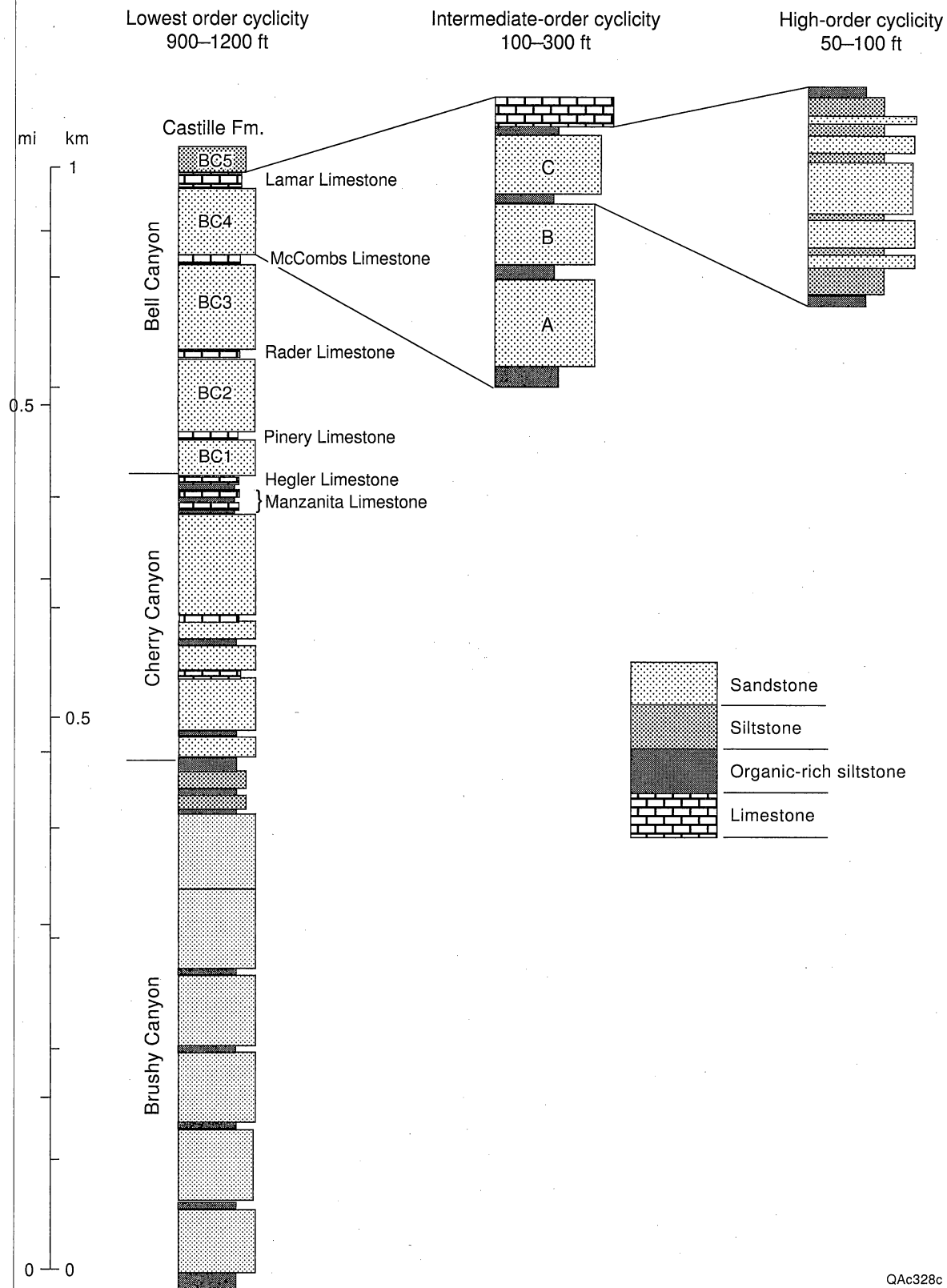
Figure 3. Diagram illustrating stratigraphic cyclicity within Delaware Mountain Group. Three scales classified as low, intermediate, and high have been recognized.

The Bell Canyon Formation contains five limestone tongues that include (from oldest to youngest) the Hegler, Pinery, Rader, McCombs, and Lamar. The limestone tongues are composed of decimeters-thick beds of graded carbonate mudstone (fig. 4). They extend basinward from the shelf margin and subdivide the Bell Canyon Formation into intermediate-scale cycles informally referred to as BC-1 through BC-5 in ascending stratigraphic order (see fig. 3). The intermediate-scale cycles are 30 to 90 m thick and are further subdivided by thin organic-rich siltstones into units referred to as high-frequency cycles (Gardner, 1992). The high-frequency cycles are 6 to 30 m thick and tend to show a trend of upward-increasing followed by upward-decreasing sandstone content.

The cyclic successions of the Delaware Mountain Group have been interpreted by a number of researchers to reflect frequent changes in relative sea level during their deposition (Meissner, 1972; Fischer and Sarnthein, 1988). During highstands in relative sea level, sands were trapped behind a broad, flooded carbonate shelf and were prevented from entering the basin. Thin, widespread, organic-rich siltstones accumulated on the basin floor through the slow settling of marine algal material and airborne silt. Basinal limestones were deposited by sediment gravity flows that originated from the slumping of carbonate debris along the flanks of a steep, rapidly aggrading carbonate platform. During subsequent lowstands in relative sea level, the carbonate shelf was exposed and sandstones bypassed to the basin floor. Textural characteristics of the sands, the absence of clay-sized material, and the lack of channels on the shelf strongly suggest that wind was an important agent in delivering the sands to the basin margin where they accumulated as large sand masses (Fischer and Sarnthein, 1988). Slumping of the sand masses along the shelf edge generated dense sediment-rich mixtures that moved downslope and into the basin as turbulent sediment gravity flows (Payne, 1976; Berg, 1979; Jacka, 1979; Zelt and Rossen, 1995; Bouma, 1996). Paleocurrent indicators suggest that sand entered the basin from the Northwest Shelf and Central Basin Platform (Williamson, 1978). The flows passed through channels and emerged on the basin floor where they spread as unconfined flows. Flows that spilled over channels deposited sediment to form levees adjacent to the channels. Laterally

7

Figure 4. Photographs of graded carbonate mudstone, Lamar limestone, Bell Canyon Formation, West Texas.

extensive siltstones were deposited from suspension by fallout of airborne silt or by silt derived from density interflows (Harms, 1974; Williamson, 1978; Harms and Williamson, 1988).

Data and Methods

Study Area

The Bell Canyon Formation is exposed in the Delaware Mountains of West Texas (see fig. 1). The exposure extends to the southeast for a distance of about 80 km, roughly parallel to the direction of sediment transport that is to the south and southeast in this part of the Delaware Basin (Williamson, 1979). The outcrops examined in this study are located on Cowden Ranch, Culberson County, Texas, about 25 km to the southeast of the Guadalupe Mountains (fig. 5). Shelf-to-basin correlations indicate that the outcrops examined were deposited in a basin-floor setting about 18 km from the basin slope (Sonnenfeld, 1991; Kerans and Fitchen, 1995).

Outcrop work focused on characterizing stratigraphic and facies relationships at interwell scale within the uppermost high-order cycle of the intermediate-scale cycle BC-3 (see fig. 3). The top of this high-order cycle is the McCombs Limestone, and the base is the first regionally correlative organic-rich siltstone. This cycle shows an overall trend of upward-increasing grain size and bed thickening followed by a trend of upward-decreasing grain size and bed thinning. The scale and position of this high-order cycle is analogous to the highly productive Ramsey Sandstone (Williamson, 1978; Dutton and others, 1997a).

Facies and stratigraphic relationships were documented in three case studies within this high-frequency cycle. The location of the case studies is shown in figure 6. A two-dimensional view of the facies and bedding architecture within a channel-levee complex is illustrated at a study area referred to as Wild Horse Draw (see fig. 6). A three-dimensional view of the stacking pattern of channels, levees, and lobes within a single high-order cycle is examined at a study area referred to as Willow Mountain (see fig. 6). Regional facies and stratigraphic relationships within the high-order cycle are illustrated in a cross section that passes through the Willow Mountain

9
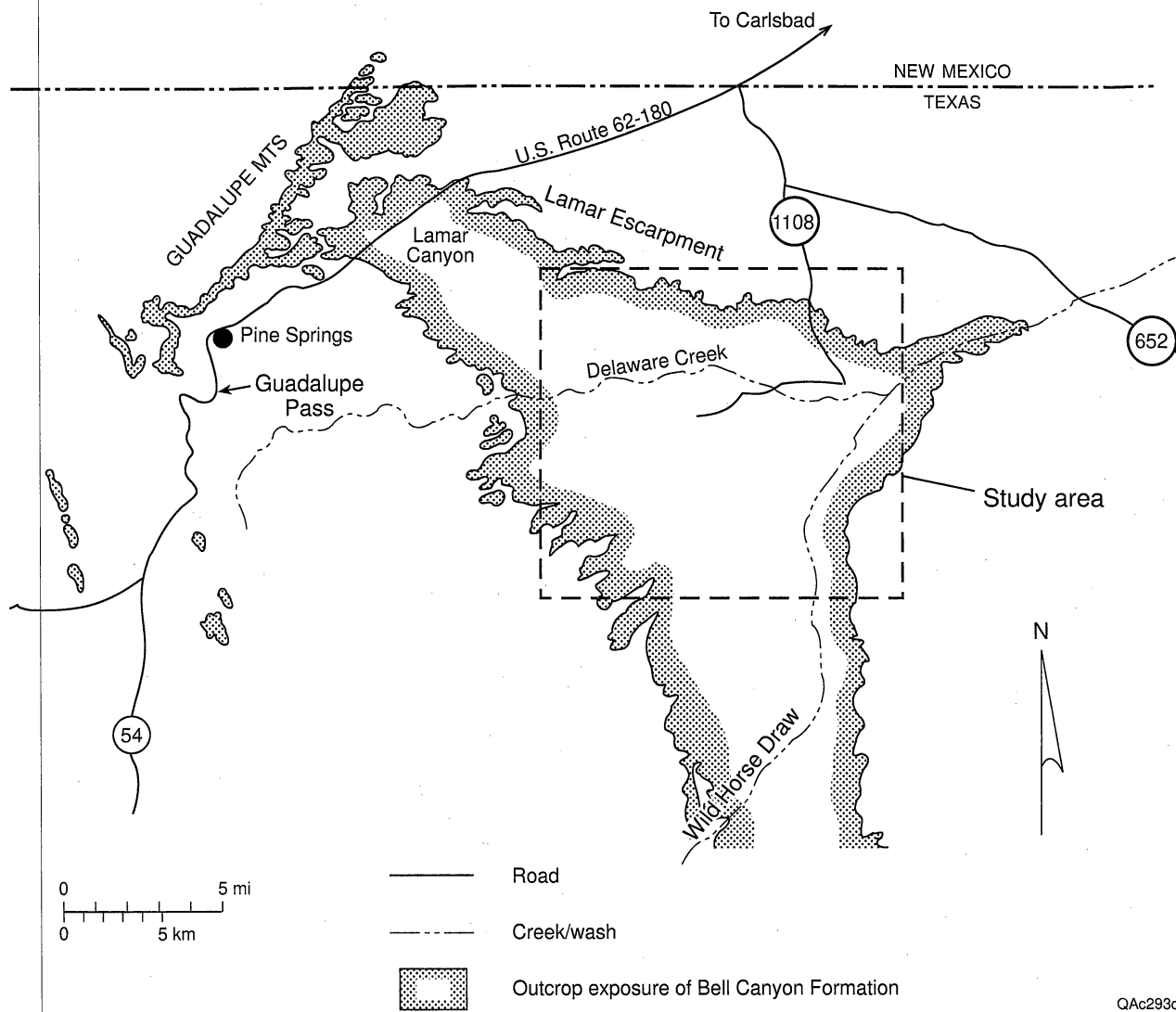
Figure 5. Map showing location of study area and outcrop exposure of Bell Canyon Formation, West Texas and southeast New Mexico.

10
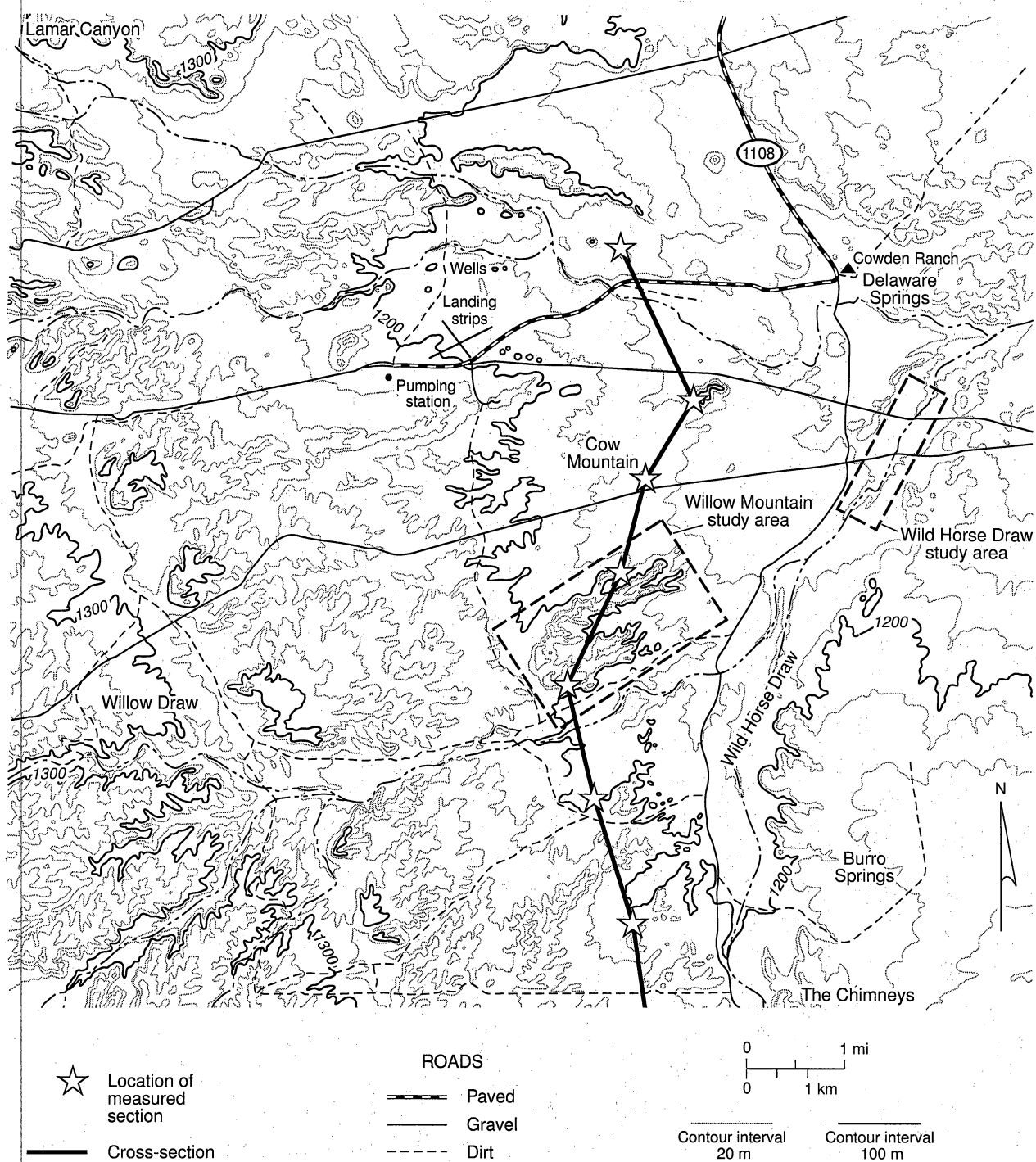
Figure 6. Map showing location of case study areas, Culberson County, West Texas.

11

study area and extends in a north-to-south fashion for a distance of about 7.5 km, roughly parallel to the depositional axis of the system (see fig. 6).

Sedimentology

Bedding architecture and facies distribution were documented from well-exposed outcrops by mapping facies and tracing bedding surfaces between measured logs and recording their distribution on photomosaics that provided complete coverage of the outcrops. Facies is a widely used term for grouping rock types on the basis of origin or any number of similar characteristics. In this study, facies are used to define groups with similar sedimentary features at the laminae to bed scale. Bounding surfaces represent breaks in sedimentation that may be erosional or conformable. They are classified according to order and type in a hierarchy that ranges from individual laminae to basin-wide unconformities or flooding surfaces. The mapping of facies together with bedding surfaces has proved to be a useful approach for dividing ancient rocks into sediment bodies that are depositionally related and characterized by their geometry, lithology, bedding architecture, and scale (Allen, 1982; Friend, 1983; Miall, 1985).

Facies

Six facies were described and categorized by number. Characteristics of the six facies are summarized in table 1.

Facies 1 is an organic-rich, laminated siltstone that lacks the extremely fine, parallel lamination of Facies 2 (fig. 7a). It ranges in thickness from a few centimeters to a few decimeters and often occurs as a relatively thin, discontinuous drape at the base of a channel or at the top of a sandstone bed. The base of the organic-rich siltstone is often gradational with underlying massive, graded, and ripple-laminated sandstone beds. The top of the organic-rich siltstone often displays an abrupt contact with overlying sandstones or laminated siltstones. Burrowing is common, especially near the top of the bed. The characteristics and position within an upward-

12

Table 1. Facies characteristics of Bell Canyon sandstones and siltstones.

Facies	Description	Bed Aspect	Transport Mechanisms	Depositional Setting
Facies 1 Massive, organic-rich siltstone	Dark-gray to black. Lacks extremely fine, parallel lamination of facies 1.	Thickness: 0.02 m to 1.0 m Length: 10 m to 1000 m	Suspension deposition from turbidity current. Similar to E division of Bouma sequence.	May occur as discontinuous drapes along the base of channels or along the top of sandstone beds.
Facies 2 Finely laminated, organic-rich siltstone	Dark-gray to black. Often interbedded with centimeters-thick volcanic ash beds.	Thickness: 0.01 m Length: 10's km	Suspension fallout of pelagic matter and airborne silt.	Deposition during prolonged periods of sediment starvation.
Facies 3 Laminated siltstone	Light-tan to brown. Extremely even parallel lamination that is a fraction of a millimeter to a few millimeters thick.	Thickness: 0.01 m to 10 m Length: Kilometers in length	Regular fluctuations in the settling of marine algal material and airborne silt, or silt derived from low-density interflows.	Occur as laterally extensive sheets that mantle underlying deposits.
Facies 4 Thin-bedded sandstones and siltstones	Current lamination, consisting of ripple drift and to a lesser extent horizontal, are the dominated sedimentary structures.	Thickness: 0.05 m to 10 m Length: 10 to 100 m	Deposition from waning turbidity currents. Similar to BCD division of Bouma sequence.	Deposited along flanks of channel by flows that spill over channel margin.
Facies 5 Structureless sandstone	Sandstones lack lamination and have a massive appearance. Floating siltstone clasts, water escape features, and load structures are other common features.	Thickness: 0.1 m to 10 m Length: 100's to 1000's m	Rapid depositon from sediment gravity flow. Equivalent to A division of Bouma sequence.	Deposited at mouths of channels and in overbank areas by unconfined flows. May also occur within upper channel fill.
Facies 6 Cross-laminated sandstone	Dune-scale cross-lamination that varies from infilled scours to climbing dunes.	Thickness: 0.2 m to 20 m Length: 10's to 100's m	Deposition from confined, turbulent, sediment gravity flows.	Largely confined to channels.

13

Figure 7a. Core photograph of massive, organic-rich siltstone (Facies 1) from Ramsey Sandstone at Ford Geraldine Unit, Culberson County, West Texas.

fining sequence suggest this facies is similar to the E division of the Bouma sequence and is interpreted to record the fallout from suspension of silt and organic matter from a turbulent sediment gravity flow.

Facies 2 is a dark-gray to black, finely laminated, organic-rich siltstone. The fine laminations are the result of tan to light-gray siltstone laminae that are a fraction of a millimeter thick and alternate with dark, organic-rich laminae that are a millimeter to several millimeters thick (fig. 7b). Overall organic content varies systematically, depending on regular increases or decreases in the thickness of the organic-poor or organic-rich siltstone laminae. The organic content of these siltstones has been reported to be as high as 46 percent. Analysis of the organic matter has shown that most of it is derived from marine algal matter (Williamson, 1978; Bozanich, 1979). Fossilized bones or teeth, nodular concretions of chert, siderite, and phosphate, and thin, centimeter-thick beds of volcanic ash are common constituents. Upper and lower contacts of Facies 2 are gradational with Facies 3 and occur at the top of upward-fining laminated siltstone or at the base of the upward-coarsening laminated siltstone. Facies 2 is interpreted to have been deposited by the settling of marine algal material and airborne silt. The presence of fossils and volcanic ash beds suggests it was deposited during a prolonged period when silt and sand were prevented from entering the basin (Meissner, 1972; Harms, 1974; Williamson, 1978; Harms and Williamson, 1988; Fischer and Sarnthein, 1988; Gardner, 1992).

Facies 3 is a laminated siltstone that is similar to Facies 2 but contains considerably less organic matter. The dominant sedimentary structure is extremely even, parallel lamination produced by the regular alteration of dark, organic-rich siltstone laminae that are a fraction of a millimeter thick, with tan to light-gray siltstone laminae that are a fraction of a millimeter to 3 mm thick (fig. 8a). Individual laminae are normally graded with the transition from light to dark laminae recording a decrease in grain size and an increase in organic matter. Rarely, the siltstone laminae are truncated by shallow scours displaying a few millimeters of relief. The scoured surfaces are usually draped by overlying laminae but may occasionally be overlain by isolated current ripples that are widely spaced, display rounded profiles, and are less than a centimeter

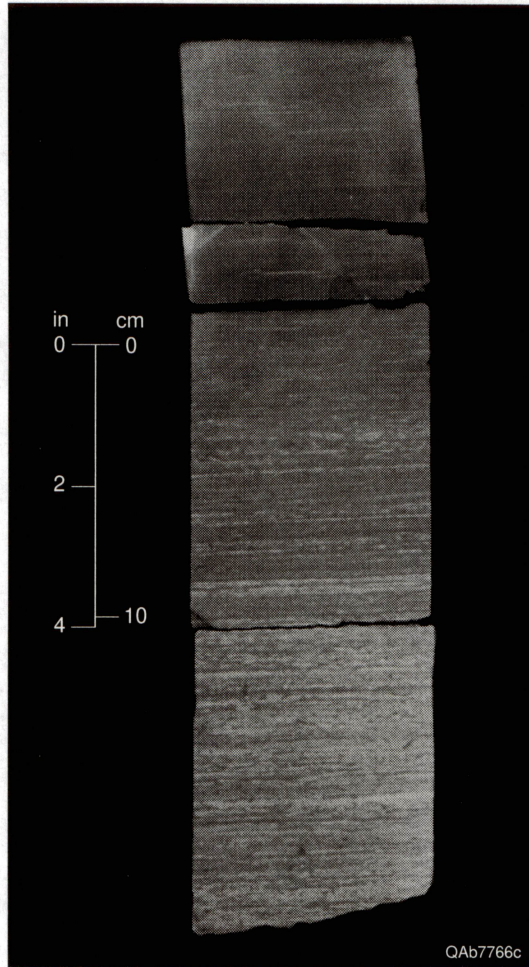Figure 7b. Core photograph of laminated, organic-rich siltstone (Facies 1) from Ramsey Sandstone at Ford Geraldine Unit, Culberson County, West Texas.
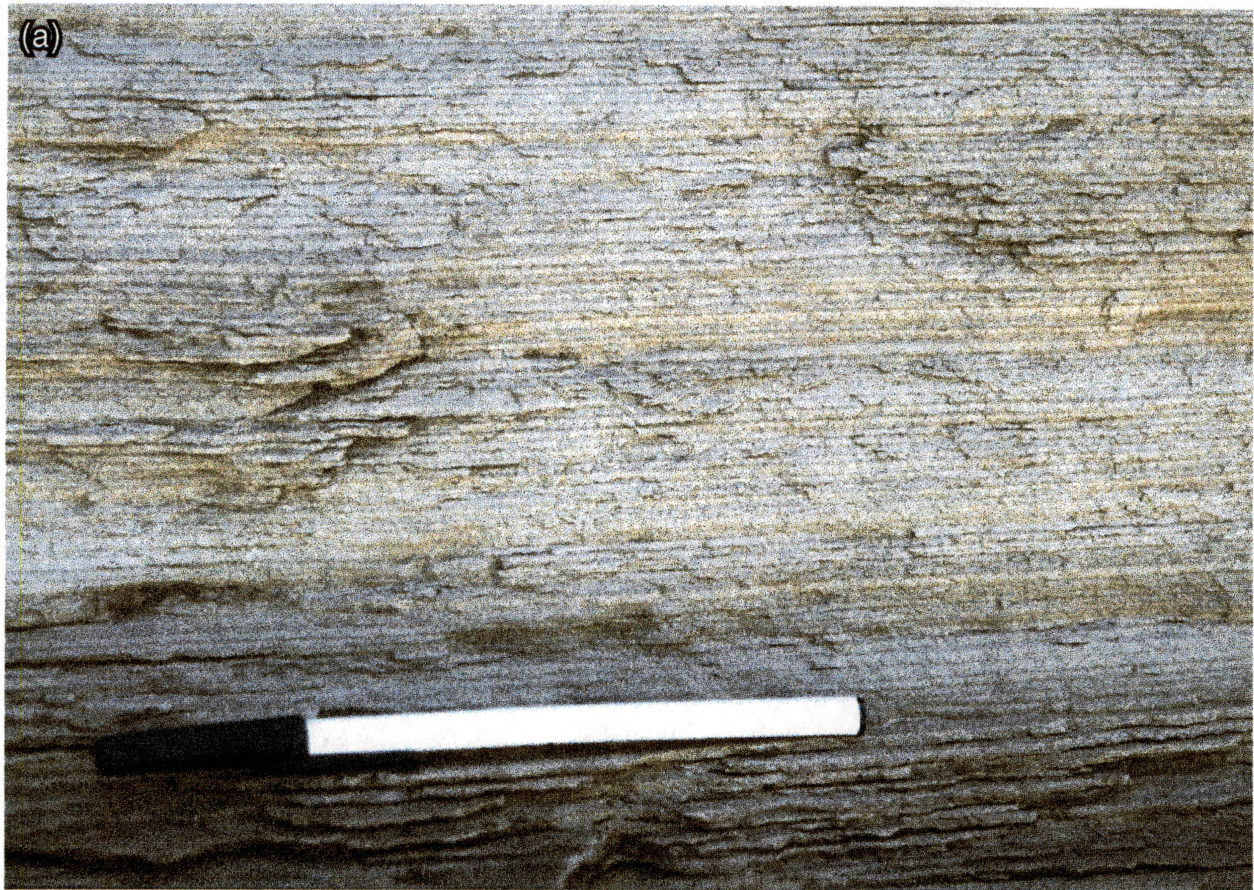
Figure 8. (a) Outcrop photograph of laminated siltstone (Facies 3) from Wild Horse Draw, Culberson County, West Texas. (b) Outcrop photograph of thin-bedded sandstones and siltstones (Facies 4) from Wild Horse Draw, Culberson County, West Texas.

thick. Burrowing is not common and is usually restricted to horizontal bedding planes. Laminae are often organized into sets that are a few centimeters to a few decimeters in thickness and show a progressive increase or decrease in lamina thickness or organic content. In turn, the sets may combine to form upward-fining or upward-coarsening successions that are as much as several meters in thickness. The laminated siltstones occur as laterally extensive sheets that mantle underlying deposits. Facies 3 is interpreted to record regular fluctuations in the settling of marine algal material with airborne silt or silt derived from low-density interflows. The presence of truncated laminae and current ripples suggests that weak bottom currents occasionally reworked the sediments.

Facies 4 is composed of thin-bedded sandstones and siltstones that are normally graded, display partial Bouma sequences (Bouma, 1962), and have abundant current lamination (fig. 8b). Sandstone beds are a few centimeters to a few decimeters in thickness and often have erosional bases. Individual beds usually fine upward, from sandstone at the base to siltstone at the top. The most common sequence of stratification types is similar to the BC or BCD division of the Bouma sequence, with beds beginning as horizontally laminated sandstone or ripple-drift, cross-laminated sandstone, and passing upward into a wavy-laminated siltstone. Graded sandstones at the base of the bed are occasionally observed. The sequence of stratification types and abundance of ripple-drift cross-lamination indicates that Facies 4 was deposited from waning, turbulent sediment gravity flows.

Facies 5 consists of sandstones that are structureless or massive in appearance (fig. 9a). Sandstone beds are several decimeters to several meters thick, are weakly graded to ungraded, and display abrupt, nonerosional bases. Flame structures and convoluted bedding contemporaneous with deposition are common along the base of many sandstone beds (fig. 9b). Dewatering features include dish and pillar structures that are most abundant in the upper portions of the beds; other features include siltstone clasts that are concentrated near the top of the bed and float in a matrix of fine sand. The lack of lamination, presence of floating clasts
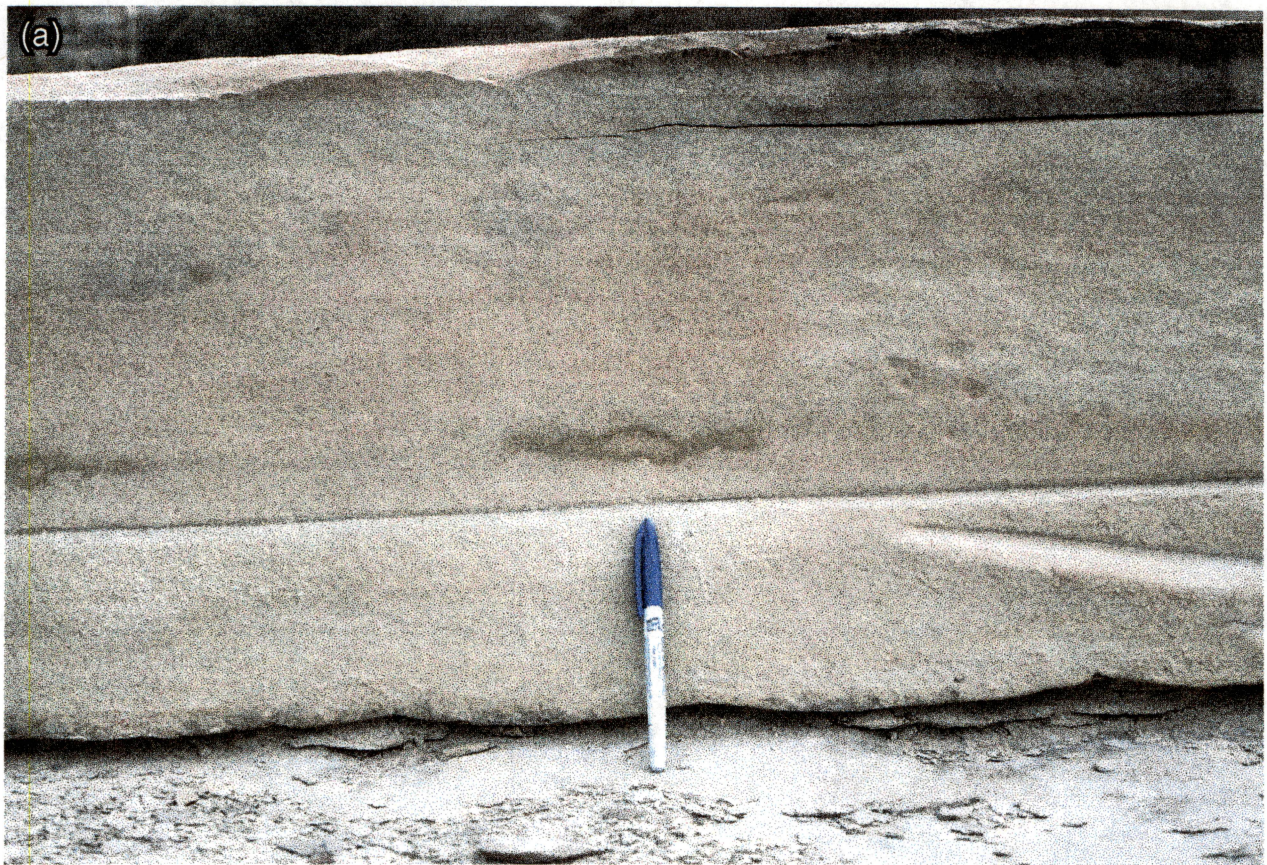
QAc232c

Figure 9. (a) Outcrop photograph of structureless sandstone (Facies 5) from Willow Mountain, Culberson County, West Texas. (b) Photograph showing deformed bedding contemporaneous with deposition (Facies 5) from Willow Mountain, Culberson County, West Texas.

19

(see fig. 9b), and abundance of water escape and load structures suggest the sandstones were rapidly deposited from high-density sediment gravity flows (Lowe, 1982; Kneller, 1996).

Facies 6 consists of sandstones displaying dune-scale cross-lamination that varies from infilled scours to climbing dunes. The infilled scours are scoop-shaped with sides inclined up to 75 degrees in dip. In plan view the scours have an elliptical to circular shape that is about 0.5 to 1.5 m long and 0.3 to 0.75 m across. Laminae onlap and overlap the margins of the scour (fig. 10a). The climbing, dune-scale cross-lamination, often referred to as a megaripple drift (Williamson, 1978; Harms and Williamson, 1988), is similar to a ripple-drift cross-lamination, only larger in scale. The most common form shows full preservation of laminae on the stoss side of the dune (fig. 10b). Laminae on the lee side of the bed have tangential bases suggesting the presence of turbulent eddies during deposition. Cross-laminated sandstones are restricted to channel fills. The scale, form, and occurrence of the cross-lamination suggest the sands were deposited from confined, highly turbulent sediment gravity flows.

Depositional Elements

Depositional elements are sediment bodies or lithosomes defined by their bounding surfaces, geometry, bedding architecture, and facies. They represent a particular process or suite of processes occurring within a depositional system (Miall, 1985). Depositional elements that are recognized within Bell Canyon include (1) amalgamated channels, (2) isolated, winged channels, (3) lobes, (4) interchannel lobes, (5) laminated siltstone sheets, and (6) organic-rich, laminated siltstone sheets. Geometry, dimensions, and lithology of the six lithosomes are summarized in table 2.

The amalgamated channels have an irregular convex-downward geometry. They are bounded at the base by an erosion surface and are composed largely of cross-laminated sandstones. The bodies are several meters to 10 m thick and a hundred to a thousand meters in

20

QAc231c

Figure 10. (a) Outcrop photograph of large-scale cross-laminated sandstone (Facies 6) from Willow Mountain, Culberson County, West Texas. (b) Outcrop photograph of climbing dunes (Facies 6) from Willow Mountain, Culberson County, West Texas.

21

Table 2. Characteristics of depositional elements.

Depositional element	Geometry	Dimensions: T-Thickness (m) W-Width (m) AR-Aspect Ratio	Lithology	Depositional Setting/Process
Condensed section	Sheet	T: 0.05 to 0.5 W: 10's km Composite sequences are up to 30 m thick and 100's km in length.	Facies 2 Gradational contacts with facies 3.	Deposition of pelagic material during prolonged period of sediment starvation. Bound stratigraphic cycles at multiple scales.
Siltstone sheet	Sheet	T: 0.1-3 W: Kilometers in length	Facies 3 May form upward-coarsening or -fining successions.	Topography mantling siltstones deposited by density interflows or airborne silt.
Lobe	Broad lens	T: 1-10 W: 1,000-10,000 AR: 100-10,000	Facies 5 Facies 6 near the top of body. Abrupt, nonerosive basal contact.	Sandy lobe deposited by unconfined sediment gravity flows at mouth of channel.
Channel	Convex downward	T: 2-20 W: 10-1,000 AR: 10-100	Facies 6 Facies 5 in upper portion of fill. Facies 1 may drape base of channel.	Incised channel or amalgamated channels.
Winged channel	Biconvex body with wings	Channel: T: 2-20 W: 10-200 AR: 10-20 Wings: T: 1-6 W: 200-2,000 AR: 100-1,000	Channel fill composed of facies 6. Wings composed of facies 4. Facies 1 may drape base of channel.	Aggradational channel levee.
Overbank lobe	Irregular	T: 1-10 W: 1,000 AR: 100-10,000	Facies 5 Facies 6 near top of body. Abrupt, nonerosive basal contact.	Overbank sandstones deposited in topographic lows by unconfined sediment gravity flows.

width parallel to depositional strike. The amalgamated channels are a highly truncated and amalgamated complex of channels that form a composite body with a larger aspect ratio (width:thickness ratio of 50:100) than an individual channel fill.

The winged-channel elements have a narrow, lenticular core flanked on both sides by beds that gradually thin and taper away from the body (fig. 11). The channel has an erosive base and is composed largely of cross-laminated sandstones. The channels range in size from several meters to 15 m in thickness and tens of meters to several hundreds of meters in width parallel to depositional strike. The flanking wings have a wedge-shaped geometry with an aspect ratio of around 100. Thickness of the flanking wings ranges from 1 to 6 m, and their length ranges from several hundred to several thousand meters. The wings consist largely of thin-bedded sandstones and siltstones or thick-bedded massive sandstones that tend to become finer grained farther from the channel. Paleocurrents within the wings deviate by about 15 degrees away from the axis of the channel. The winged channels are interpreted as aggradational channel fills flanked by winglike levees that maintained the channel margins (Mutti and Normark, 1987). The channels are interpreted to have been deposited by confined turbidity currents. The channel wings are interpreted to have been deposited by unconfined turbidity currents that spilled over the margin of the channel.

The lobes are broad lens-shaped to convex-upward bodies. They generally lack an erosive base and are composed chiefly of medium- to thick-bedded massive sandstones. Thicknesses reach as much as 10 m with aspect ratios on the order of 100 to 10,000. The geometry and abundance of structureless sandstone suggest the lens-shaped bodies were deposited as sandy lobes at the mouths of channels by unconfined, highly depletive sediment gravity flows.

The interchannel lobes are irregularly shaped sandstone bodies, internally similar to the broad, lens-shaped bodies. They lack an erosive base and consist chiefly of massive sandstones with lesser amounts of cross-laminated sandstones. Width and thickness are poorly correlated, and geometry appears to be closely associated with underlying topography. Stratigraphic relationships indicate they are contemporaneous with or succeed associated channel-levee

23

BOUNDING SURFACES

═══ Bed or bedset

──── Type 2

▬ ▬ ▬ Type 3

ELEMENT

Lam Laminated siltstone
Ch   Channel
Lv   Levee
Ob   Overbank

QAc295c
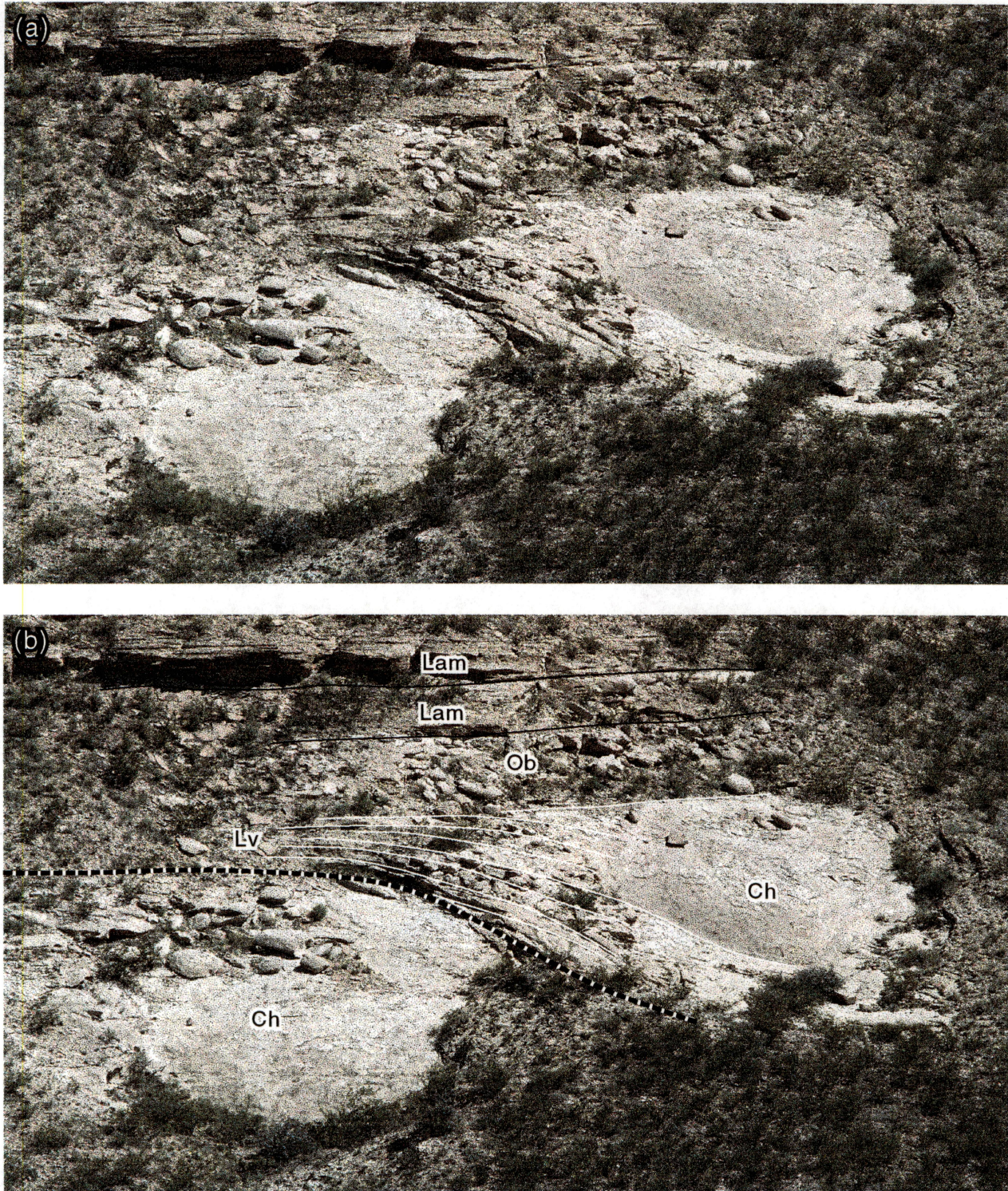
Figure 11. Outcrop photograph of channel-levee deposit from Willow Mountain, Culberson County, West Texas.

deposits. Features of the sandstone and bedding relationships indicate the irregularly shaped bodies were deposited as interchannel lobes within topographic lows that existed between adjacent channel levees.

The laminated siltstones occur as sheets that mantle underlying deposits. The sheets are less than a meter to more than several meters in thickness. Over an area of 5 to 6 km there is little variation in thickness except where the laminated siltstones have been incised by overlying channels. The sheets of laminated siltstone were not observed to drape a channel base or margin or to occur as part of a channel fill. The uniform thickness and lateral extent suggest that the sheets were deposited from suspension by the settling of airborne silt or silt derived from laterally extensive, low-density interflows.

The sheets of organic-rich siltstones are similar to the sheets of laminated siltstone but are thinner and less frequent. They occur at the top of an upward-fining succession of laminated siltstone or at the base of an upward-coarsening succession of laminated siltstone. The organic-rich siltstone sheets are interpreted to be condensed sections deposited by slow settling of marine algal matter during a prolonged period when the basin was starved of sand and silt. Their distinctive lithology and lateral extent make them excellent correlation markers.

These depositional elements or lithosomes are organized in a systematic fashion to form cyclic successions referred to as high-frequency cycles. The cycles are bounded by organic-rich siltstones that display gradational contacts with overlying and underlying laminated siltstones. The laminated siltstone sheets may combine to form composite sequences that are as much as 10 m thick and tens of kilometers in length. In the lower half of the cycle, the laminated siltstones tend to coarsen upward and are interstratified with broad, lens-shaped sandstone bodies that show an upward-bed-thickening trend. This succession is locally incised and replaced by amalgamated channels that pass upward into winged-channel-form bodies interstratified with the broad, irregularly shaped sandstone bodies. The winged channels display crosscutting relationships and stack vertically and laterally to form multistoried complexes. Channel orientation within a complex varies by as much as 90 degrees. An upward-fining succession of

25

laminated siltstones interstratified with broad, lens-shaped sandstone bodies that display an upward-bed-thinning trend abruptly overlies the deposits and caps the cycle.

The high-frequency cycle is interpreted to record deposition from a system of channel-levees with attached lobes. The multistoried channel complex records repeated episodes of channel aggradation and avulsion. The systematic change in cycle architecture indicates the system prograded into the basin, aggraded, and then retrograded. Bounding, organic-rich siltstones record periods when sediment was prevented from entering the basin.

Case Studies

Wild Horse Draw

At Wild Horse Draw, a complex of crosscutting channels and interchannel deposits are extremely well exposed. The exposure is about 800 m in length and aligned parallel to depositional strike. A map of the study area and the location of lithologic logs are shown in figure 12. The bedding architecture and distribution of facies were documented along the west wall of the wash and shown in figure 13. Paleochannel trends were mapped between adjacent walls of the wash.

The complex of crosscutting channels and interchannel deposits is bounded by sheets of organic-rich, laminated siltstones (see fig. 13). The channel complex is up to 6 m thick, and the bounding laminated siltstones are up to 2 m thick. The channel complex overlies an erosive surface that locally incises through the underlying laminated siltstone. Erosion surfaces within the channel complex have several meters of relief and divide the channel complex into three sediment bodies or lithosomes. The lithosomes are 4 to 5 m thick and hundreds of meters wide. Erosional surfaces are occasionally overlain by a relatively thin, massive, organic-rich siltstone. The lithosomes have a lens-shaped geometry with a thick, sandy channel fill that is flanked by wedges of thin-bedded sandstones and siltstones. The thin-bedded sandstones and siltstones thin and taper away from the channel fill. Paleochannel trends were mapped between adjacent walls of the wash: the paleochannel directions range from S30°W to S45°E (fig. 14).

26
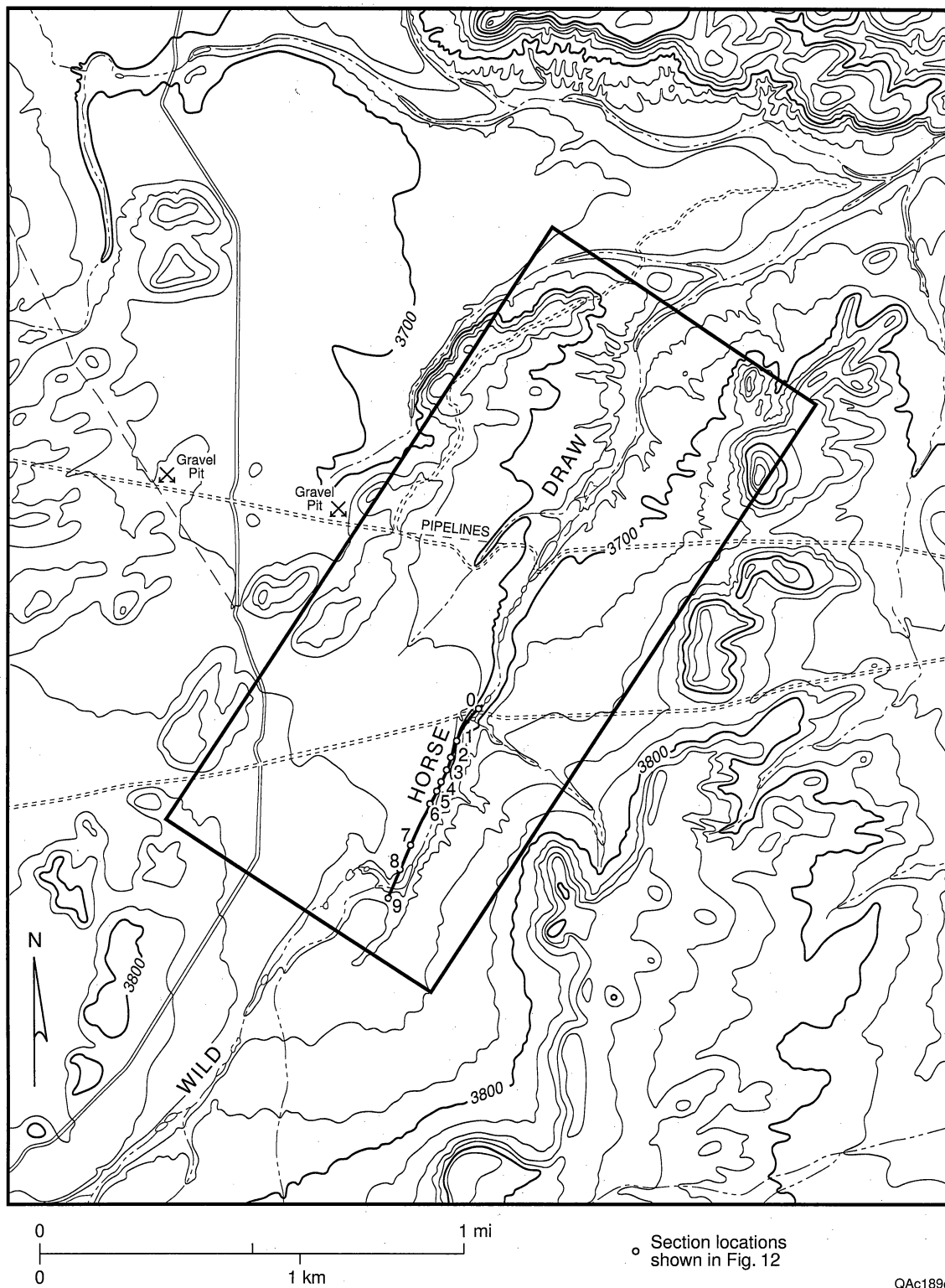
Figure 12. Map of Wild Horse Draw study area showing location of measured logs and cross section.

27
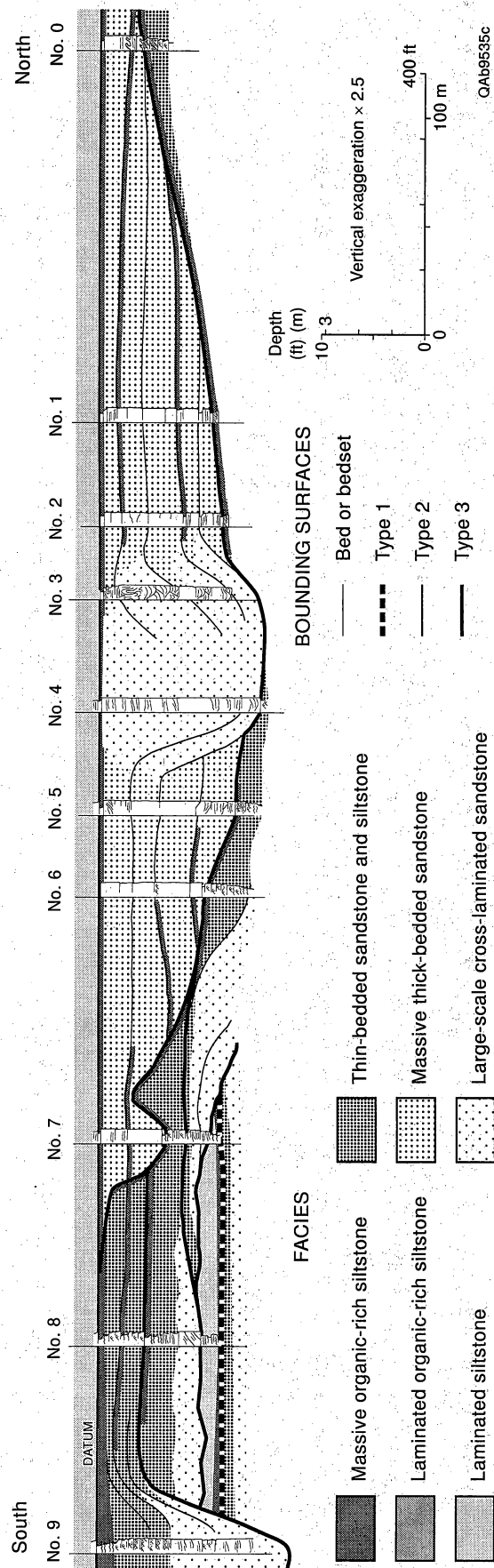
Figure 13. Diagram illustrating facies and bedding architecture from Wild Horse Draw. Exposure is from the north end of the wash along the west wall.

28
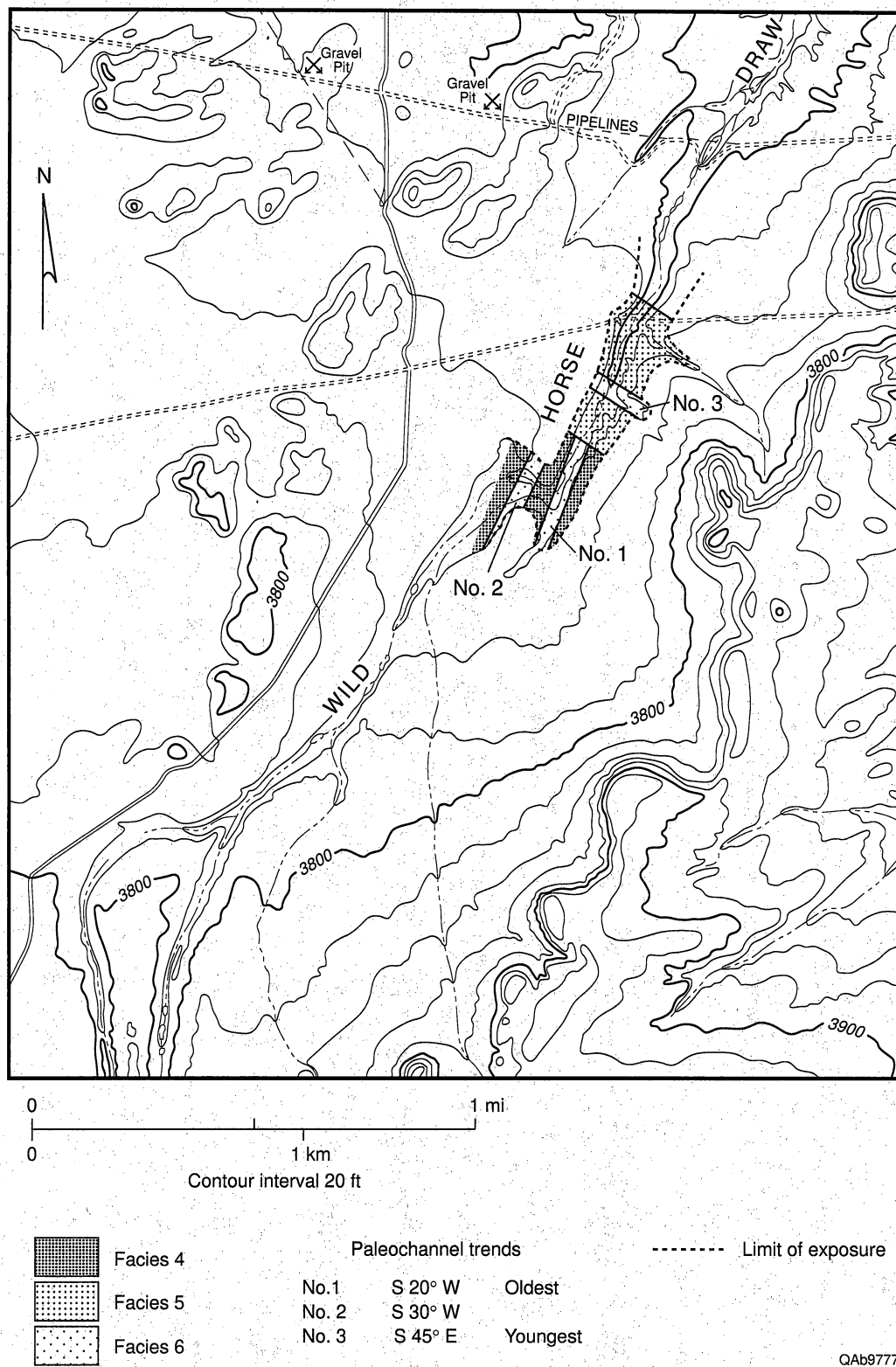
Figure 14. Plan-view map showing paleochannel trends from Wild Horse Draw.

The channel fills are 4 to 5 m thick and 30 to 50 m across. They have a massive appearance and are composed chiefly of large-scale cross-laminated sandstones. Portions of the fill, especially near the top and center of the channel, are massive and often have dewatering and dish structures. Angular to well-rounded siltstone clasts that are up to several centimeters in diameter are occasionally present near the base of the channel.

The margins of the channel are draped by sandstone beds that can be traced from the channel fill into adjacent interchannel areas. Within the channel fill, individual beds have a sigmoidal geometry that is 3 to 4 m in height and as much as 1 m thick. Beds dip as much as 17 degrees toward the axis of the channel. On both sides of the channel, the beds are stacked vertically and slightly offset toward the center of the channel (fig. 15). As a result, opposing channel margins are relatively symmetrical and appear as mirror images. Beds that extend over the margin of the channel rapidly flatten and show a change from cross-laminated sandstones within the channel fill to massive and parallel-laminated sandstones over the margin. As the beds are traced laterally away from the channel they gradually thin and pinch out over several hundred meters by downlapping onto an erosional surface. Beds flanking the channel fills also tend to show systematic changes in facies. As a whole they tend to become finer grained and more thinly bedded away from the axis of their respective channels. Individual beds generally show a change from massive and parallel-laminated sandstones to thin-bedded, ripple-laminated sandstones and siltstones away from the channel axis. In the interchannel areas, individual beds or bedsets are often overlain by thin, discontinuous, massive, organic-rich siltstones. The massive, organic-rich siltstones are up to 10 cm thick and pinch out toward the channel. Flame structures are common along the base of many of the massive sandstones and tilt away from the channel axis by about 15 degrees.

Beds flanking channel fills also show variation in facies composition. The beds flanking the two oldest channel fills are composed largely of thin-bedded sandstones and siltstones that internally show extremely complex and irregular bedding geometries. By contrast, beds that

flank and are contemporaneous with the youngest channel fill consist largely of massive sandstones that, despite thinning and pinching out, show little lateral variation in the facies.

The bedding architecture and biconvex geometry suggest the channels were maintained by levee deposits that tended to aggrade vertically during deposition with little or no lateral migration. The channel stacking pattern suggests that individual channels were capable of aggrading 3 or 4 m above the surrounding area before becoming unstable and avulsing into topographically low interchannel areas. The lens-shaped geometry of the channel fills is interpreted to reflect differences in depositional topography rather than differences in compaction between sandy channel fills and silty interchannel areas. Interchannel beds that are immediately adjacent to the channel margin tend to thin abruptly toward the channel and in some cases display onlapping relationships. It is also important to note that interchannel areas experience significant erosion or scour immediately following each avulsion event. The restriction of cross-laminated sandstones to channel fills indicates that they were deposited by confined turbidity currents. In contrast, levees and interchannel deposits are composed of massive sandstones and thinly bedded sandstones and siltstones, suggesting that they were deposited by unconfined turbidity currents that spilled over the channel margins. The internal architecture and stacking pattern of channels observed at Wild Horse Draw are interpreted to record three episodes of channel development and avulsion (fig. 16). Each episode consists of a series of events that include (1) widespread erosion, (2) channel-levee aggradation, (3) channel filling, and (4) channel avulsion.

Willow Mountain

At Willow Mountain, the stacking pattern of channels and lobes was documented over an area of several square kilometers. A map of the study area and location of lithologic logs are shown in figure 17. Stratigraphic relationships from the northern half of the mountain are illustrated in five cross sections that are aligned in an east-to-west fashion parallel to the

South

North

Match line A

Match line A

Match line A

Match line A
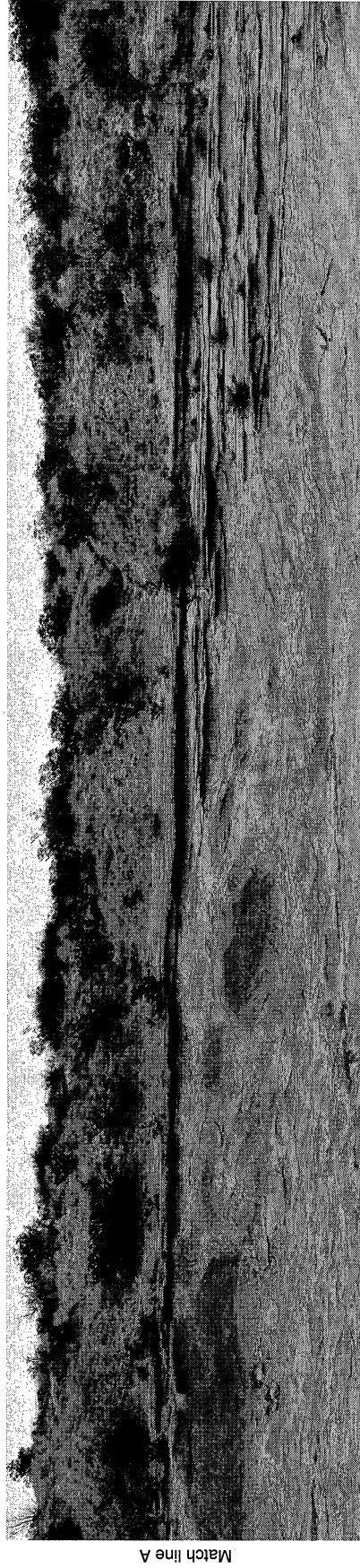
QAc339(b)c

Figure 15. Photograph of channel, Wild Horse Draw.

South
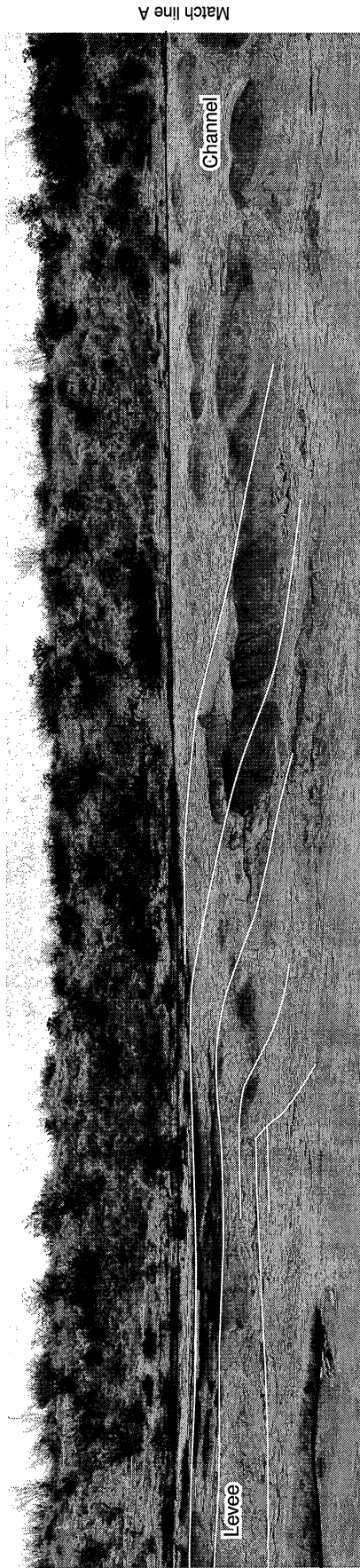
North

Channel

Levee

Levee

Levee

Match line A

Match line A

QAc339(a)c

BOUNDING SURFACES

Bed or bedset   Type 2   Type 3

Figure 15 (cont.)

33
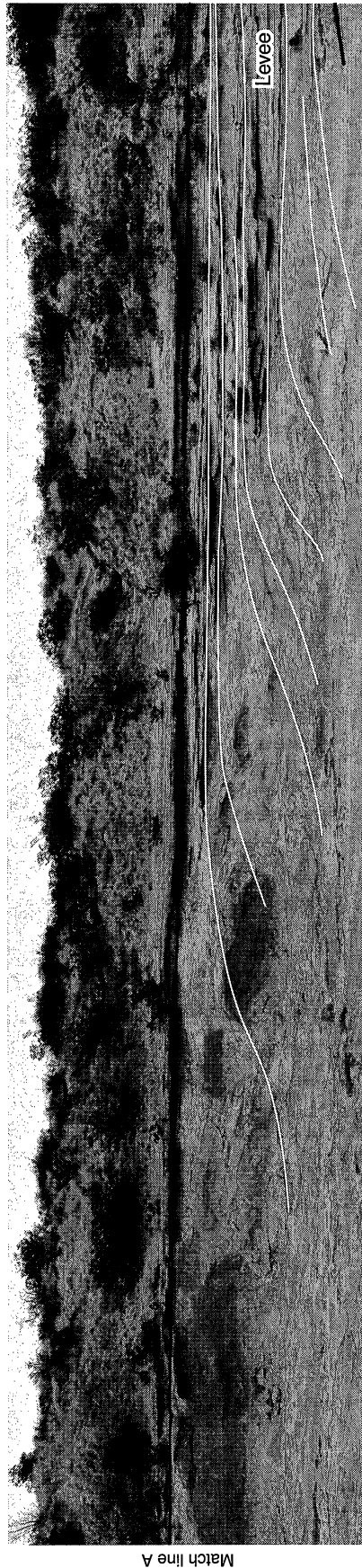
I. Suspension deposition of mantling organic-rich siltstone and laminated siltstone

South   North
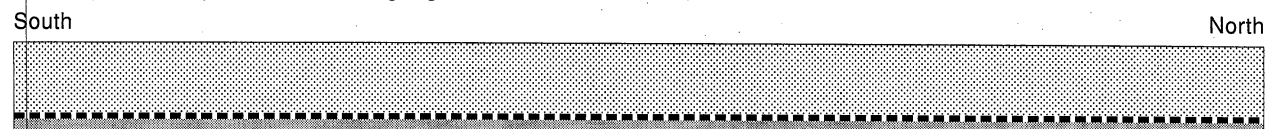
II. Erosion followed by deposition of channel levee (channel direction: S 20° W)

South   North

III. Avulsion followed by deposition of 2nd channel levee (channel direction S 30° W)

South   North

IV. Avulsion followed by deposition of 3rd channel levee (channel direction S 45° E)
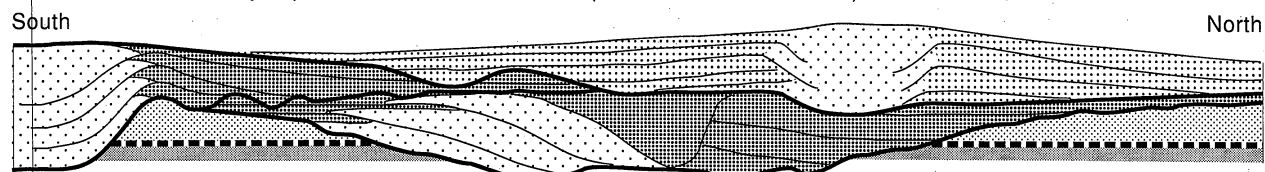
South   North

V. Suspension deposition of mantling organic-rich siltstone and laminated siltstones

South   North

FACIES

Laminated organic-rich siltstone

Laminated siltstone

Thin-bedded sandstone and siltstone

Massive thick-bedded sandstone

Large-scale cross-laminated sandstone

BOUNDING SURFACES

—— Bed or bedset

▬▬▬▬ Type 1

—— Type 2

▬▬ Type 3
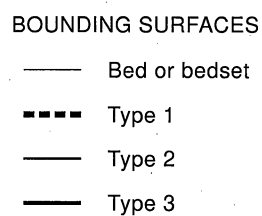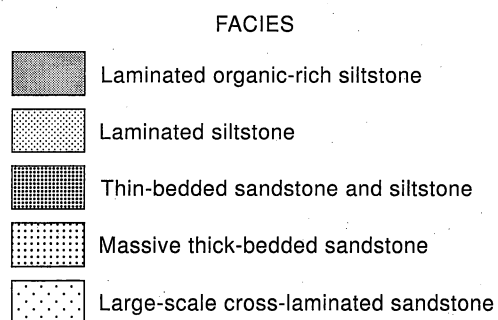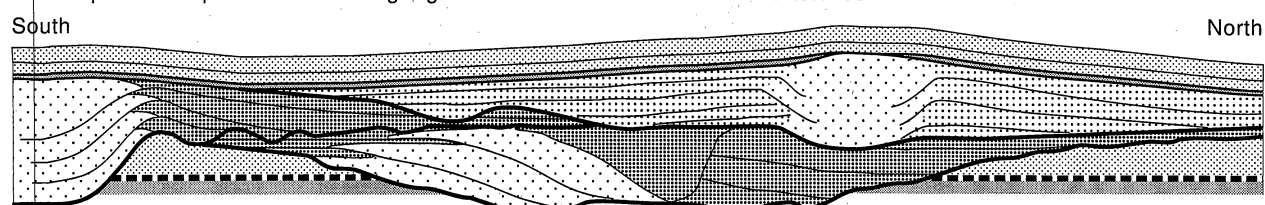
QAc239c

Figure 16. Diagram illustrating the interpreted sequence of events for Wild Horse Draw.

34
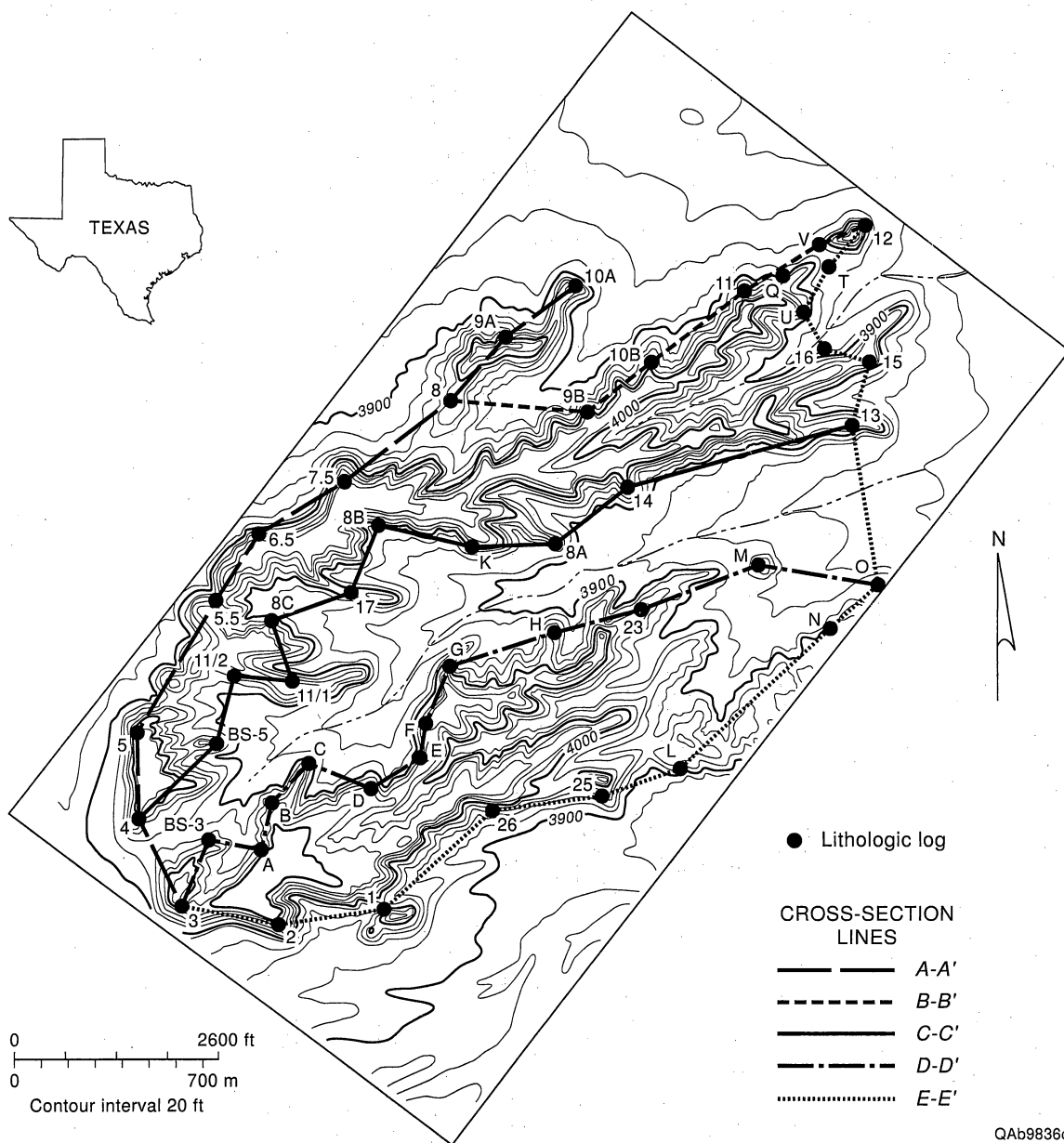
Figure 17. Map of Willow Mountain study area showing location of measured logs and cross sections.

35

depositional strike of the system (figs. 18 through 22). The cross sections are 1 to 3 km in length and are spaced about 0.25 to 0.35 km apart.

The high-frequency cycle is 15 to 20 m thick and bounded at the base and the top by thin (30-to 60-cm-thick), organic-rich laminated siltstones. Both the overlying and underlying organic-rich laminated siltstones have transitional contacts with Facies 3 and can be traced across the entire study area of 50 km^2. Within the high-order cycle, sandstone thickness ranges from 0.3 to 18 m and varies systematically with an upward-bed-thickening trend followed by an upward-bed-thinning trend. In some cases the lower upward-bed-thickening trend has been replaced by a relatively thick, erosive-based sandstone channel that is uniform to upward fining.

Sandstones in the upper and lower half of the cycle display a broad tabular or lens-shaped geometry. Individual sandstones are up to several meters thick and thin toward the east (fig. 23). The sandstones are interstratified with sheets of laminated siltstone that are between 1 and 2.5 m thick and show little lateral variation in composition or in thickness. Contacts between the tabular sandstones and siltstone sheets are abrupt but nonerosional. The middle of the cycle consists of a heterogeneous mix of narrow channel-form sandstone bodies and broad, irregularly shaped sandstone bodies interstratified with wedges of thin-bedded sandstone and siltstone (fig. 24). The channel-form bodies are up to 20 m thick and several hundred to a thousand meters wide. The channels are aligned in a northwest-to-southeast fashion and extend for several kilometers parallel to depositional dip. Within the complex, channel stacking patterns change in a systematic fashion. In the lower part, the channel-form bodies are highly amalgamated and truncated. In the middle part, they are vertically stacked in an offset pattern and are flanked by wedges of thin-bedded sandstone and siltstone similar to the Wild Horse Draw study area. In the upper part, they bifurcate and are flanked by broad, irregularly shaped sandstone bodies.

The high-order cycle is interpreted to have been deposited by a system of channels and levees with attached lobes. Vertical trends suggest the system initially prograded basinward (southeast), then aggraded, and finally, retrograded (fig. 25). Initially, clastic sediments were prevented from entering the basin and organic-rich laminated siltstones were deposited by the
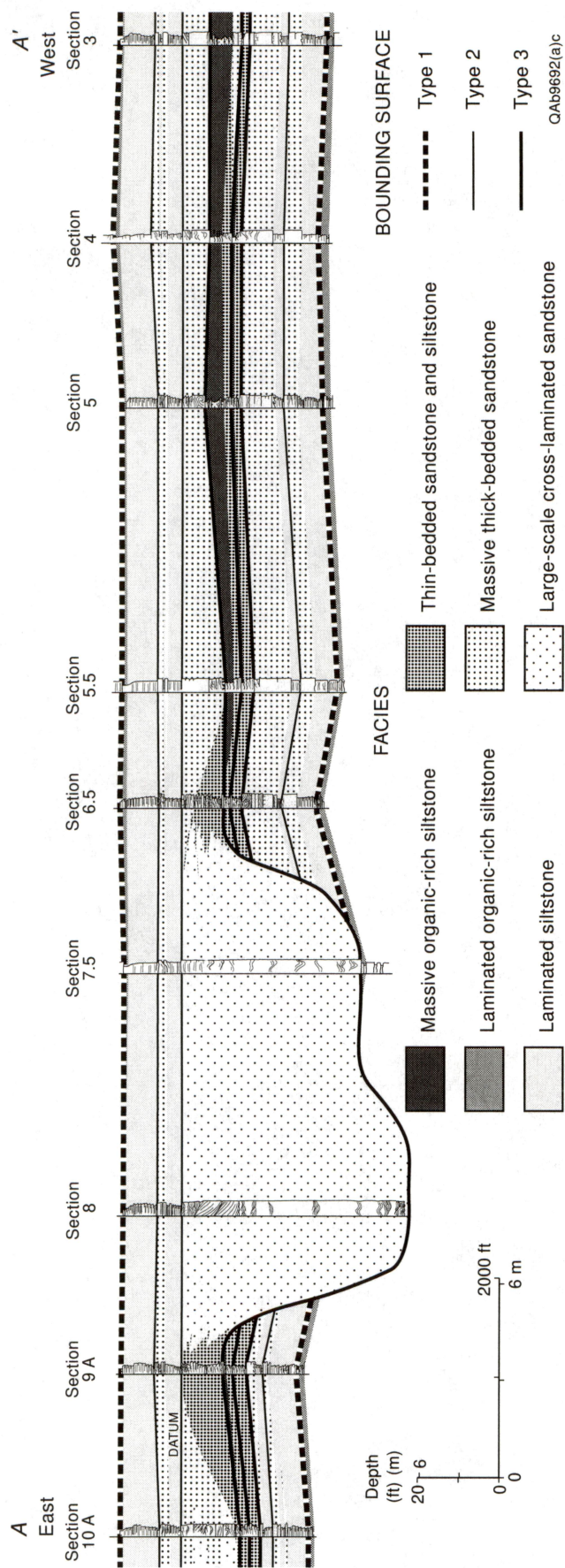
Figure 18. Cross section A–A' (see fig. 16 for location) showing distribution of facies and traces of key surfaces within a single high-order cycle, Bell Canyon Formation.
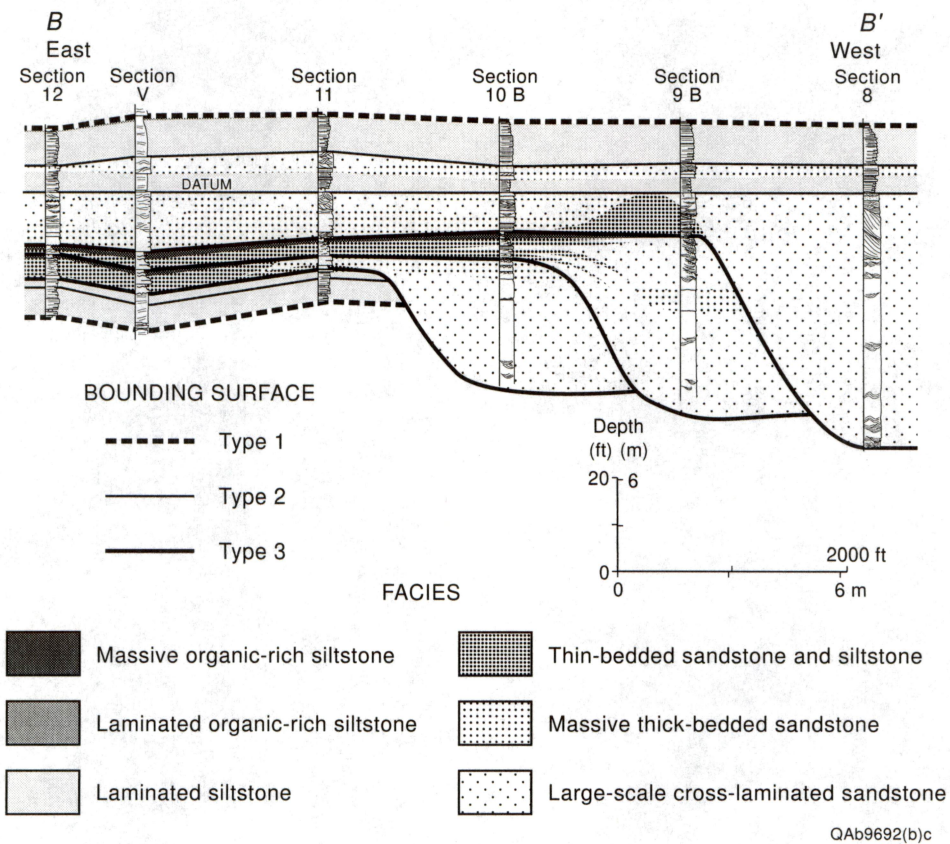
Figure 19. Cross section B–B′ (see fig. 16 for location) showing distribution of facies and traces of key surfaces within a single high-order cycle, Bell Canyon Formation.

Figure 20. Cross section C–C' (see fig. 16 for location) showing distribution of facies and traces of key surfaces within a single high-order cycle, Bell Canyon Formation.

39

Figure 21. Cross section D–D′ (see fig. 16 for location) showing distribution of facies and traces of key surfaces within a single high-order cycle, Bell Canyon Formation.

40

E'
East

Section Section Section Section Section Section Section Section Section Section Section Section Section Section Section Section
3 2 1 26 25 L N M 13 15 16 U T 12

E
West

DATUM

DATUM

Depth
(ft) (m)
20 — 6

0 — 0

3000 ft

900 m

QAb9694c

FACIES

BOUNDING SURFACE

Thin-bedded sandstone and siltstone

Massive thick-bedded sandstone

Large-scale cross-laminated sandstone

Massive organic-rich siltstone

Laminated organic-rich siltstone

Laminated siltstone

Type 1

Type 2

Type 3

Figure 22. Cross section E–E' (see fig. 16 for location) showing distribution of facies and traces of key surfaces within a single high-order cycle, Bell Canyon Formation.

41

BOUNDING SURFACES
----- Type 1   —— Type 2   —— Type 3

QAc331c
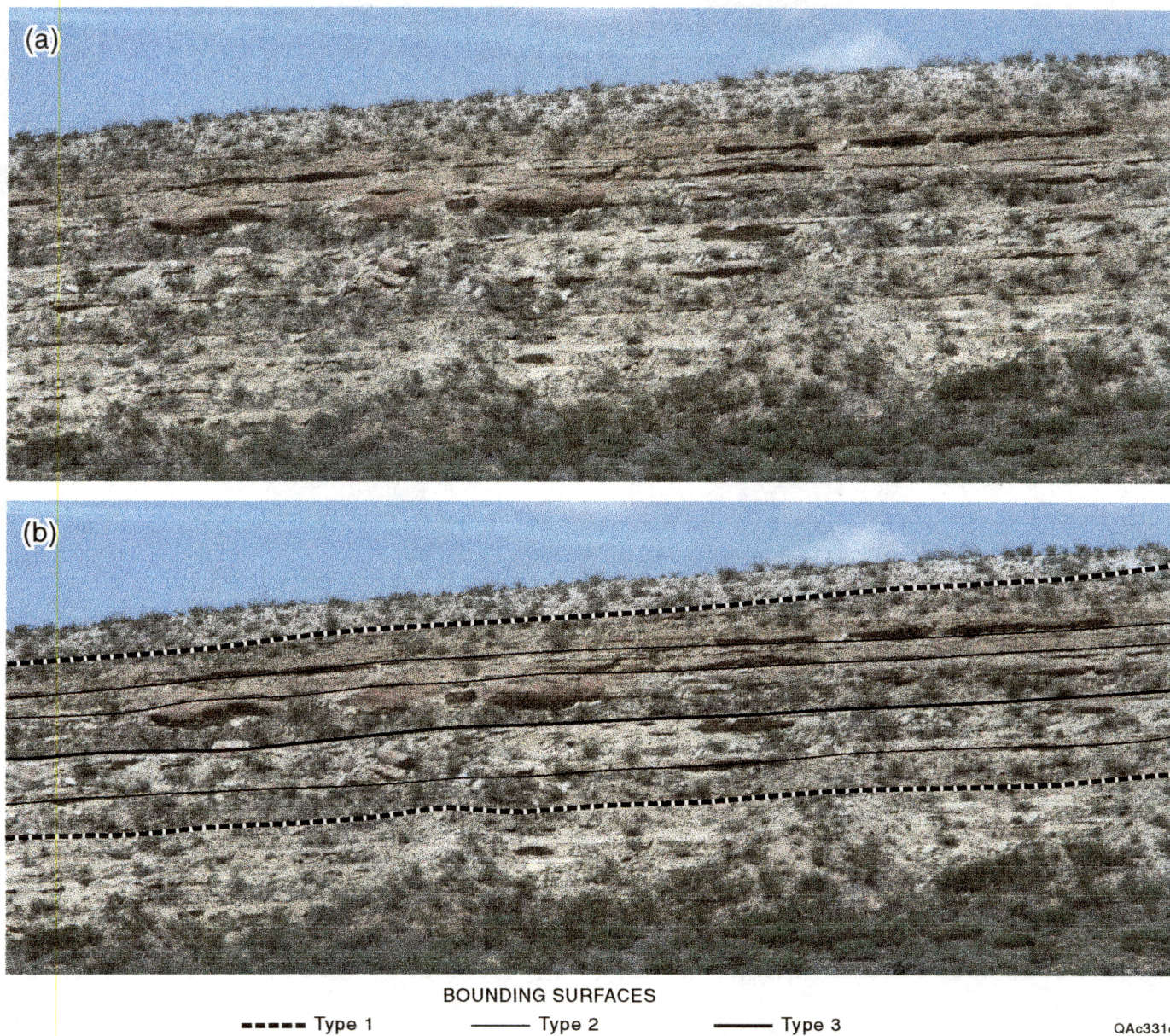
Figure 23. Photograph illustrating sandstone architecture of high-order cycle. Photograph is from Willow Mountain between lithologic logs 4 and 5 (see fig. 17 and cross section A–A′).

Figure 24. Photograph showing correlation of offset channels within high-order cycle. Photograph is from Willow Mountain between lithologic logs 8 and 10A.

BOUNDING SURFACES

▪▪▪ Type 1   ―― Type 2   ―― Type 3

ELEMENT

Lam Laminated siltstone   Ch Channel   Lv Levee   Ob Overbank

QAc330c

43

I. Deposition of silt and organic matter from suspension
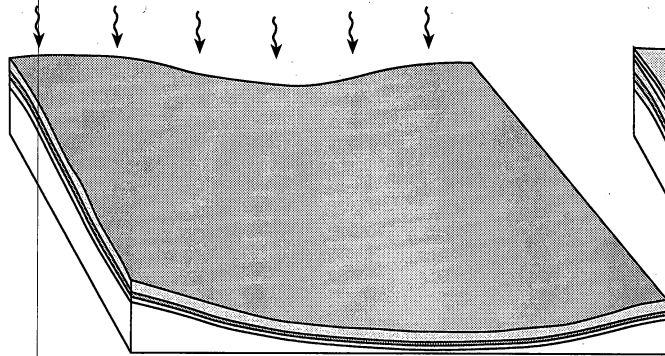
III. Deposition of channel and levee deposits/may be preceeded by erosion
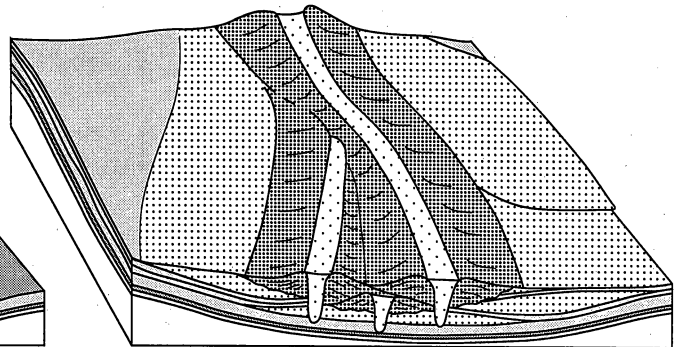
II. Deposition of lobes and laminated siltstones
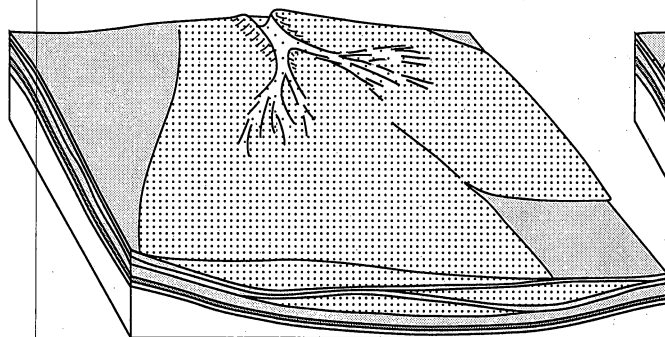
IV. Deposition of lobes in interchannel areas
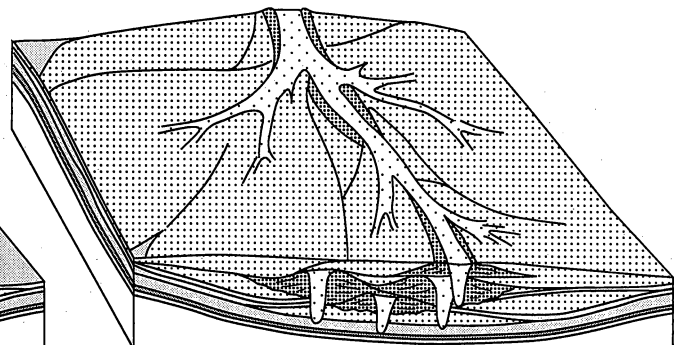
V. Deposition of silt and organic matter from suspension

5-30 m

0.5-5 km
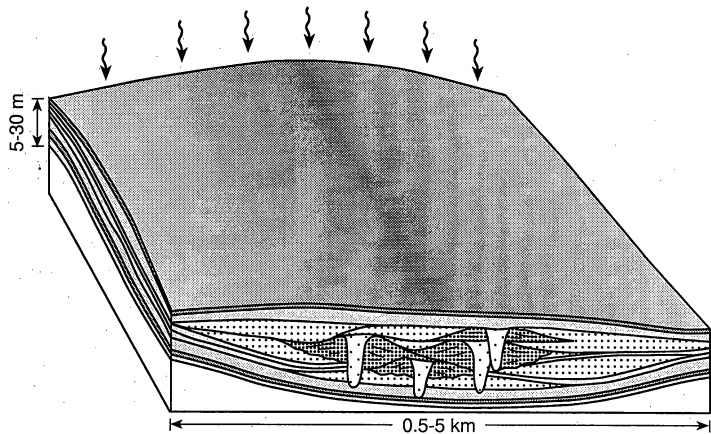
QAc186c

FACIES

Organic-rich laminated siltstone

Laminated siltstone

Thin-bedded, rippled, and horizontally laminated sandstone and siltstone

Massive sandstone

Cross-stratified sandstone

Figure 25. Diagram illustrating depositional facies model for high-order cycle examined at Willow Mountain.

44

slow settling of pelagic and organic material, airborne silt settling from suspension (step I). The upward-bed-thickening succession of broad, lens-shaped sandstone bodies interstratified with sheetlike, laminated siltstones in the lower half of the cycle was deposited during the initial progradational phase (step II). As the system continued to prograde, the sandstone lobes and sheets of laminated siltstones were partially eroded and replaced by a system of amalgamated channels. Upward, the system shows a gradual change from amalgamated channels to narrow, widely spaced channels flanked by well-developed levees interpreted to represent the aggradational part of the system (step III). The retrogradational part of the system is represented by bifurcating channels flanked by interchannel lobes (step IV) that are in turn abruptly overlain by an upward-fining and bed-thinning succession of sheetlike, laminated siltstones interstratified with broad, lens-shaped sandstone bodies (step V).

Regional Cross Section

A more regional view of facies and stratal relationships within the high-order cycle is illustrated in a cross section that extends south from Delaware Wash for a distance of about 7.5 km roughly parallel to the depositional axis of the system (fig. 26). In the cross section, the channel-levee complex exposed at Willow Mountain appears to pass out of the plane of the cross section. Finer-grained levees that flank the margins of the channel complex form wedges that gradually thin and pinch out to the northeast and southwest over a distance of about 2 km. Farther to the south (basinward), near the southern end of Cowden Ranch, the high-order cycle progressively thins to about 12 m and consists of a single sandstone body that is about 6 m thick and has bounding laminated siltstones. The sandstone body has a broad tabular geometry, has an abrupt but nonerosive base, and is composed largely of structureless sandstones. Organic-rich siltstones above the sandstone body indicate that it correlates with the overbank sandstone lobes at Willow Mountain.
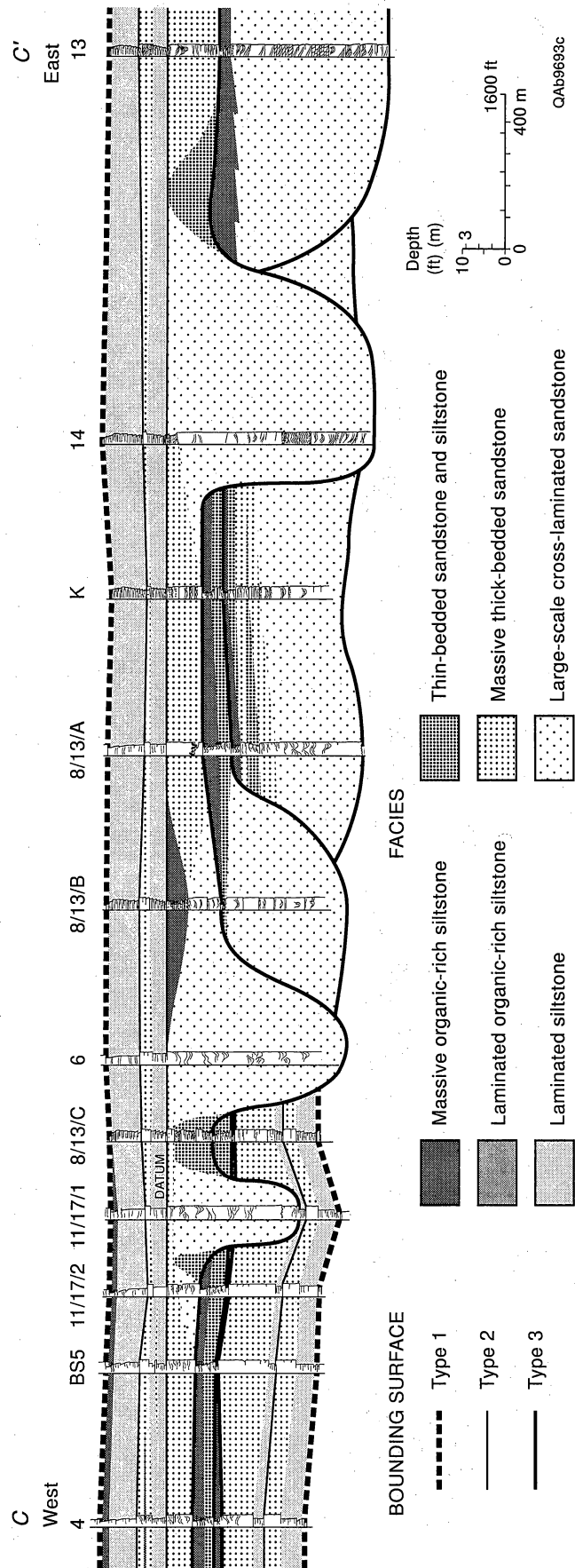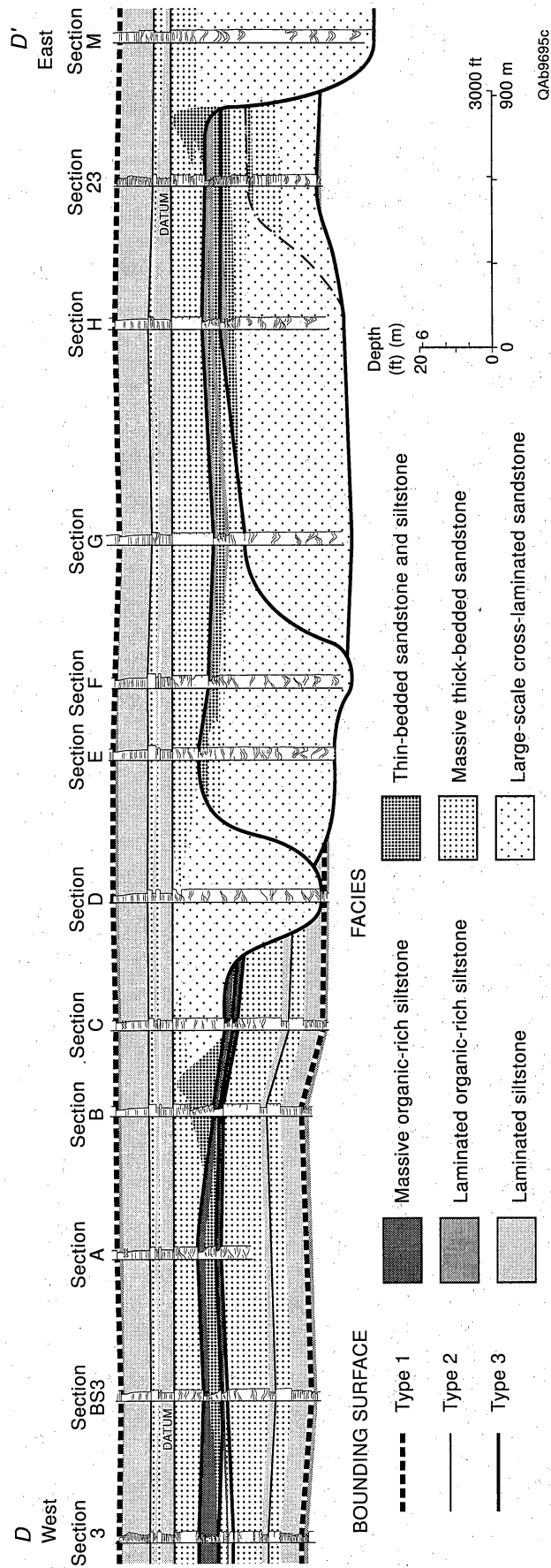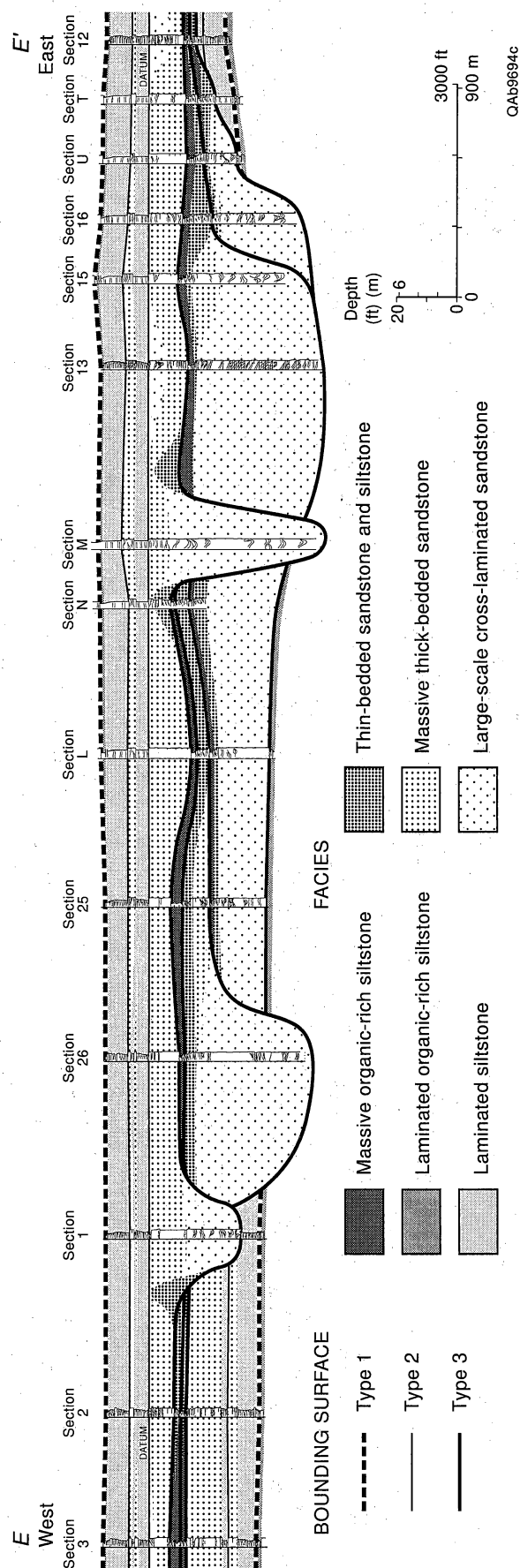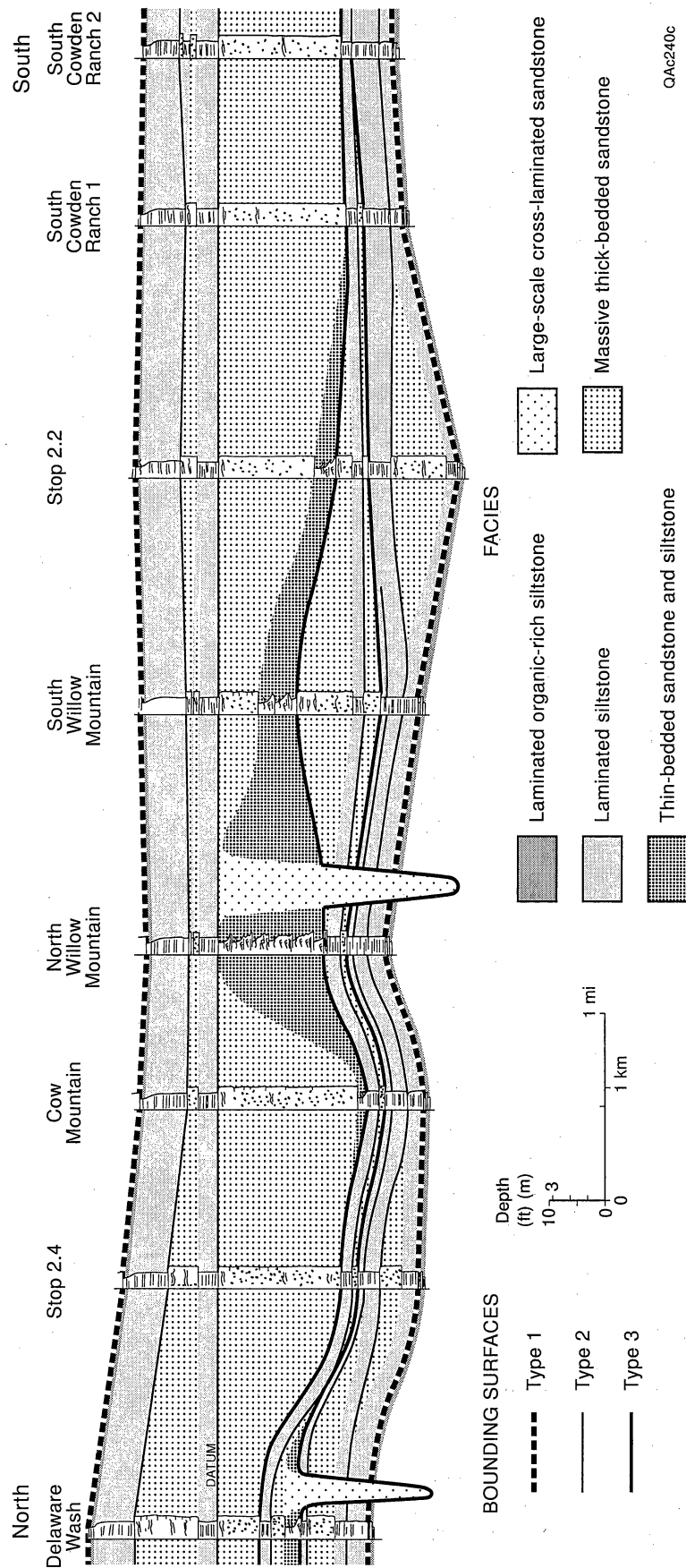
Figure 26. Cross section showing distribution of facies and traces of key surfaces within single high-order cycle. Cross section extends south from Delaware Wash for a distance of about 7 mi.

To the north (shelfward) near Delaware Wash, the high-order cycle gradually thickens to more than 23 m. At this position it appears that there are three distinct channel levees with attached lobe complexes. The first two complexes step basinward, whereas the youngest steps back toward the shelf. The basal and uppermost complexes correlate with channel-levee and lobe complexes that are older and younger, respectively, than the one exposed at Willow Mountain. The separate channel-levee and lobe complexes appear to be on the order of several tens of kilometers wide. However, the lack of outcrop exposure does not allow the limits of these elements to be defined precisely. Patterns of thickening and thinning also suggest that the complexes are stacked in a compensating, offset fashion with younger complexes avulsing into and filling topographic lows.

A final observation of importance is that the thickness of the laminated siltstones within the high-order cycle remains relatively constant from one end of the cross section to the other. Changes in thickness within the high-order cycle are largely related to increases or decreases in sandstone thickness. The constant thickness of the laminated siltstones also suggests they would be useful correlation markers at the reservoir and field scale.

SECTION 2: DATA STRUCTURE AND MAPPING METHODS

Geologic Data

A three-dimensional reservoir model of facies architecture within a high-order cycle was constructed for the Willow Mountain case study using data collected from a series of closely spaced, strike-parallel outcrop exposures.

Three types of bounding surfaces and lithosomes were recognized and mapped:

1. The Type 1 bounding surface is a relatively flat nonerosional surface. Type 1 surfaces are always marked by an abrupt change from organic-rich siltstone to laminated siltstone (Facies 2). Type 1 surfaces occurred at the base and top of the high-order cycle.

2. The Type 2 bounding surface is also a relatively flat nonerosional surface marked by an abrupt change to a laminated siltstone. These surfaces may overlie Facies 1, 3, 4, 5, or 6—any facies except Facies 2.

3. The Type 3 bounding surface is a relatively high-relief surface that varies from erosional to nonerosional.

The bounding surfaces defined three types of lithosomes:

1. The Type 1 lithosome is bounded at the base by a Type 2 bounding surface and at the top by a Type 1 bounding surface. Type 1 lithosomes consist of an upward-fining succession of laminated siltstones at the base that are gradually replaced by organic-rich siltstones at the top.

2. Type 2 lithosomes are bounded at the base by a Type 2 bounding surface and at the top by either a Type 2 or a Type 3 bounding surface. Type 2 lithosomes consist of an upward-coarsening succession that passes from laminated siltstone at the base to massive sandstone or, rarely, into large-scale cross-laminated sandstones at the top.

3. Type 3 lithosomes are bounded at the base by a Type 3 bounding surface and at the top by either a Type 2 or a Type 3 bounding surface. These lithosomes consist of an upward-fining succession of sandstones and siltstones that vary from relatively thin successions of thin-bedded sandstones and siltstones to relatively thick successions of large-scale cross-laminated sandstones or massive sandstones overlain by thin-bedded successions of sandstones and siltstone.

The Type 1 lithosome is interpreted to be distal-fan deposits overlain by a condensed section; Type 2 is interpreted to be composed of sandy lobes and distal fan deposits; and Type 3 is interpreted to be a complex of channel-levee and overbank deposits. The channel-levee complexes vary in composition, from largely amalgamated channels to widely spaced channels separated by levee and overbank deposits.

Drafting the Maps

The original set of maps was drafted by hand and was based upon measured sections and other outcrop data. These maps are attached in appendix A. The maps overlie a base map of the study area (see fig. 17) that displays the topographic elevation and locations of lithologic logs. The study area is about 2,000 m in length and 1,000 m across and is aligned in a southwest-by-northeast fashion. The average paleocurrent of the channels is to the southeast so that the long axis of the study area is a near-strike section to the channels.

On the basis of systematic changes in facies, the cycle was divided into mappable rock bodies or lithosomes. Lithosomes were correlated between adjacent cross sections (figs. 18 through 22), and topography maps were created for each bounding surface (see table 3). Proportion and isopach maps were used to define the distribution of facies within each lithosome (see table 3). A total of nine surfaces were mapped, defining eight rock bodies or lithosomes. All topography maps are relative elevations above or below the G (yellow) surface. Each lithosome is composed of two or three facies that are arranged in a regular or predictable fashion. The distribution of facies within each lithosome was defined by mapping the proportion or thickness of all but one of the facies. A total of 10 facies maps were created for the 8 lithosomes. The distribution of the unmapped facies within each lithosome was defined as either (1) the difference between the total lithosome thickness and the combined thickness of the mapped facies or (2) one minus the combined proportions of the mapped facies.

Digitizing the Maps

A total of 20 hand-contoured maps (9 bounding surfaces and 11 facies isopach or proportion maps) were scanned and digitized with NDS (Neuralog Digitizing System, Neuralog, Inc., 1997). NDS semiautomatically digitizes the maps and verifies them by overlaying the original and digitized contours on a graphics screen. This step needs to be quite precise, especially for maps with very closely spaced contours. The maps used in the Willow Mountain study had closely

49

Table 3. Structure and characteristics of bounding surfaces and lithosomes.

Lithosome (ordered from bottom to top)	Bounding surface (ordered from bottom to top)	Type	Composition (facies ordered from bottom to top)	Thickness (ft)	Depositional element
	I-Brown (9)	1			
8		1	3/2	7 – 8	Distal fan and condensed section
	H-Red (8)	2			
7		2	3/5	1 – 3	Distal fan and sandy lobe
	G-Gray (7)	2			
6		2	3/5	3 – 4.5	Distal fan and sandy lobe
	F-Yellow (6)	2			
5		3	4/6/5	12 – 50	Channel-levee and overbank
	E-Orange (5)	3			
4		3	6/5/4	0 – 40	Channel-levee and overbank
	D-Green (4)	3			
3		3	6/5/4	0 – 30	Channel-levee and overbank
	C-Blue (3)	3			
2		2	3/5	0 – 12	Distal fan and sandy lobe
	B-Purple (2)	2			
1		2	3/5	0 – 8	Distal fan and sandy lobe
	A-Black (1)	1			

spaced and complex-shaped contours to reflect channels in bounding-surface maps and channel-fill, -levee, and overbank deposits in lithofacies maps (see figs. A4, A5, A6, A11, A12, A13, A14, and A15).

A rectangular mapping domain was chosen with the origin in the northwest corner. The x-axis is nearly parallel to the depositional strike. The dimensions of the rectangle are 4,000 ft along the y-axis and 8,800 ft along the x-axis (approximately 1,200 by 2,640 m). The grid interval (50 by 50 ft; approximately 15 by 15 m) was chosen as a compromise that adequately preserved the detailed features of the maps while still keeping the model small enough that it was manageable for 3-D modeling, gridding, and simulation.

Four mapping software packages were tested for the conversion of digitized contour maps to gridded maps: CPS-3 version 4.5 (Schlumberger-GeoQuest, 1997), GES version 7.5 (Geographix, 1997; Landmark, 1997a), PCMS (PC Mapping System) version 2.0 (Zycor, 1986), and Z-map Plus 3.0 (Landmark, 1997b). Because these maps are so complex, none of the mapping programs gave satisfactory results if used without modification. One of the reasons for these poor results was the sudden change in slope across from the low-dip interchannel areas to steeply dipping channel margins (see figs. A4, A5, A6, and A14). In addition, there are large areas where the elevation or thickness was nearly constant (see figs. A2, A6, A7, A8, and A10). In such cases, small oscillations and errors can destroy the features that are trying to be captured. In the most difficult cases, the maps had channels (with rapid slope changes) adjacent to nearly flat zones (see figs. A11, A12, A13, A15, and A16).

After several iterations, a combined approach of using PCMS for primary gridding and CPS-3 for detailed editing was established. PCMS automatically creates several cross-sectional profiles across strike and dip direction of the map. The profiles help guide the gridding process, especially when sudden changes in slope and/or curvature are encountered. PCMS is a PC-DOS based program without a modern graphic user interface, so CPS-3 was chosen to work in tandem with PCMS to edit the grids.

First, extra contours were drawn in areas with high curvature to influence the gridding and to control the slope change. Second, polygons were drawn in large flat areas to blank the grid to zero for pinch-outs or to set the grid to a constant for flat zones. Third, a "cut-and-paste" approach was used to accommodate the situation of adjacent curved and flat areas (figs. A4, A5). The steeply sloped channel area of the contour map was cut out to grid separately. Then, the resulting map was clipped and pasted back into the relatively flat grid. Individual grid points along the suture between the two maps were examined and modified to ensure smoothness. These steps were repeated until satisfactory results were obtained. After all the maps were gridded, the facies isopach and proportion maps were converted to elevation maps; these maps are used to indicate the lithofacies boundary within lithosomes. The stacking order and meaning of all maps are summarized in table A1.

SECTION 3: PRODUCING THE THREE-DIMENSIONAL GRIDDED MODEL

The structure of the maps was selected to facilitate the construction of a three-dimensional model: all maps have a common origin and orientation, and the maps are designed so that they will correctly sum to the correct thicknesses or proportions between the key bounding surfaces. Still, considerable checking and editing are required to ensure that the three-dimensional model accurately captures the map-view features of each of the depositional elements, to make certain that surfaces do not cross, and to create an accurate gridded representation of the reservoir architecture. Once the model has been reconciled in this way, it is a relatively straightforward process to create a cornerpoint geometry description for use in reservoir simulation.

Geocellular Model Construction

The 3-D geocellular modeling program Stratamodel (Landmark, 1997b) was chosen to build this 3-D outcrop geological model. In the construction the following procedures were used:

1. All the maps were verified in 3-D display to make certain that surfaces did not cross and pinch-outs occured at the correct location.

2. The bounding surfaces and facies maps were stacked using "Framework Modeling." This produced reasonable and accurate depositional orders and patterns. Many iterations of checking, editing, regridding, and rebuilding are required to ensure that the framework of the geocellular model accurately represents the outcrop-based reservoir model.

3. The internal facies composition was introduced using the "Model Operation" for individual facies units.

4. After the model was completed, displays of cross sections, isosurfaces (using the "Geobody" function), and modeled surfaces were built for visualization and analysis.

5. Finally, the finished model was converted to a cornerpoint grid for a commercial reservoir simulator.

Strike cross sections verified that the geometry of the lithosomes was correctly represented in the geocellular model (see fig. 27). The complex stacking of the various channel sandstones is very clear in this cross section. The reservoir model can be further dissected by looking at individual facies: such a view separates channel, levee, and distal facies (see fig. 28). Several of the lithosome bounding surfaces are shown in fig. 29; the branching channel is immediately apparent. Figures 30 and 31 show how the facies distribution is related to key surfaces in the reservoir model. In the construction of the reservoir model, many surfaces truncated lower surfaces. In figure 32, the green surface is shown crossing the orange and blue surfaces (the mesh pattern is used for transparency). More views are included in appendix B and on the accompanying CD-ROM (vol. 2).

Cornerpoint Grid Construction

With the model reconciled by viewing and editing the geocellular model, the gridded arrays of elevation for each of the surfaces can be converted into a cornerpoint geometry description that can be imported into reservoir visualization and simulation software.
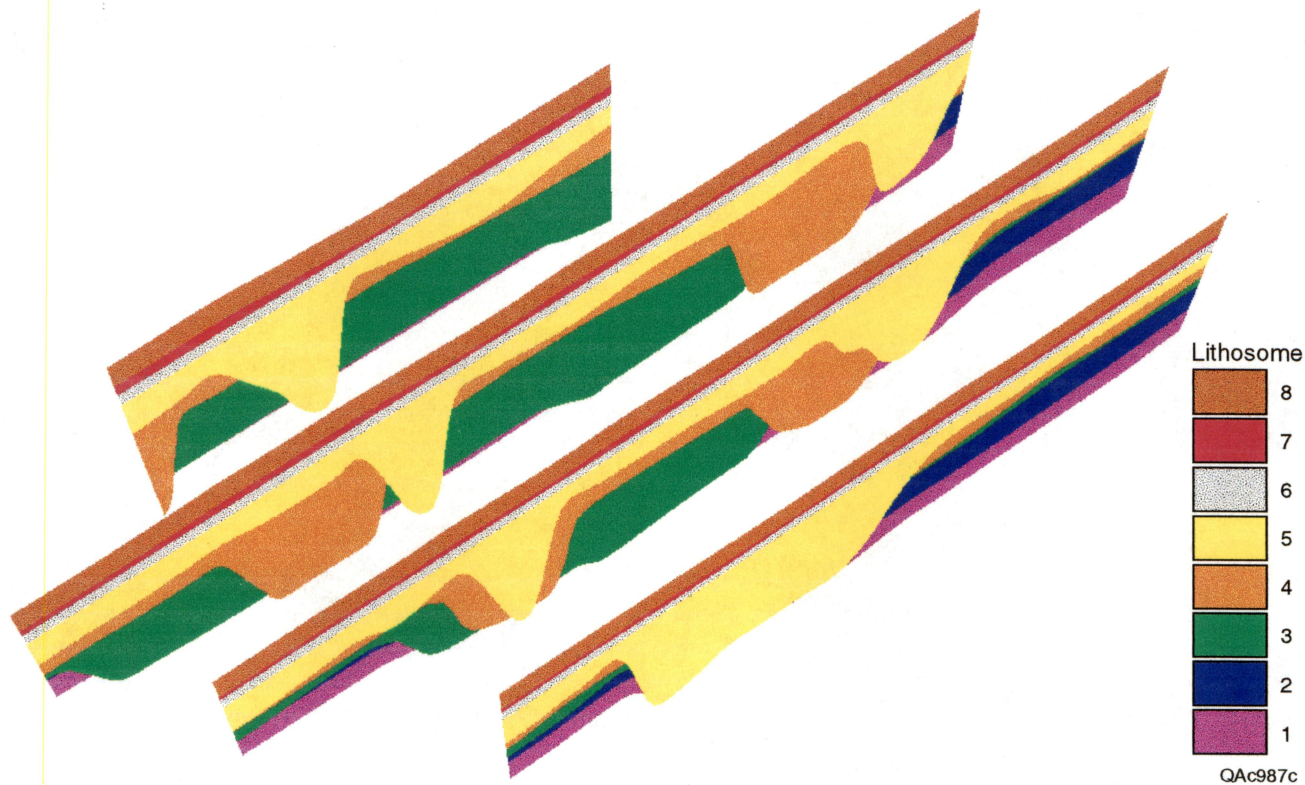
Figure 27. Lithosome stacking and truncation displayed along the near-strike section from geocellular model (along the x direction).
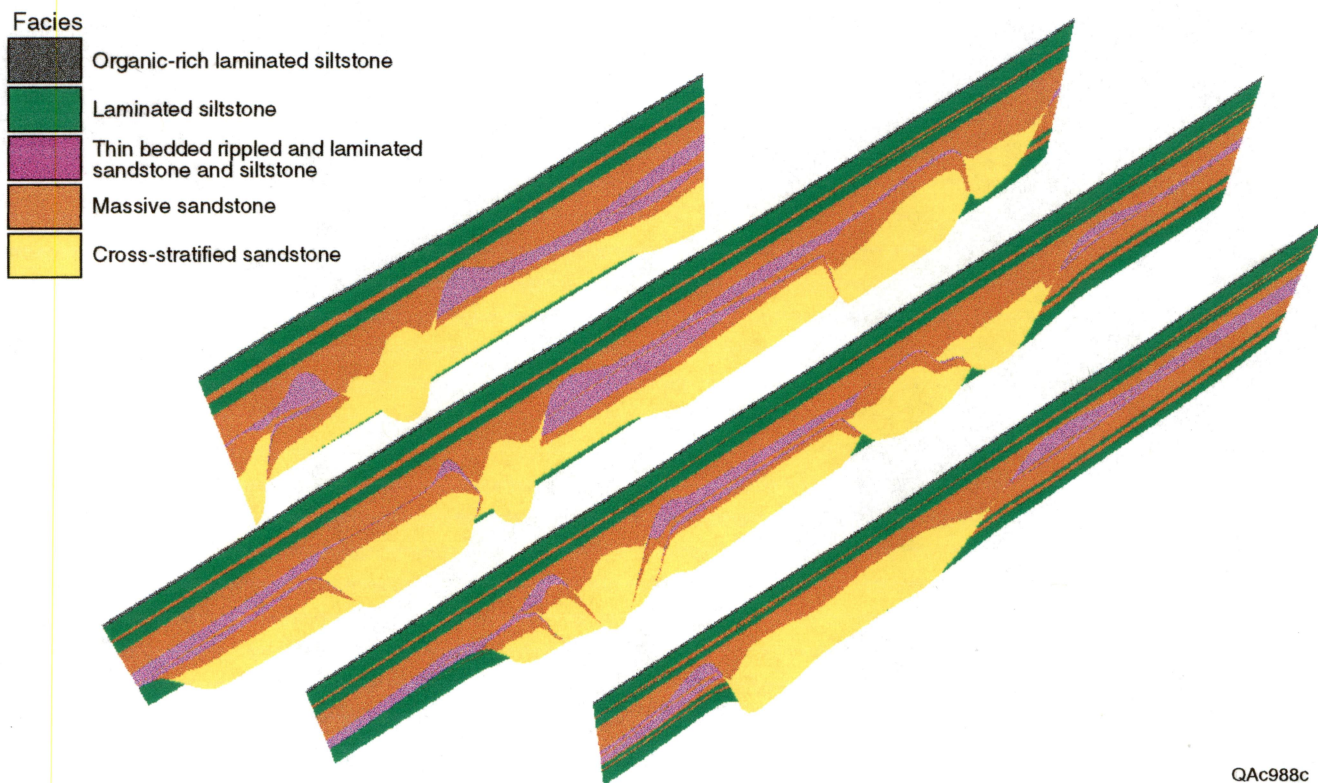
Figure 28. Facies distribution on near-strike section from geocellular model (along the x direction).

Bounding
surface

▨	5
▨	4
▨	3
▨	2
▨	1

QAc989c

Figure 29. Bounding surfaces stacked to form the model. This view shows the purple, blue, green, orange, and yellow surfaces.

Facies

▨	Organic-rich laminated siltstone
▨	Laminated siltstone
▨	Thin bedded rippled and laminated sandstone and siltstone
▨	Massive sandstone
▨	Cross-stratified sandstone

QAc990c
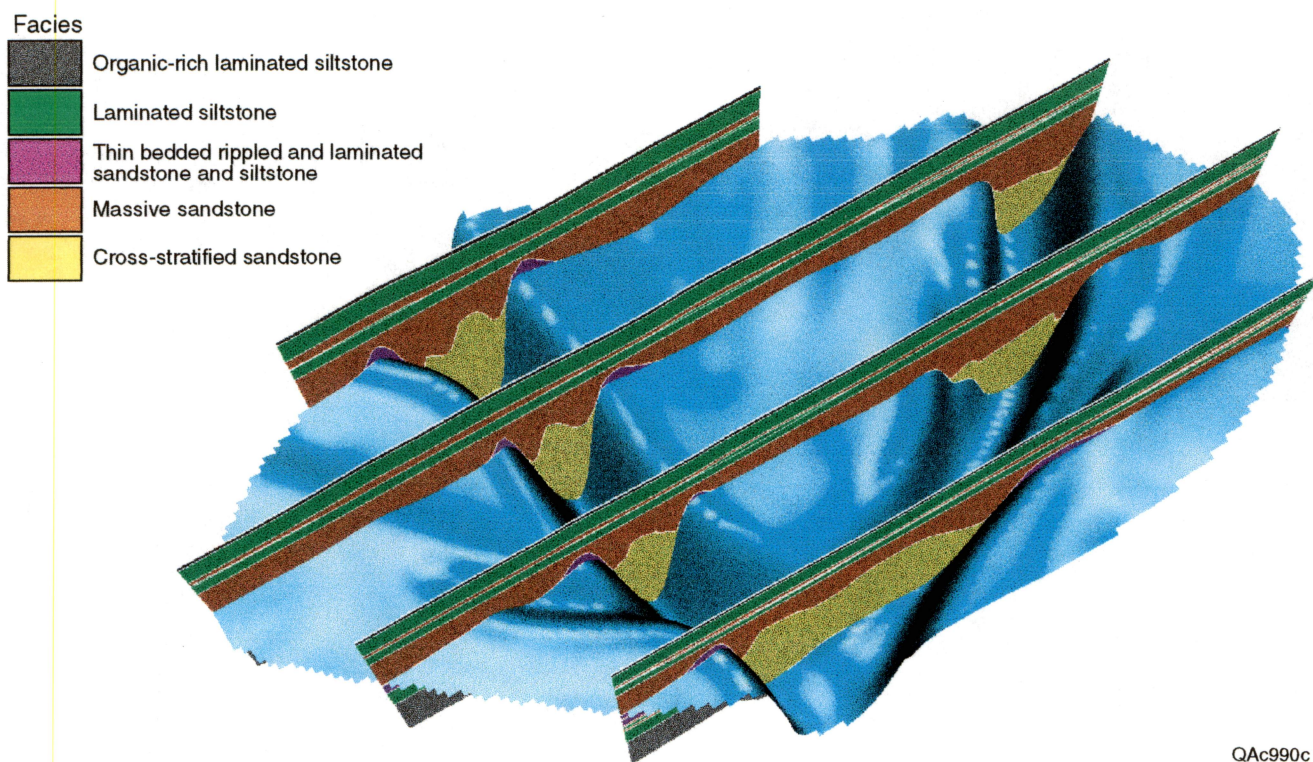
Figure 30. Facies distribution on strike section related to the blue surface 2.

Facies

- Thin bedded rippled and laminated sandstone and siltstone
- Massive sandstone
- Cross-stratified sandstone
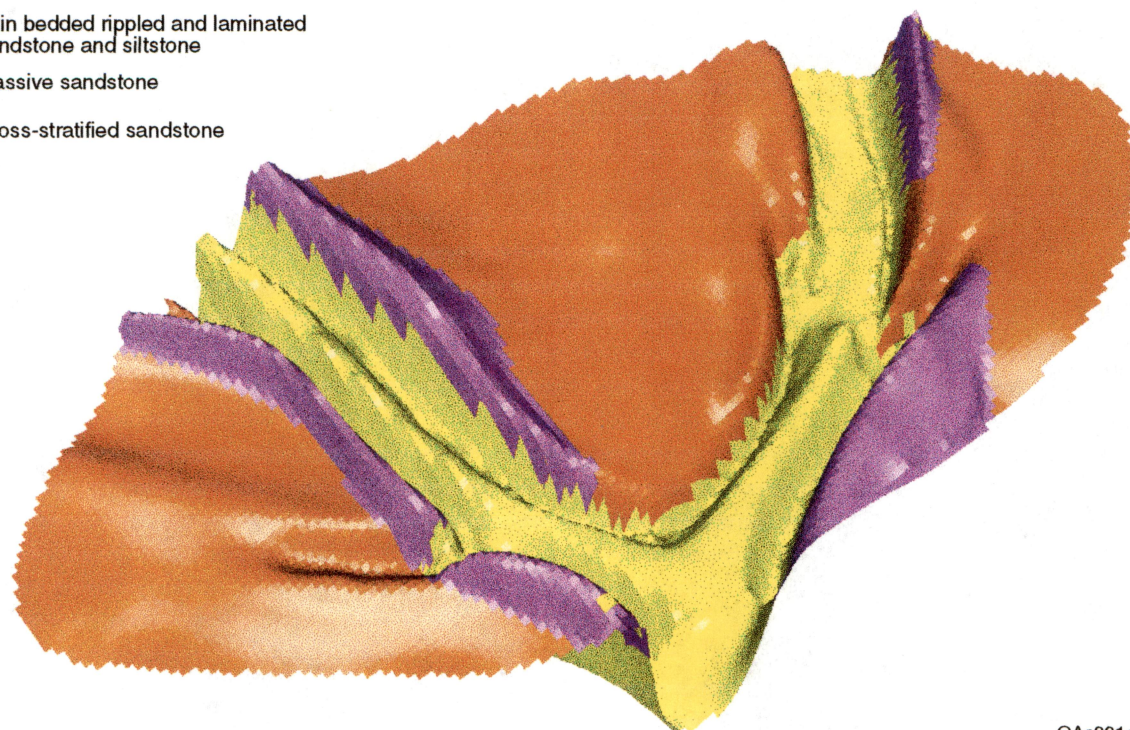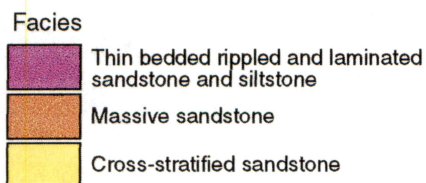
QAc991c

Figure 31. Channel facies (Facies 6, shown in yellow) and levee facies (Facies 4, shown in purple) layered on the orange bounding surface. This shows how lithosome composition was controlled within the model.

Bounding surface

- 4
- 3
- 2
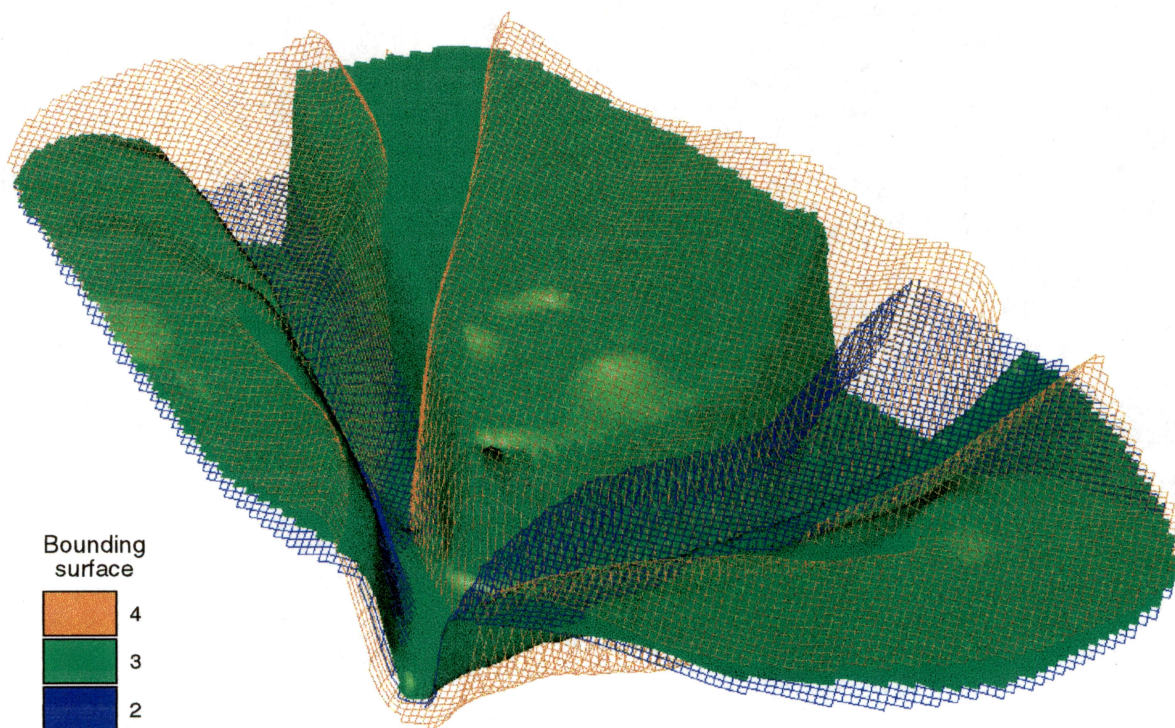
QAc992c

Figure 32. Truncating relationships between the blue, green, and orange bounding surfaces. In the area of the channels, the surfaces can be seen to cross. The compound surfaces, defined by this crossing or truncation, will form the boundaries of the lithosomes in the gridded model.

Editing the Grid

The maps form the basis for the cornerpoint model. The surface elevation maps are stacked in the order specified by the geologist. The 9 lithosome-bounding surfaces and 11 facies maps combine to give 8 lithosomes and a total of 19 simulation model layers. The stacking order, lithosome number, map name, and a brief description of each map are given in table A1. The properties of the facies are given in table C1. Stacking order, lithosome number, facies, fraction of areal coverage, and average thickness for each simulation layer are given in table C2.

Several data verification steps must be applied during grid construction. First, all maps must be checked to ensure that their origins, units, orientations, and dimensions are consistent. Second, each pair of maps must be examined, to ensure that there are no points where they cross. If the crossing is small (in this study, 0.10 ft or approximately 5 cm), then the value is simply reset. If the crossing is larger, the error is flagged and the maps must be corrected before gridding can proceed. Third, void blocks must be detected and set so that the gridded model contains no blocks that extend beyond the intended study area. The process of flagging the void blocks is particularly important right along the edge of the intended study area. Along this edge, each grid cell contains some cornerpoints that are defined and other cornerpoints that are "missing." Reservoir simulation software can detect most void blocks automatically, but gridding software must flag the edge blocks as voids before the geometry is imported into the simulator. Otherwise, odd-shaped blocks around the model periphery will make visualization difficult and simulation all but impossible.

A set of C-language routines (named "Stackmaps") was written to perform the grid verification and editing. The Stackmaps program reads a control file that specifies the names of the maps, the stacking order, names of output files, gridding tolerances, and so on. The gridding control file used to construct the Willow Mountain model is included on CD-ROM Vol. 2. After performing the verification and editing, Stackmaps writes a set of summary and geometry files.

The geometry is specified by the trajectory of the cornerpoints ("COORD" record; Intera, 1994), the cornerpoint elevations ("ZCORNER" record), and a list of active block flags ("ACTNUM" record). All geometry files have header sections giving relevant grid data. Relatively minor modifications are needed to make the geometry files compatible with other simulators (Computer Modeling Group, 1997). The geometry files are included on volume 2 of the CD-ROM set transmitted with this report. The source code, header files, a make file, and an IRIX 6.2 executable for Stackmaps are also included on volume 2, as are example input and output files. The gridded model has 267,520 cells; only 102,482 cells are active.

Viewing the Cornerpoint Grid

The reservoir model was loaded into simulation software (Intera, 1994). The simulator completed the geometry calculations and initialized the model using ideal gas properties and an assumed set of saturation functions. Flow was not simulated; only the static model was analyzed. The simulator input files are included in volume 2 of the CD-ROM set.

The rock properties were set using core data from the Ford Geraldine Unit (Dutton and others, 1997a and b). The geometric mean permeability (see table C1) was loaded into the x-direction permeability, and the arithmetic mean porosity (see table 1) was loaded into the porosity array. To increase the usefulness of the 3-D visualization, facies were loaded into the simulator as the y-direction permeability and lithosome numbers were loaded as the z-direction permeability. The y-direction and z-direction permeability arrays would have to be reset before this reservoir model could be used in flow simulation.

The reservoir simulator output files were reformatted for input to a 3-D visualization program (Intera, 1994). The entire model is shown in figure 33; note the axes to indicate the orientation of the view. The channelized bodies are especially complex in shape, as shown in figure 34. A 3-D visualization program can spin the model and take it apart. Views of all eight lithosomes are shown in figures C1-C8. Several sequences of views were animated and recorded
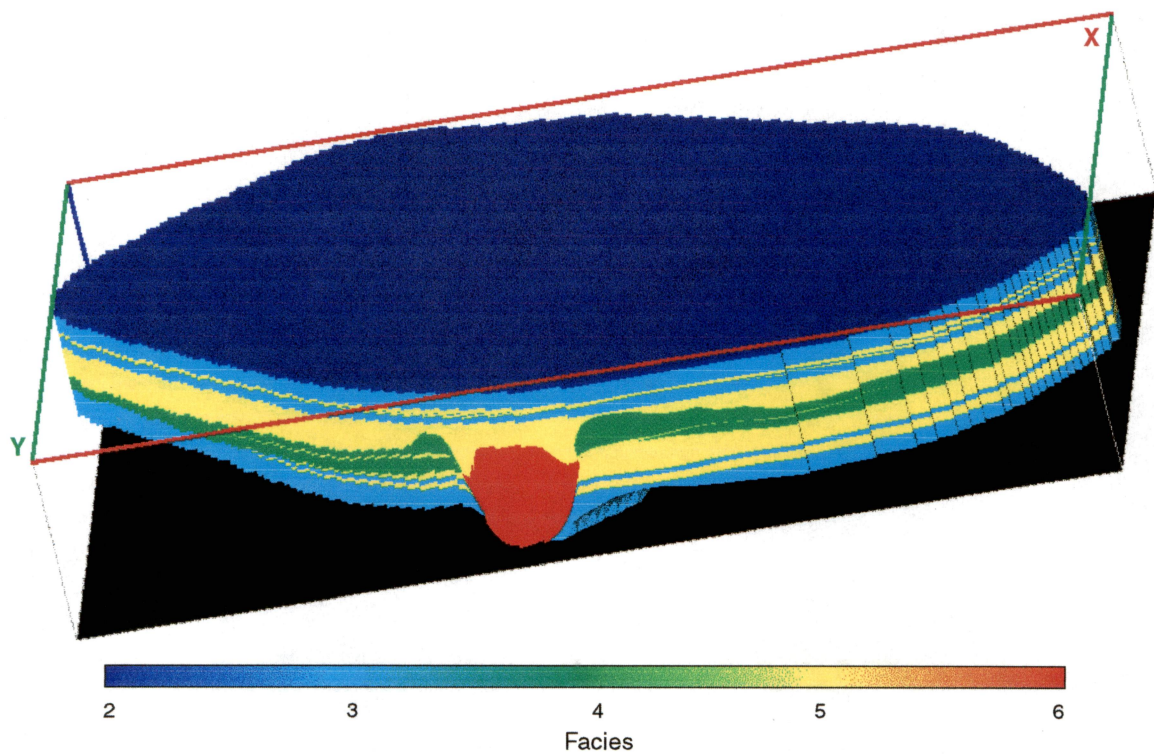
58

Figure 33. Perspective view of the complete three-dimensional reservoir model, with color indicating facies. The vertical scale has been exaggerated by a factor of 20.
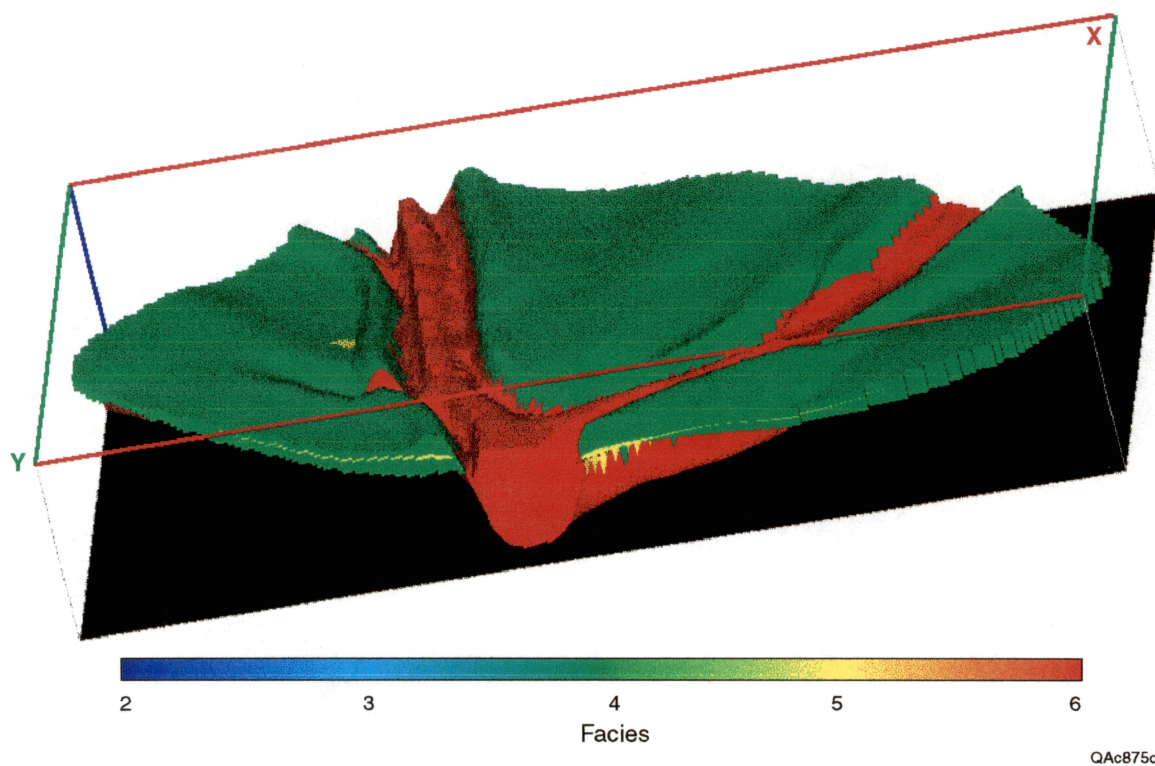

Figure 34. Perspective view of the channel and levee facies within Lithosome 4. Color indicates facies. The vertical scale has been exaggerated by a factor of 20.

in QuickTime format. In the four animations, the layering of the model is dissected, the channel-body geometry is highlighted, the grid is shown, and views from many perspectives are compiled. Because the animations are composed of a small number of frames, they are best viewed by stepping through the animations frame-by-frame. The animations can be viewed without special software; only a QuickTime player or plug-in is needed. The images and animations are included on volume 2 of the CD-ROM set.

CONCLUSIONS AND RECOMMENDATIONS

1. High-frequency cycles within the Bell Canyon Formation of the Delaware Mountain Group in the Permian-age Delaware Basin have been studied in outcrop, deterministically mapped in three dimensions, and represented using contour maps, a geocellular model, and a cornerpoint geometry description.

2. The deep-water clastic systems contain facies and depositional elements that reflect slow settling into a distal basin setting, overbank deposition of low-density turbidity currents, unconfined flow of turbidity currents, and channelized flow of higher-density turbidity currents.

3. The facies associations and bedding geometries indicate that the depositional elements include highly continuous distal siltstone layers, lobe and interchannel lobe deposits, channels, and channels with attached levee deposits.

4. The stacking pattern of these elements reflects progradation, aggradation, and retrogradation within the high-frequency cycles at Willow Mountain and Wild Horse Draw.

5. The exposures at Willow Mountain are continuous and extensive, and allow construction of deterministic maps of key surfaces and lithosome composition.

6. The maps prepared for the Willow Mountain outcrop data set were stacked and a three-dimensional reservoir model was created. The three-dimensional geocellular and cornerpoint models are consistent with the field observations.

7. The three-dimensional models can be further manipulated using geocellular modeling software, or imported to reservoir simulation or seismic modeling software.

8. The key data sets, selected images, and other items of interest are included on CD-ROM's transmitted with this report. The contents of the CD's are summarized in appendix D.

ACKNOWLEDGMENTS

REFERENCES

Allen, J. R. L., 1982, Studies in fluviatile sedimentation: bars, bar-complexes, and sandstone sheets (low-sinuosity braided streams) in the Brownstones (L. Devonian), Welsh Borders: Sedimentary Geology, v. 33, 237–293.

Berg, R. R., 1979, Reservoir sandstones of the Delaware Mountain Group, southeast New Mexico, *in* Sullivan, N. M., ed., Guadalupian Delaware Mountain Group of West Texas and southeast New Mexico, Symposium and Field Trip Conference Guidebook: Society of Economic Paleontologists and Mineralogists (Permian Basin Section) Publication 79-18, p. 75–95.

Bouma, A. H., 1962, Sedimentology of some flysch deposits: a graphic approach to facies interpretation: Amsterdam, Elsevier, 168 p.

Bouma, A. H., 1996, Initial comparison between fine- and coarse-grained submarine fans and the Brushy Canyon Formation sandstones: the Brushy Canyon play in outcrop and subsurface: concepts and examples: Guidebook, Permian Basin Section, SEPM, Publication No. 96-38, p. 41–59.

Bozanich, R. G., 1979, The Bell and Cherry Canyon Formations, Eastern Delaware Basin, Texas: lithology, environments, and mechanisms of deposition: *in* Sullivan, N. M., ed., Guadalupian Delaware Mountain Group of West Texas and southeast New Mexico, Symposium and Field Trip Conference Guidebook: Society of Economic Paleontologists and Mineralogists (Permian Basin Section) Publication 79-18, p. 121–141.

Computer Modeling Group, 1997, IMEX (version 97) Advanced oil/gas reservoir simulator: Calgary, Alberta, Canada.

Dutton, S. P., Asquith, G. B., Barton, M. D., Cole, A. G., Gogas, J., Malik, M. A., Clift, S. J., and Guzman, J. I., 1997a, Application of advanced reservoir characterization, simulation, and production optimization strategies to maximize recovery in slope and basin clastic reservoirs, West Texas (Delaware Basin): The University of Texas at Austin, Bureau of Economic Geology, draft annual report prepared for the U.S. Department of Energy, 187 p.

Dutton, S. P., Malik, M. A., Clift, S. J., Asquith, G. B., Barton, M. D., Cole, A. G., Gogas, J., and Guzman, J. I., 1997b, Geologic and engineering characterization of Geraldine Ford field, Reeves and Culberson Counties, Texas: The University of Texas at Austin, Bureau of Economic Geology, Topical Report No. 2, work performed under Contract No. DE-FC22-95BC14936 for the U.S. Department of Energy, 138 p.

Fischer, A. G., and Sarnthein, M., 1988, Airborne silts and dune-derived sands in the Permian of the Delaware Basin: Journal of Sedimentary Petrology, v. 58, p. 637–643.

Folk, R. L., 1974, Petrology of sedimentary rocks: Austin, Hemphill Publishing Company, 182 p.

Friend, P. F., 1983, Towards the field classification of alluvial architecture or sequences: *in* Collinson, J. D. and Lewin, J., eds., Modern and ancient fluvial systems: International Association of Sedimentologists Special Publication No. 6, p. 345–354.

Gardner, M. H., 1992, Sequence stratigraphy of eolian-derived turbidites: patterns of deep water sedimentation along an arid carbonate platform, Permian (Guadalupian) Delaware Mountain Group, West Texas, *in* Mruk, D. H., and Curran, B. C., eds., Permian Basin exploration and production strategies: applications of sequence stratigraphic and reservoir characterization concepts: West Texas Geological Society Publication 92-91, p. 7–12.

GeoGraphix, Inc., 1997, GeoGraphix Exploration System (GES) version 7.5 Reference guide: Denver, Colorado.

Harms, J. C., 1974, Brushy Canyon Formation, Texas: a deep-water density current deposit: Geological Society of America Bulletin, v. 85, p. 1763–1784.

Harms, J. C., and Williamson, C. R., 1988, Deep-water density current deposits of Delaware Mountain Group (Permian), Delaware Basin, Texas and New Mexico: American Association of Petroleum Geologists Bulletin, v. 72, p. 299–317.

Intera Information Technologies, Ltd., 1994, 95A Eclipse 100 Reference manual: Henley-on-Thames, Oxfordshire, England.

Jacka, A. D., Thomas, C. M., Beck, R. H., Williams, K. W., and Harrison, S. C., 1969, Guadalupian depositional cycles of the Delaware Basin and Northwest Shelf, *in* Cyclic sedimentation in the Permian Basin: West Texas Geological Society Symposium, p. 152–196.

Jacka, A. D., 1979, Deposition and entrapment of hydrocarbons in Bell Canyon and Cherry Canyon deep-sea fans of the Delaware Basin, *in* Sullivan, N. M., ed., Guadalupian Delaware Mountain Group of West Texas and southeast New Mexico, Symposium and Field Trip Conference Guidebook: Society of Economic Paleontologists and Mineralogists (Permian Basin Section) Publication 79-18, p. 104–120.

Kerans, C., Fitchen, W. M., Gardner, M. H., Sonnenfeld, M. D., Tinker, S. W., and Wardlaw, B. R., 1992, Styles of sequence development within uppermost Leonardian through Guadalupian strata of the Guadalupe Mountains, Texas and New Mexico, *in* Mruk, D. H., and Curran, B. C., eds., Permian Basin exploration and production strategies: applications of sequence stratigraphic and reservoir characterization concepts: West Texas Geological Society Publication 92-91, p. 1–6.

Kerans, C. and Fitchen, W. M., 1995, Sequence hierarchy and facies architecture of a carbonate-ramp system: San Andres Formation of the Algerita Escarpment and Western Guadalupe Mountains, West Texas and New Mexico: The University of Texas at Austin, Bureau of Economic Geology, Report of Investigations No. 235, 86 p.

Kneller, B., 1996, When is a turbidity current not a turbidity current? A question of mobility? (abs.): American Association of Petroleum Geologists Annual Convention, Official Program, v. 5, p. A76.

Landmark Graphics Corporation, 1997a, Z-Map Plus version 3.0 Reference manual: Houston, Texas.

Landmark Graphics Corporation, 1997b, Stratamodel (Stratigraphic Geocellular Modeling) version 4.1 reference manual: Houston, Texas.

Lowe, D. R., 1982, Sediment gravity flows: II. Depositional models with special reference to the deposits of high-density turbidity currents: Journal of Sedimentary Research, v. 52, p. 279–297.

Meissner, F. F., 1972, Cyclic sedimentation in Middle Permian strata of the Permian Basin, West Texas and New Mexico, *in* Cyclic sedimentation in the Permian Basin (2d ed.): West Texas Geological Society, p. 203–232.

Miall, A. D., 1985, Architectural-element analysis: a new method of facies analysis applied to fluvial deposits: Earth Science Reviews, v. 22, p. 261–308.

Mutti, E., and Normark, W. R., 1987, Comparing examples of modern and ancient turbidite systems: problems and concepts, *in* Leggett, J. K., and Zuffa, G. G., eds., Marine clastic sedimentology: concepts and case studies: London, Graham and Trotman, p. 1–38.

Neuralog, Inc., 1997, Neuralog Digitizing System (NDS) version 2.0 User's guide: Houston, Texas.

Payne, M. W., 1976, Basinal sandstone facies, Delaware Basin, West Texas and southeast New Mexico: American Association of Petroleum Geologists Bulletin, v. 60, p. 517–527.

Schlumberger-GeoQuest, 1997, CPS-3 version 4.5 User's manual: Houston, Texas.

Sonnenfeld, M. D., 1991, High-frequency cyclicity within shelf-margin and slope strata of the upper San Andres sequence, Last Chance Canyon, *in* Meader-Roberts, Sally, Candelaria, M. P., and Moore, G. E., eds., Sequence stratigraphy, facies and reservoir geometries of the

San Andres, Grayburg, and Queens Formations, Guadalupe Mountains, New Mexico and Texas: Permian Basin Section, Society of Economic Paleontologists and Mineralogist Publication 91-32, p. 11–51.

Williamson, C. R., 1978, Depositional processes, diagenesis and reservoir properties of Permian deep-sea sandstones, Bell Canyon Formation, Texas-New Mexico: The University of Texas at Austin, Ph.D. dissertation, 262 p.

_____ 1979, Deep sea sedimentation and stratigraphic traps, Bell Canyon Formation (Permian), Delaware basin, *in* Sullivan, N. M., ed., Guadalupian Delaware Mountain Group of West Texas and southeast New Mexico, Symposium and Field Trip Conference Guidebook: Society of Economic Paleontologists and Mineralogists (Permian Basin Section) Publication 79-18, p. 39–74.

Zelt, F. B., and Rossen, C., 1995, Geometry and continuity of deep-water sandstones and siltstones, Brushy Canyon Formation (Permian) Delaware Mountains, Texas, *in* Pickering, K. T., Hiscott, R. N., Kenyon, N. H., Ricci Lucchi, F., and Smith, R. D. A., eds., Atlas of deep water environments, architectural style in turbidite systems: London, Chapman & Hall, p. 167–183.

Zycor, Inc., 1986, Personal Computer Mapping System (PCMS) version 2.0 User's manual: Austin, Texas.

Appendix A. Contour Maps.

Table A1. Maps stacking order for geocellular and cornerpoint models.

Stacking order (bottom to top)	Map name	File name	Description
1	A-Black	8.grd	Provides base elevation for entire model; base surface for Lithosome 1.
2	1-3/5	7a.grd	Separates Facies 3 (below) from Facies 5 within Lithosome 1.
3	B-Purple	7.grd	Top of Lithosome 1 and base of Lithosome 2.
4	2-3/5	6a.grd	Separates Facies 3 (below) from Facies 5 within Lithosome 2.
5	C-Blue	6.grd	Top of Lithosome 2 and base of Lithosome 3.
6	3-6/5	5b.grd	Separates Facies 6 (below) from Facies 5 within Lithosome 3.
7	3-5/4	5a.grd	Separates Facies 5 (below) from Facies 4 within Lithosome 3.
8	D-Green	5.grd	Top of Lithosome 3 and base of Lithosome 4.
9	4-6/5	4b.grd	Separates Facies 6 (below) from Facies 5 within Lithosome 4.
10	4-5/4	4a.grd	Separates Facies 5 (below) from Facies 4 within Lithosome 4.
11	E-Orange	4.grd	Top of Lithosome 4 and base of Lithosome 5.
12	5-6/4	3b.grd	Separates Facies 6 (below) from Facies 4 within Lithosome 5.
13	5-4/5	3a.grd	Separates Facies 4 (below) from Facies 5 within Lithosome 5.
14	F-Yellow	3.grd	Top of Lithosome 5 and base of Lithosome 6.
15	6-3/5	2a.grd	Separates Facies 3 (below) from Facies 5 within Lithosome 6.
16	G-Gray	2.grd	Top of Lithosome 6 and base of Lithosome 7.
17	7-3/5	1a.grd	Separates Facies 3 (below) from Facies 5 within Lithosome 7.
18	H-Red	1.grd	Top of Lithosome 7 and base of Lithosome 8.
19	8-3/2	n1a.grd	Separates Facies 3 (below) from Facies 2 within Lithosome 8.
20	I-Brown	n1.grd	Top of Lithosome 8; top of entire system.

Notes:
1. The names for the bounding surfaces of the lithosome are consistent with the stratigraphic description.
2. The convention for the surfaces within facies is : (lithosome number)-(facies below)/(facies above).
3. The file names are the names used within the cornerpoint grid construction.
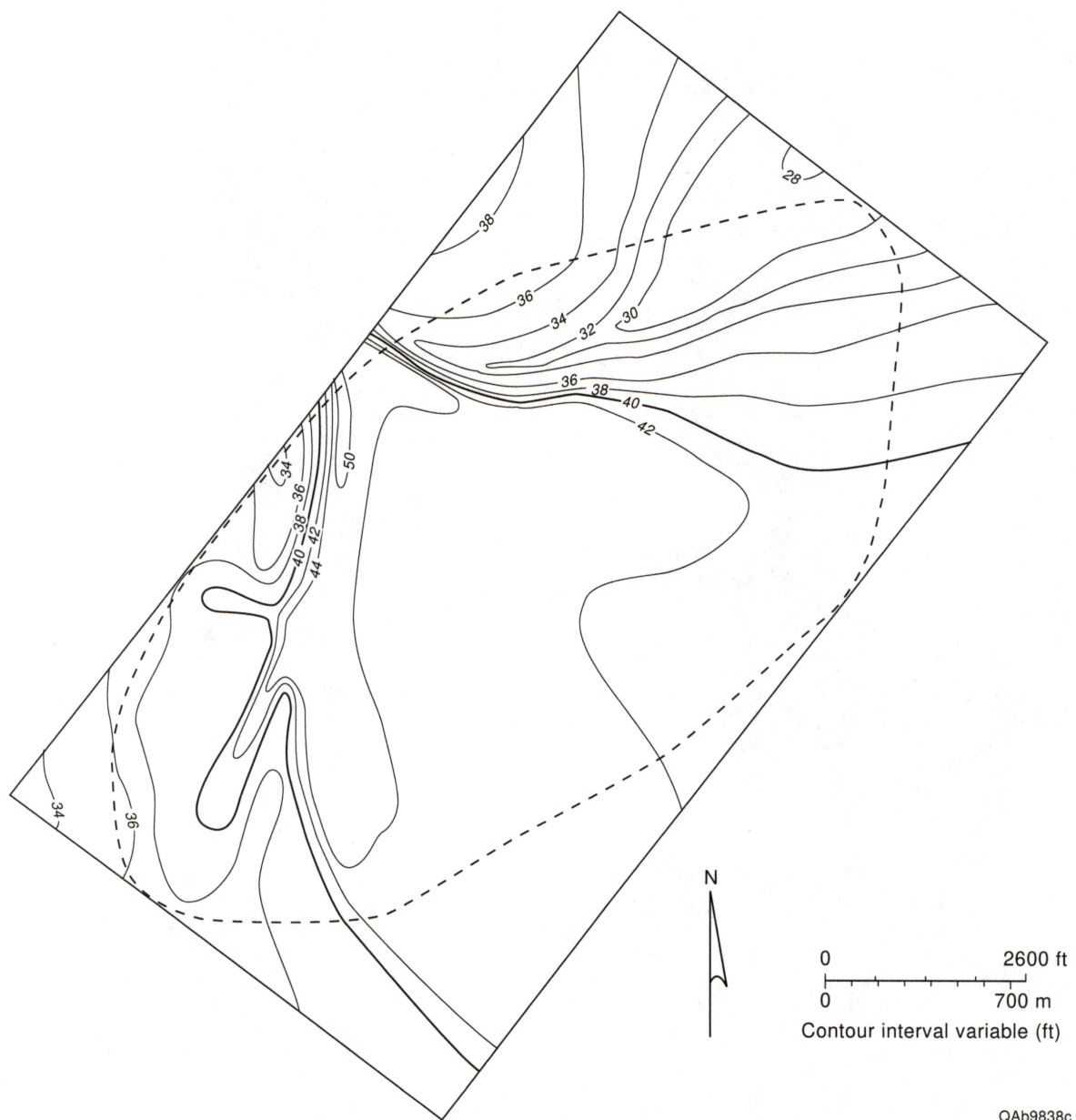
Figure A1. Topographic map on black marker A (feet below datum).
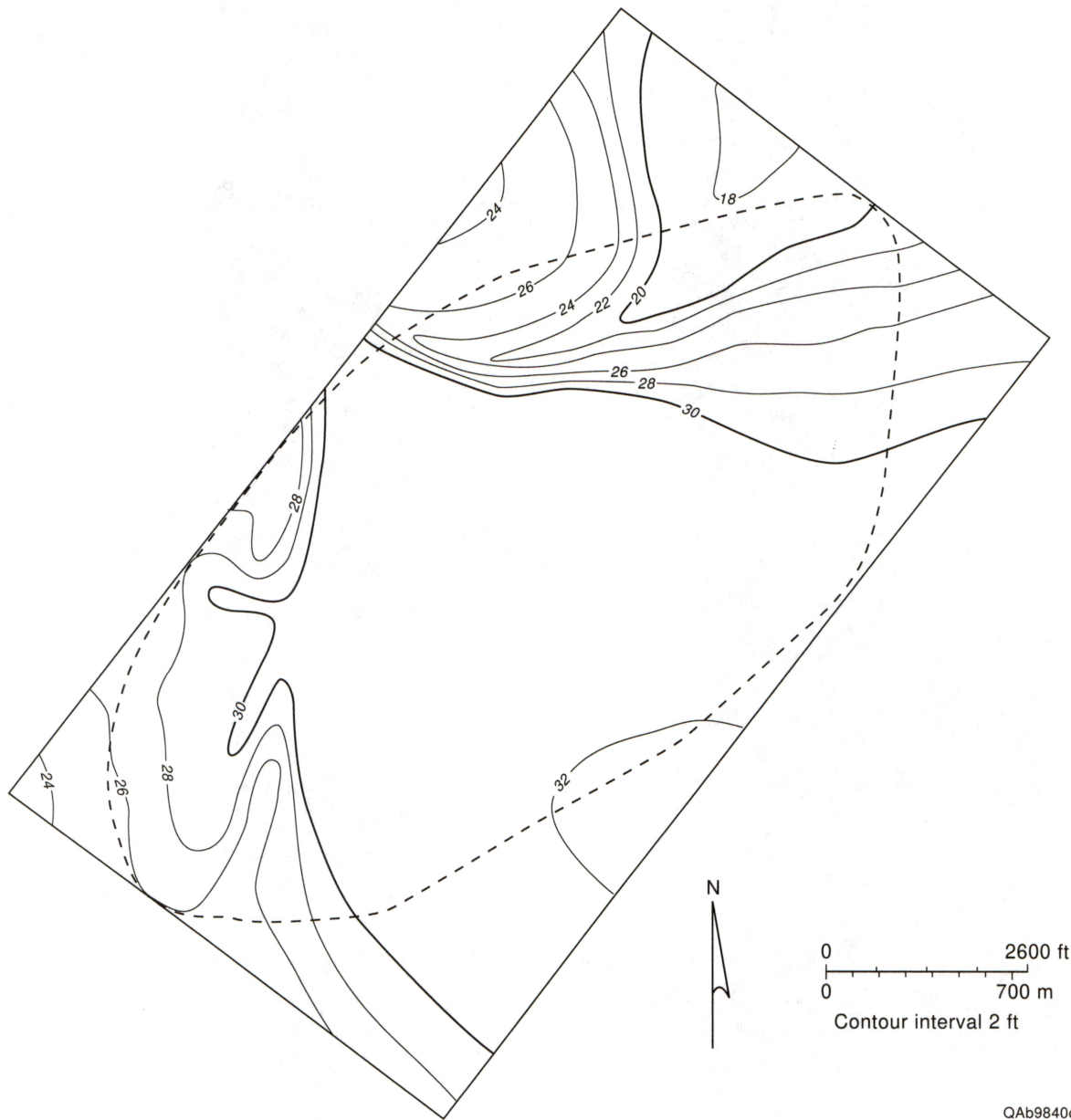
Figure A2. Topographic map on purple marker B (feet below datum).

Figure A3. Topographic map on blue marker C (feet below datum).
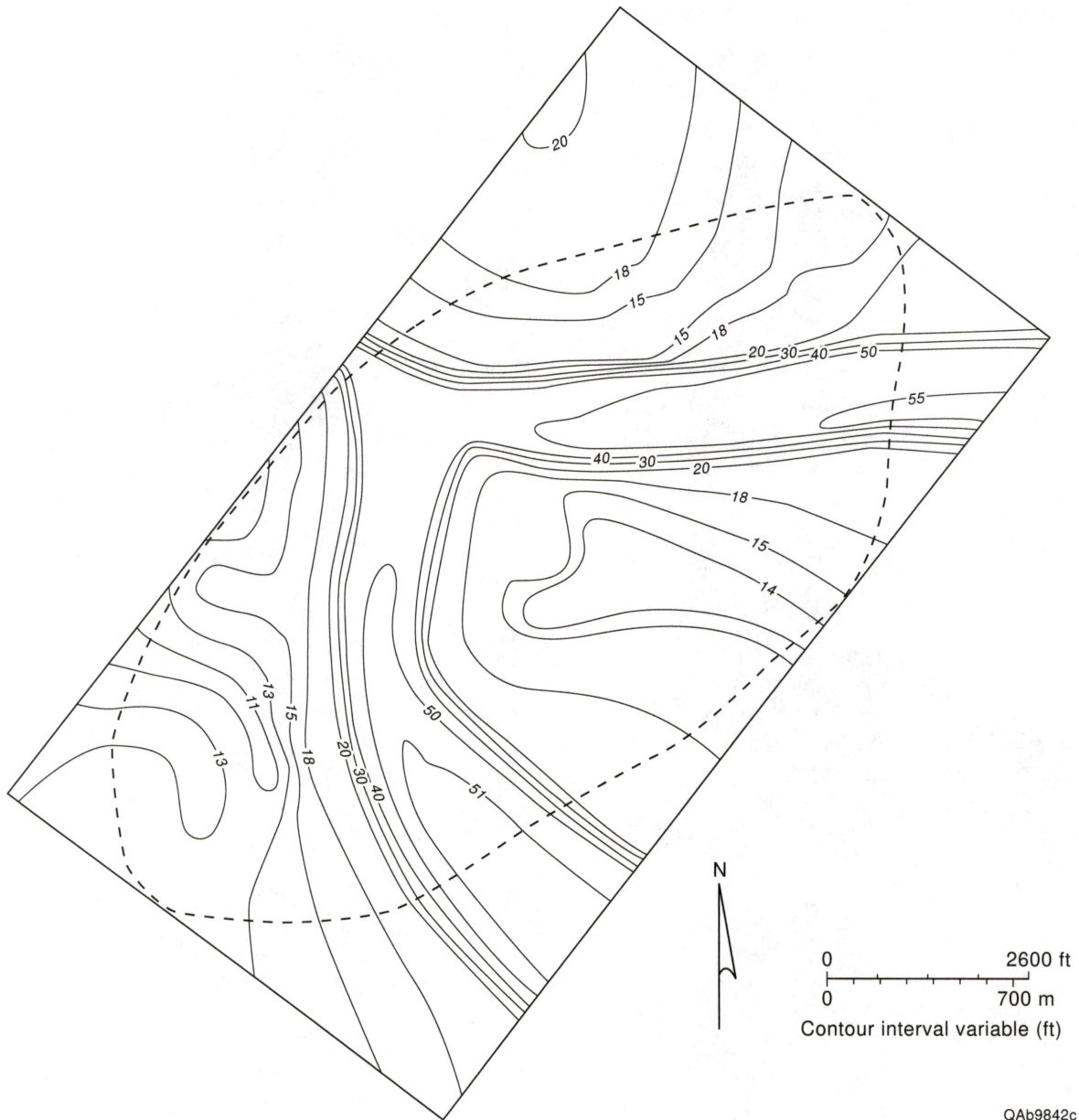
Figure A4. Topographic map on green marker D (feet below datum).
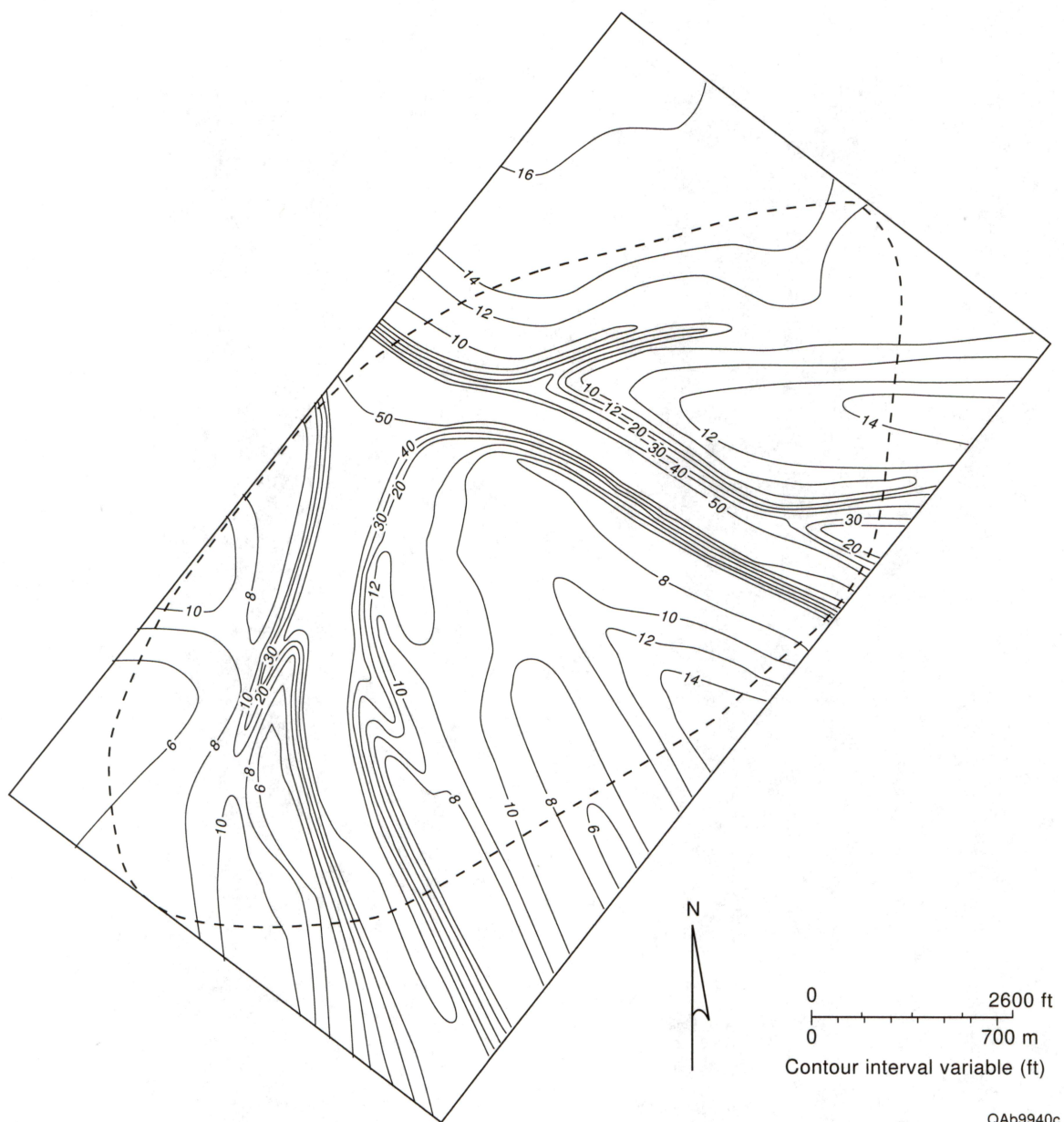
Figure A5. Topographic map on orange marker E (feet below datum).
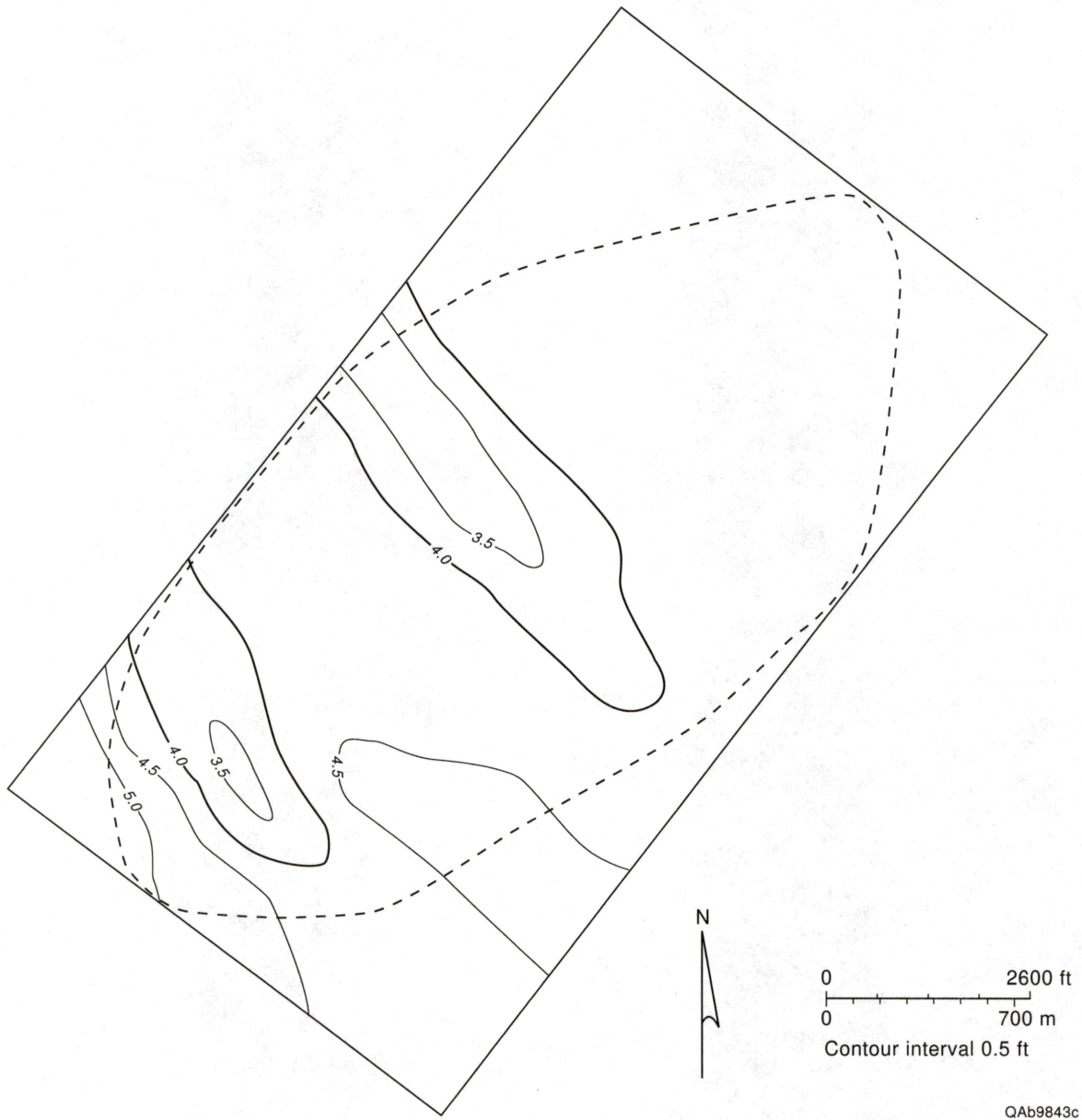
Figure A6. Topographic map on gray marker G (feet above datum).
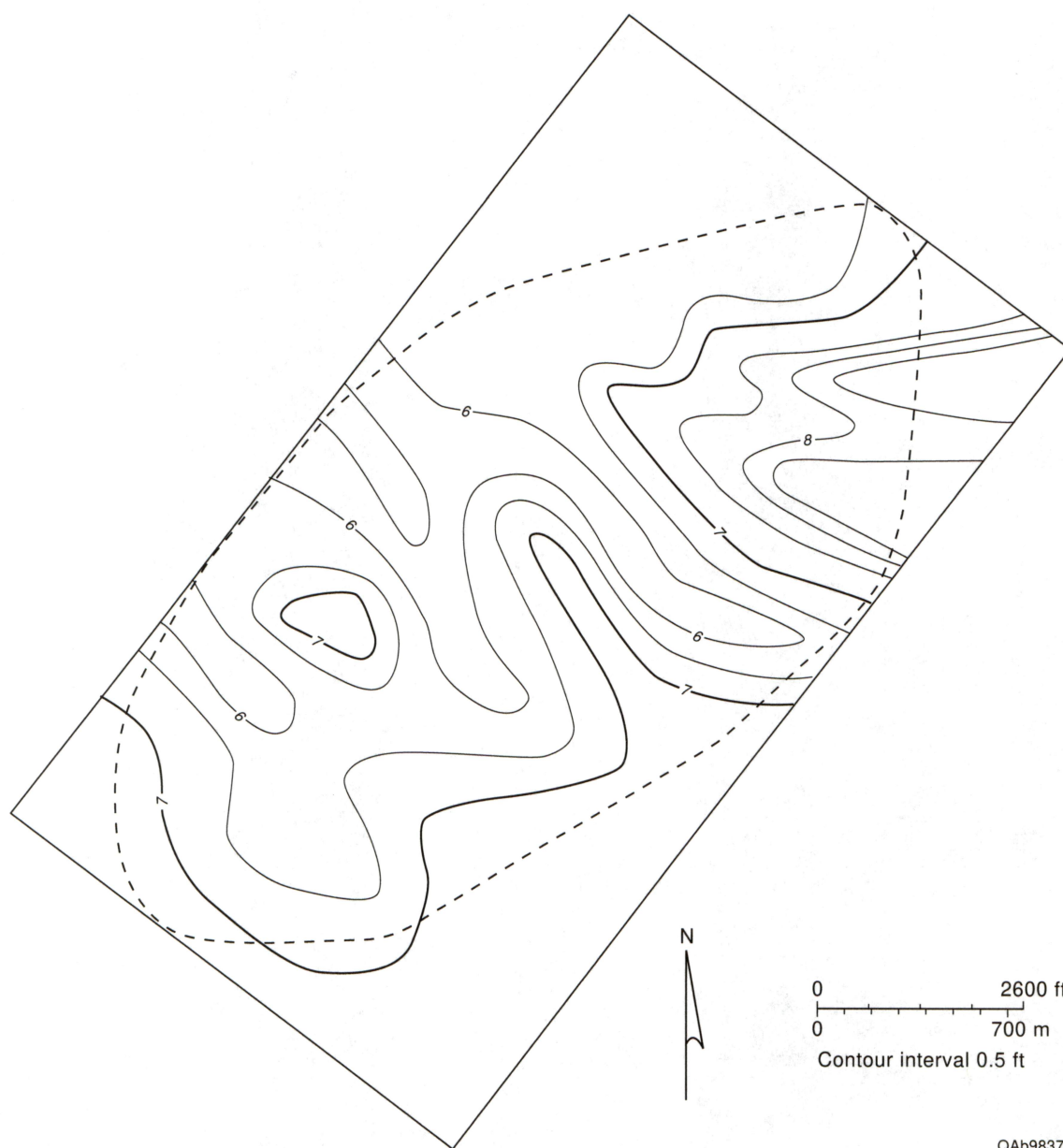
Figure A7. Topographic map on red marker H (feet above datum).
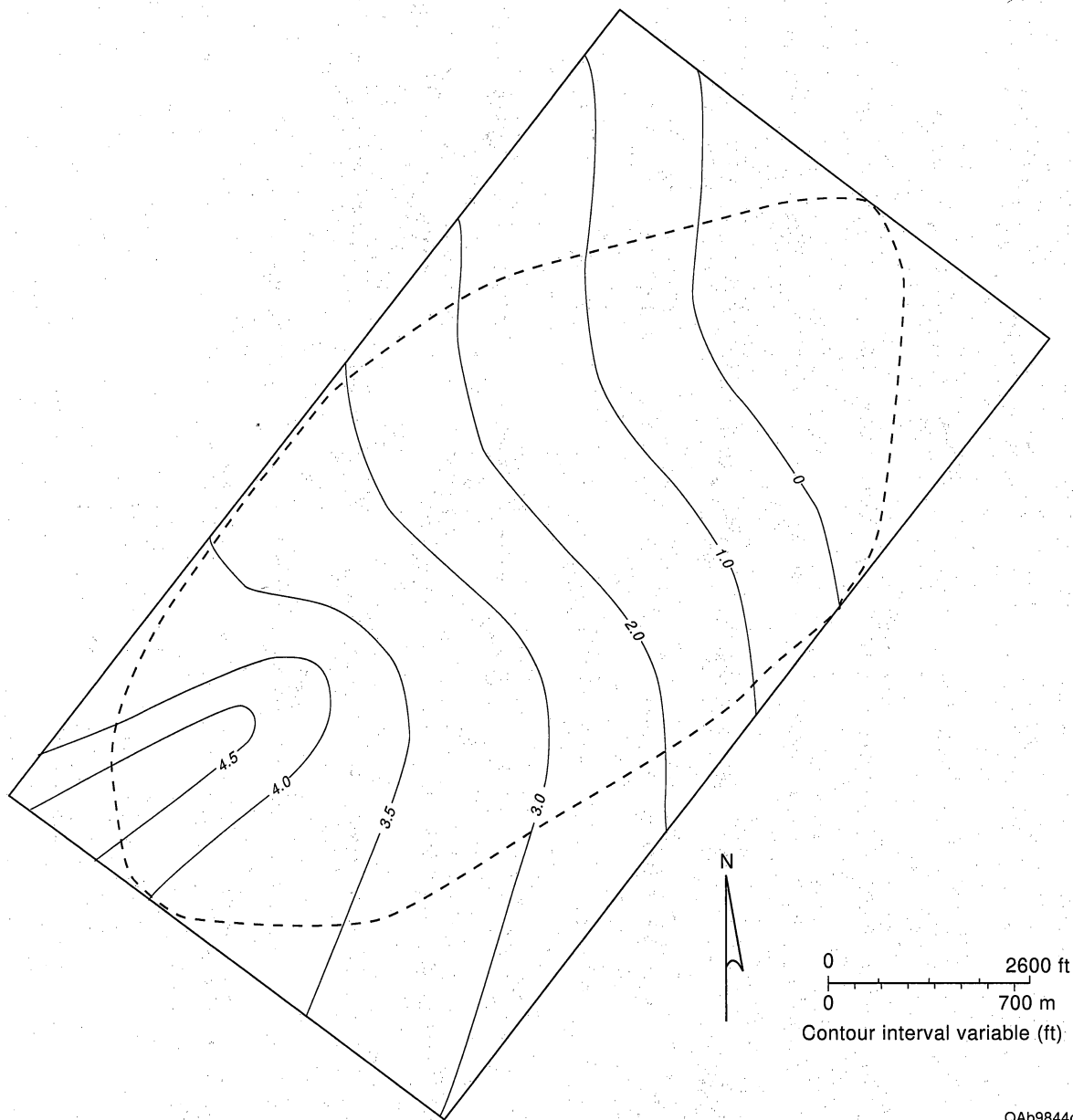
Figure A8. Isopach map (feet) of Facies 5 from Lithosome 1.

N

0					2600 ft
0					700 m

Contour interval 2 ft
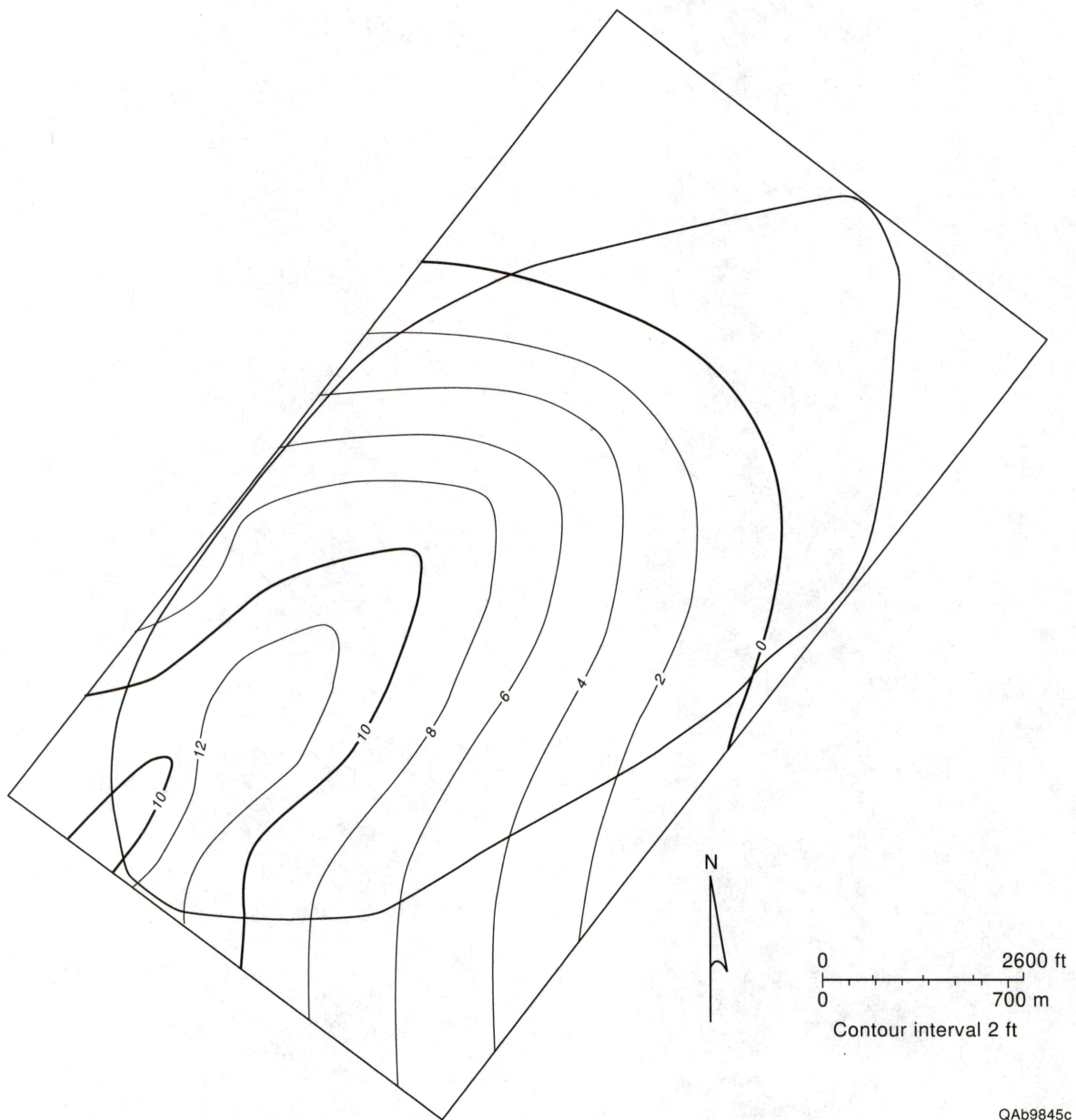
QAb9845c

Figure A9. Isopach map (feet) of Facies 5 from Lithosome 2.
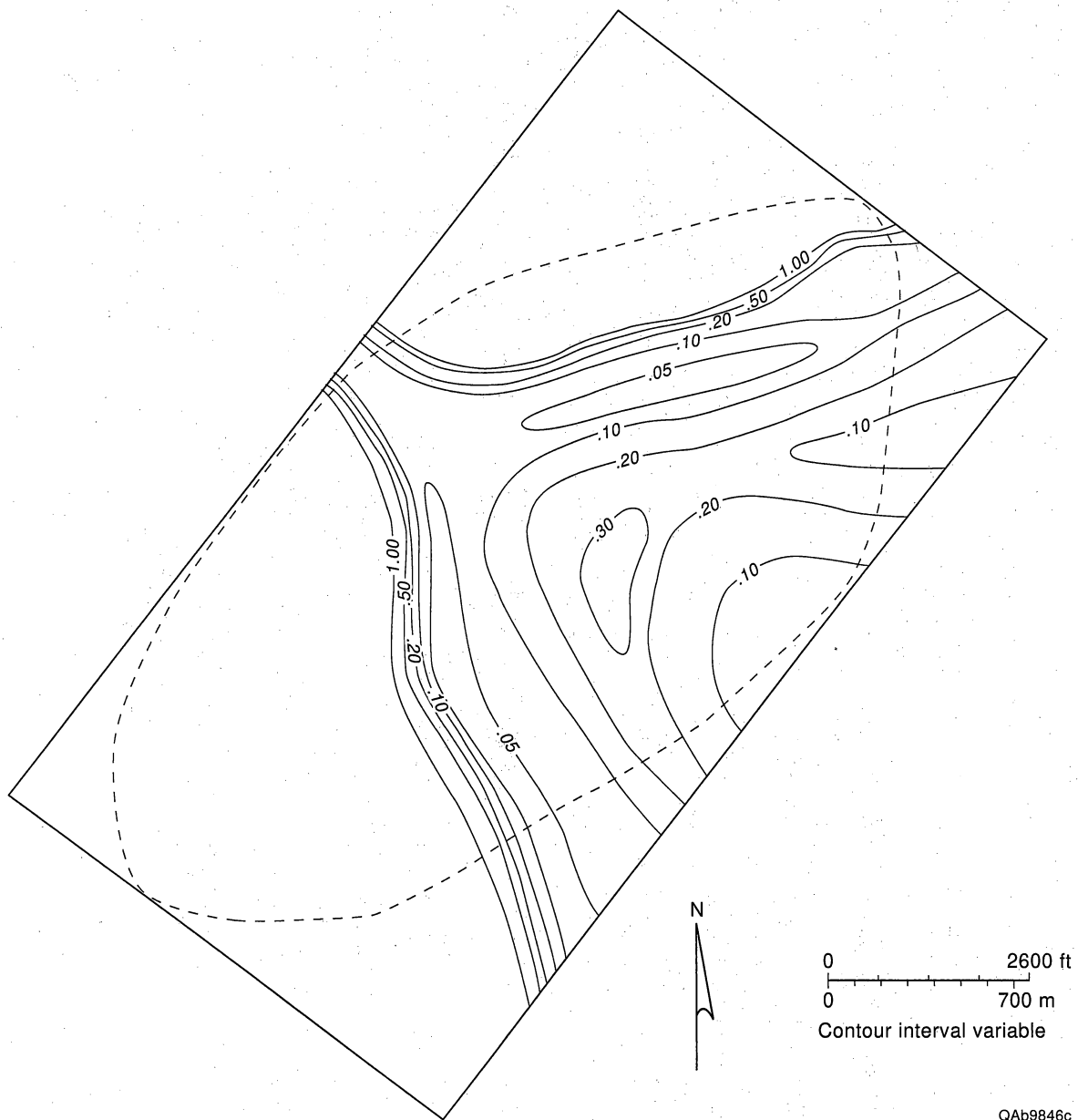
Figure A10. Proportion map for Facies 4 from Lithosome 3.

77

Figure A11. Proportion map of Facies 6 from Lithosome 3.
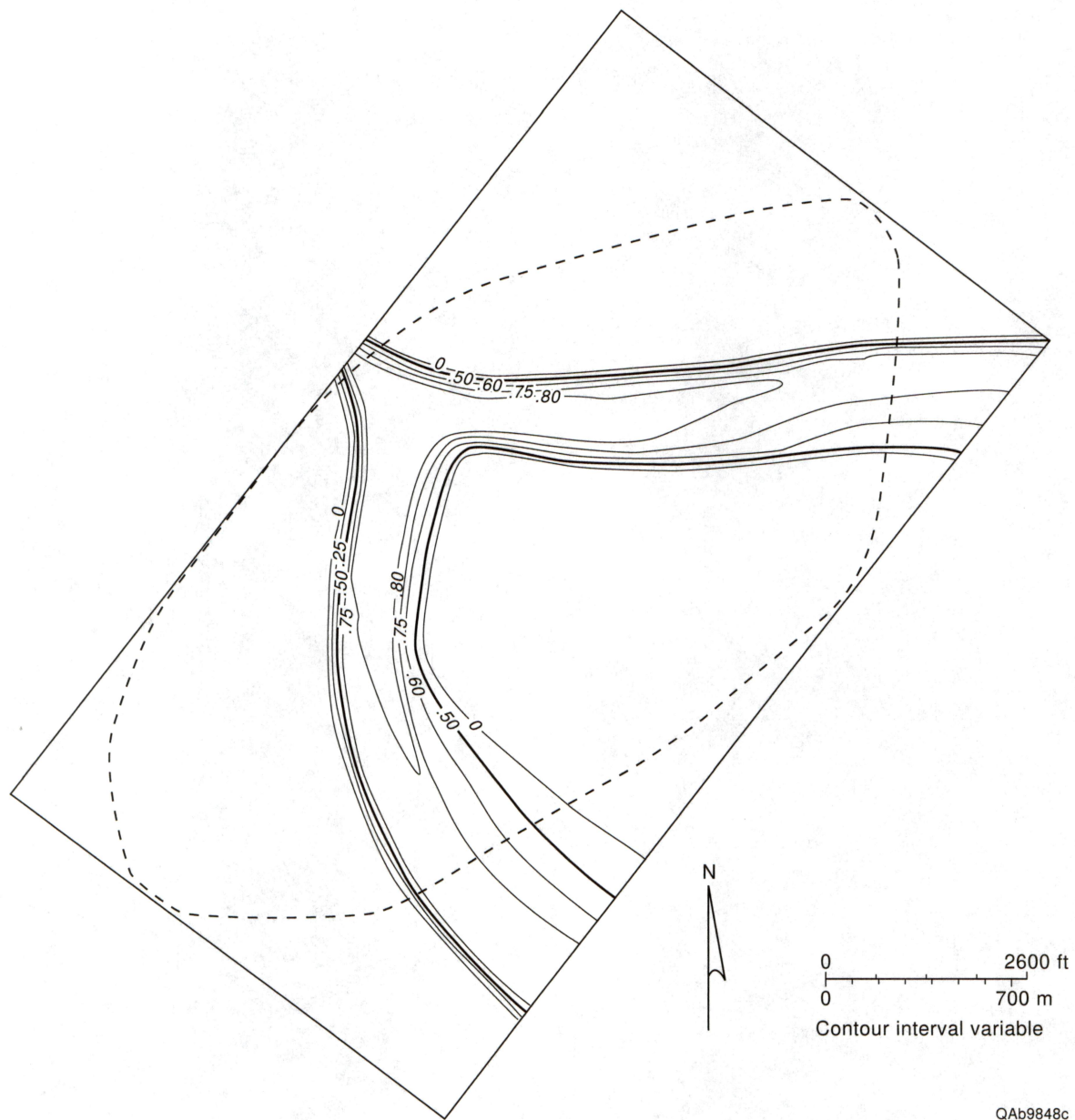
Figure A12. Proportion map of Facies 4 from Lithosome 4.

Figure A13. Proportion map of Facies 4 from Lithosome 4.
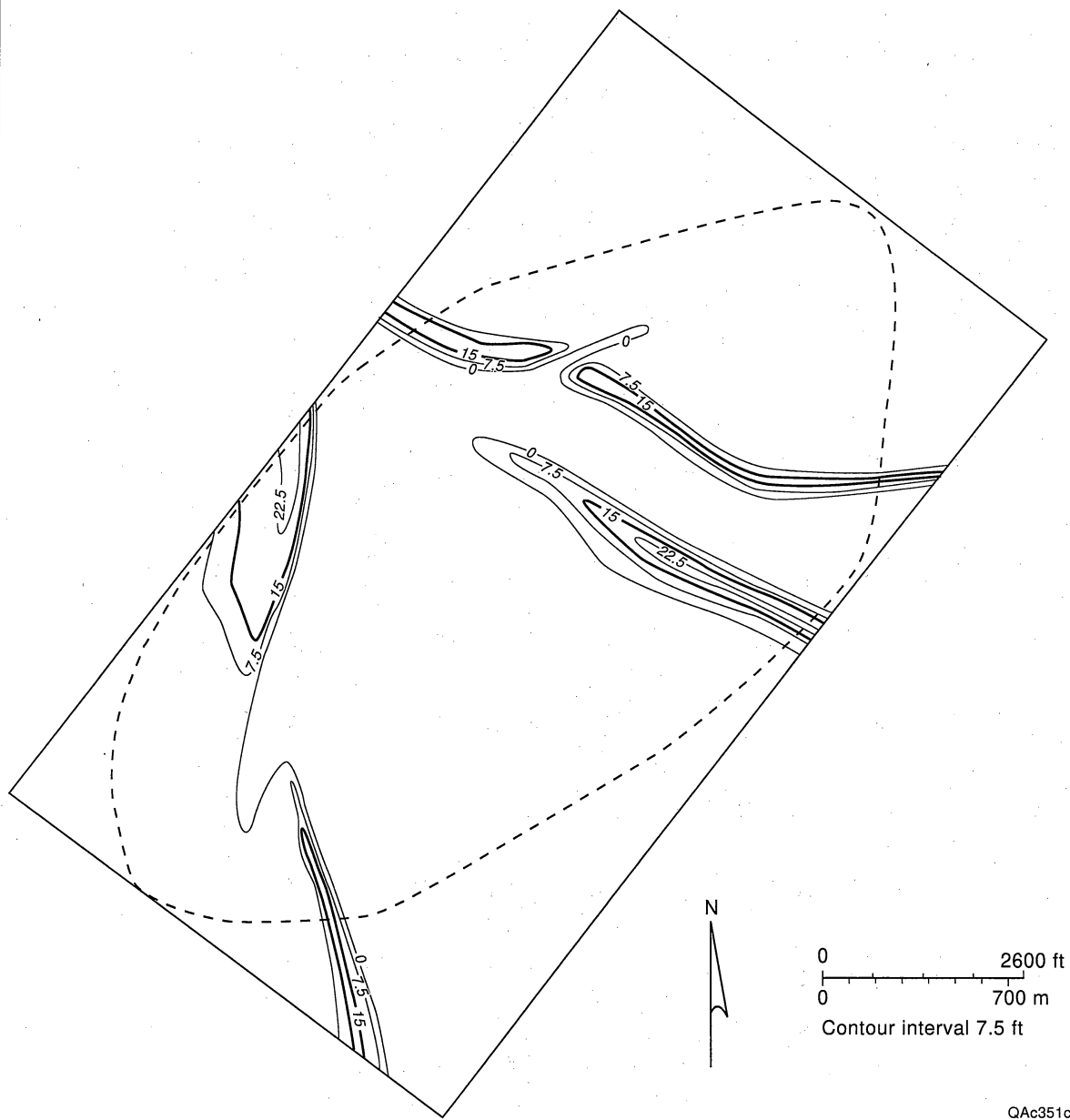
Figure A14. Proportion map of Facies 4 from Lithosome 5.
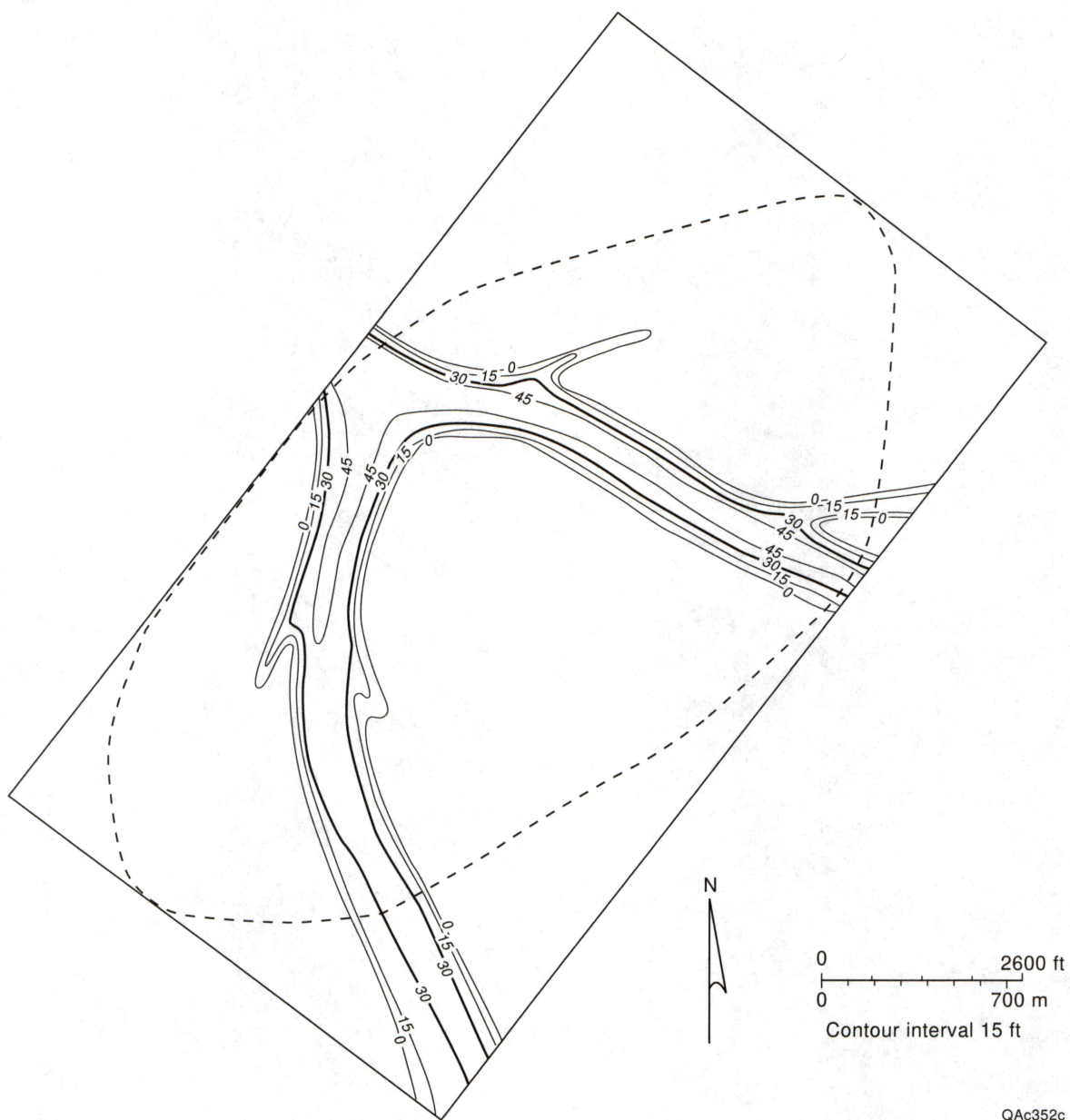
Figure A15. Proportion map of Facies 6 from Lithosome 5.
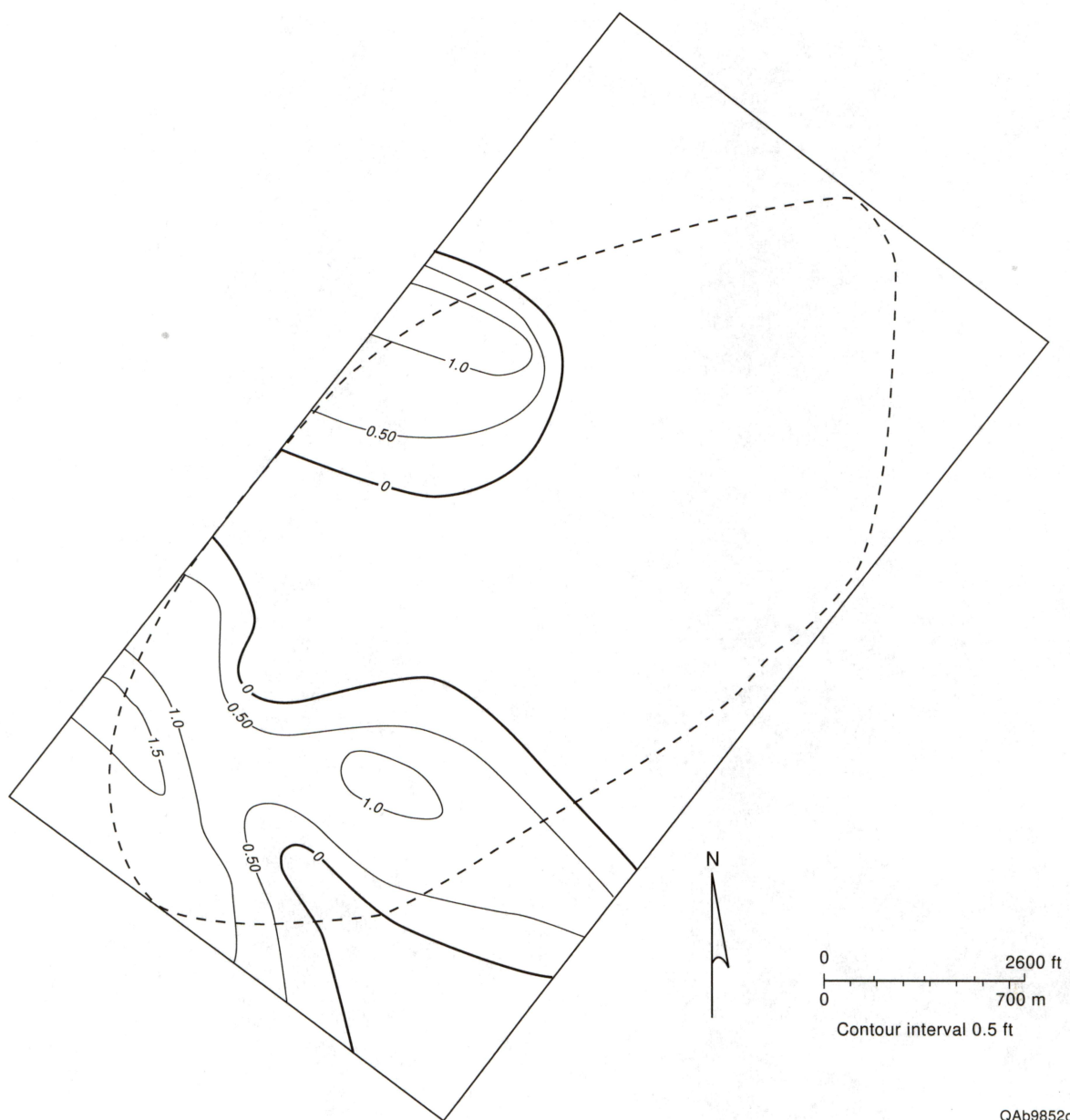
Figure A16. Isopach map (feet) of Facies 5 from Lithosome 6.
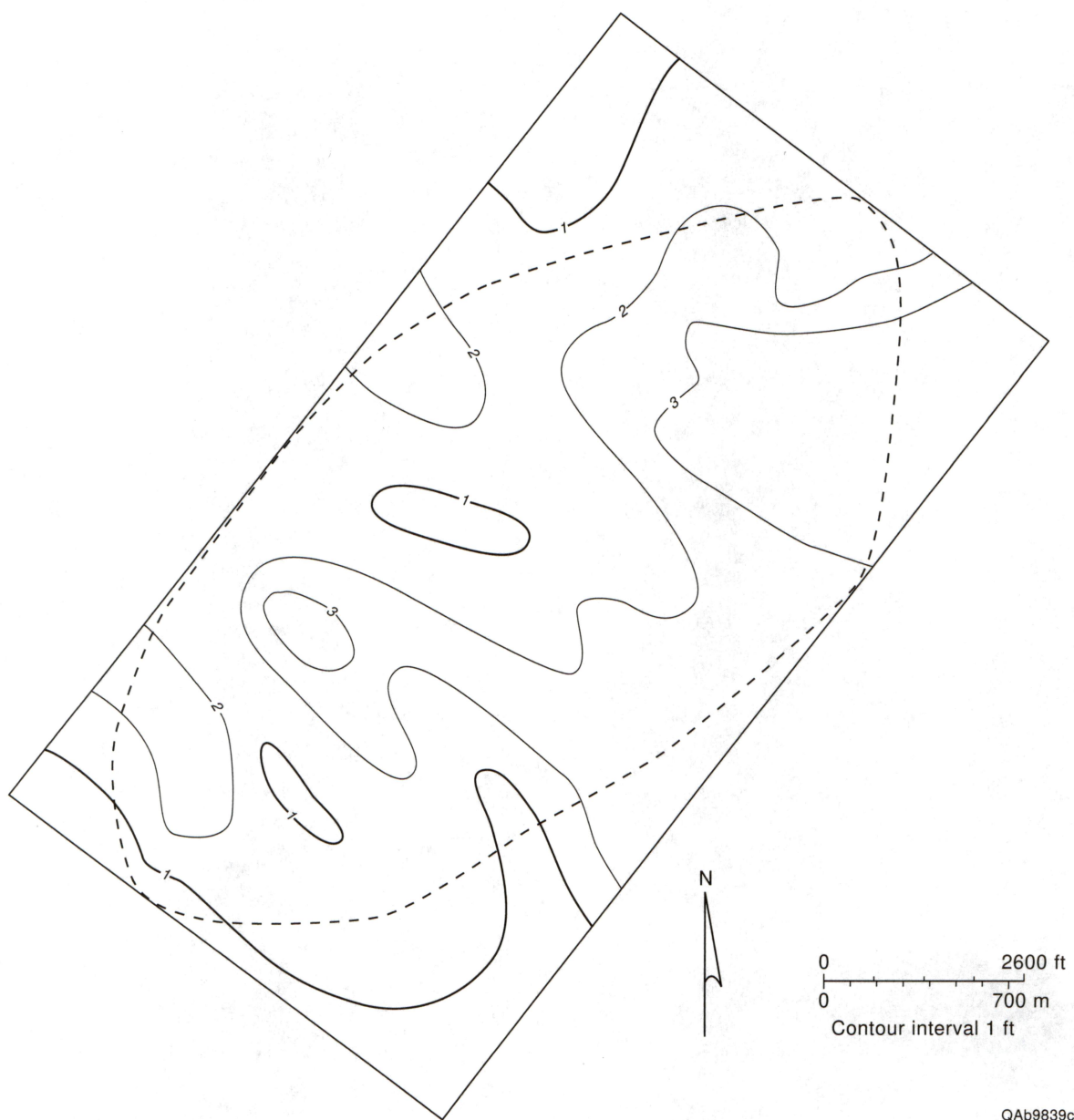
Figure A17. Isopach map (feet) of Facies 5 from Lithosome 7.

Appendix B. Views of Reservoir Model.

Facies

- Organic-rich laminated siltstone
- Laminated siltstone
- Thin bedded rippled and laminated sandstone and siltstone
- Massive sandstone
- Cross-stratified sandstone

Bounding surface

	8
	7
	6
	5
	4
	3
	2
	1

QAc993c
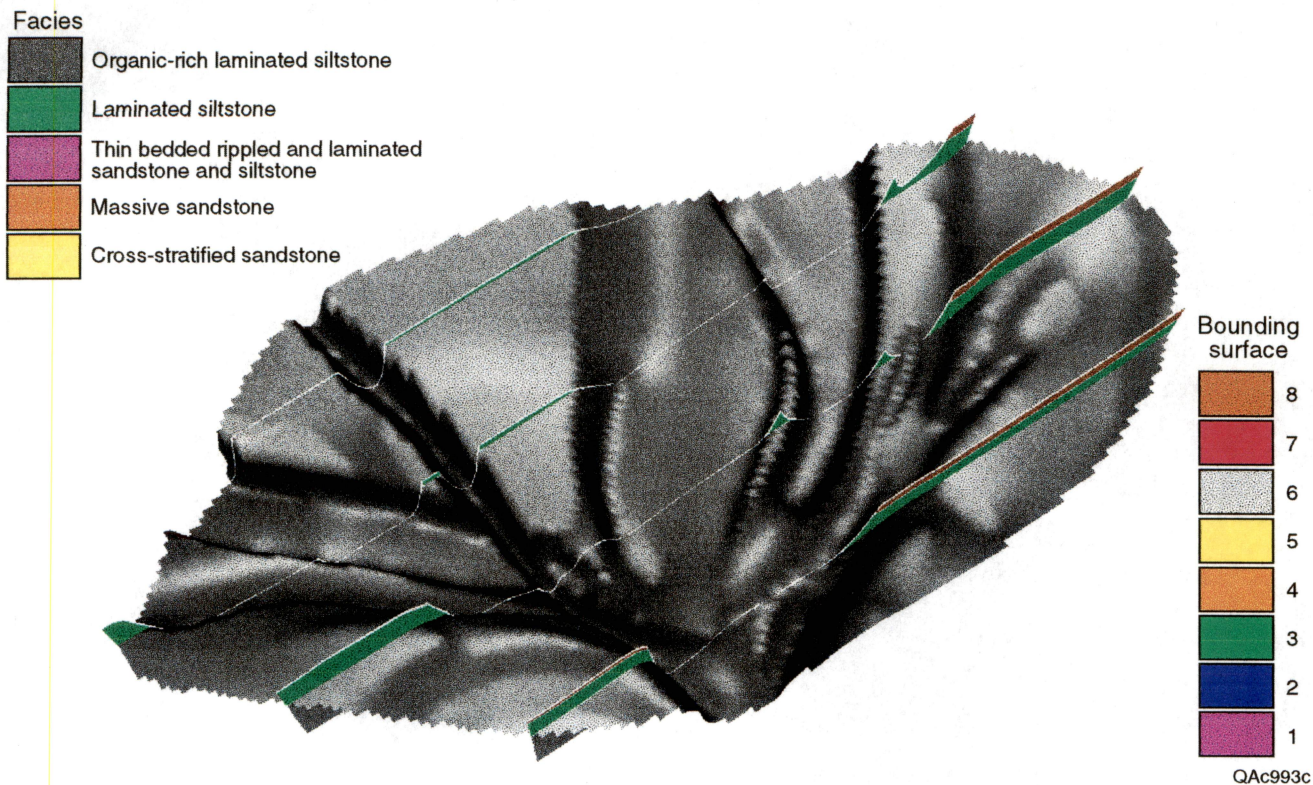
Figure B1. Facies distribution of Lithosome 1 on strike section on bottom bounding surface (black).

Facies

- Organic-rich laminated siltstone
- Laminated siltstone
- Thin bedded rippled and laminated sandstone and siltstone
- Massive sandstone
- Cross-stratified sandstone

Bounding surface

	8
	7
	6
	5
	4
	3
	2
	1

QAc994c

Figure B2. Facies distribution of Lithosome 2 on strike section on bounding surface 1 (purple).

85

Facies

- Organic-rich laminated siltstone
- Laminated siltstone
- Thin bedded rippled and laminated sandstone and siltstone
- Massive sandstone
- Cross-stratified sandstone

Bounding surface

- 8
- 7
- 6
- 5
- 4
- 3
- 2
- 1

QAc995c
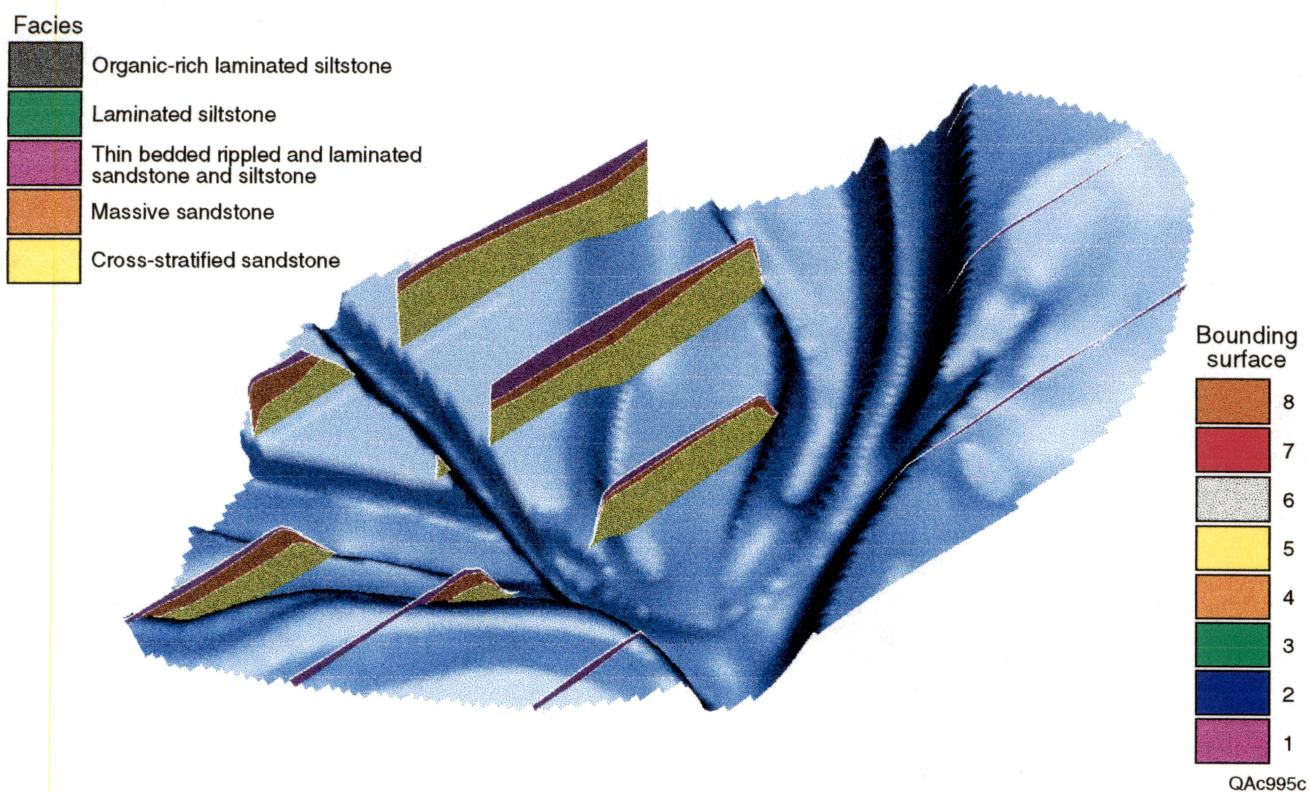
Figure B3. Facies distribution of Lithosome 3 on strike section on bounding surface 2 (blue).

Facies

- Organic-rich laminated siltstone
- Laminated siltstone
- Thin bedded rippled and laminated sandstone and siltstone
- Massive sandstone
- Cross-stratified sandstone

Bounding surface

- 8
- 7
- 6
- 5
- 4
- 3
- 2
- 1

QAc996c
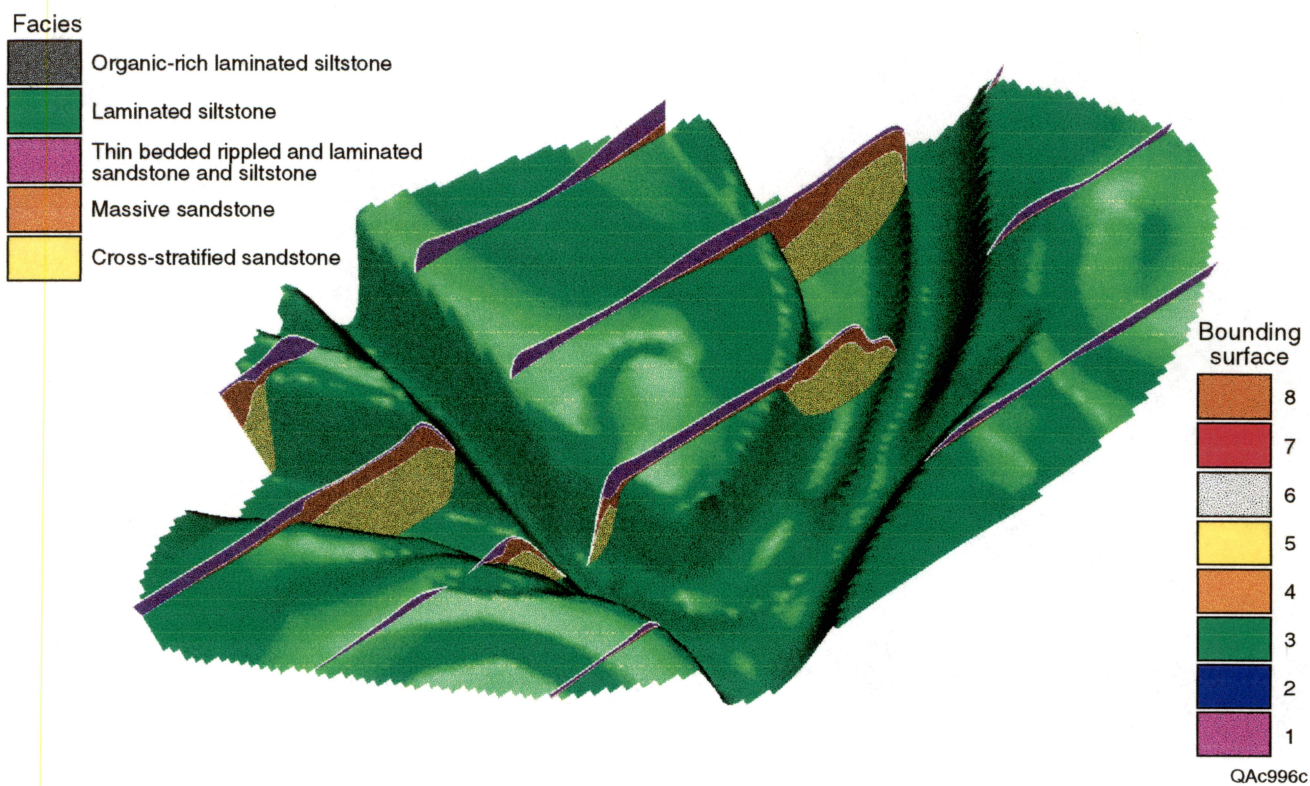
Figure B4. Facies distribution of Lithosome 4 on strike section on bounding surface 3 (green).

Facies

- Organic-rich laminated siltstone
- Laminated siltstone
- Thin bedded rippled and laminated sandstone and siltstone
- Massive sandstone
- Cross-stratified sandstone

Bounding surface

	8
	7
	6
	5
	4
	3
	2
	1

QAc997c
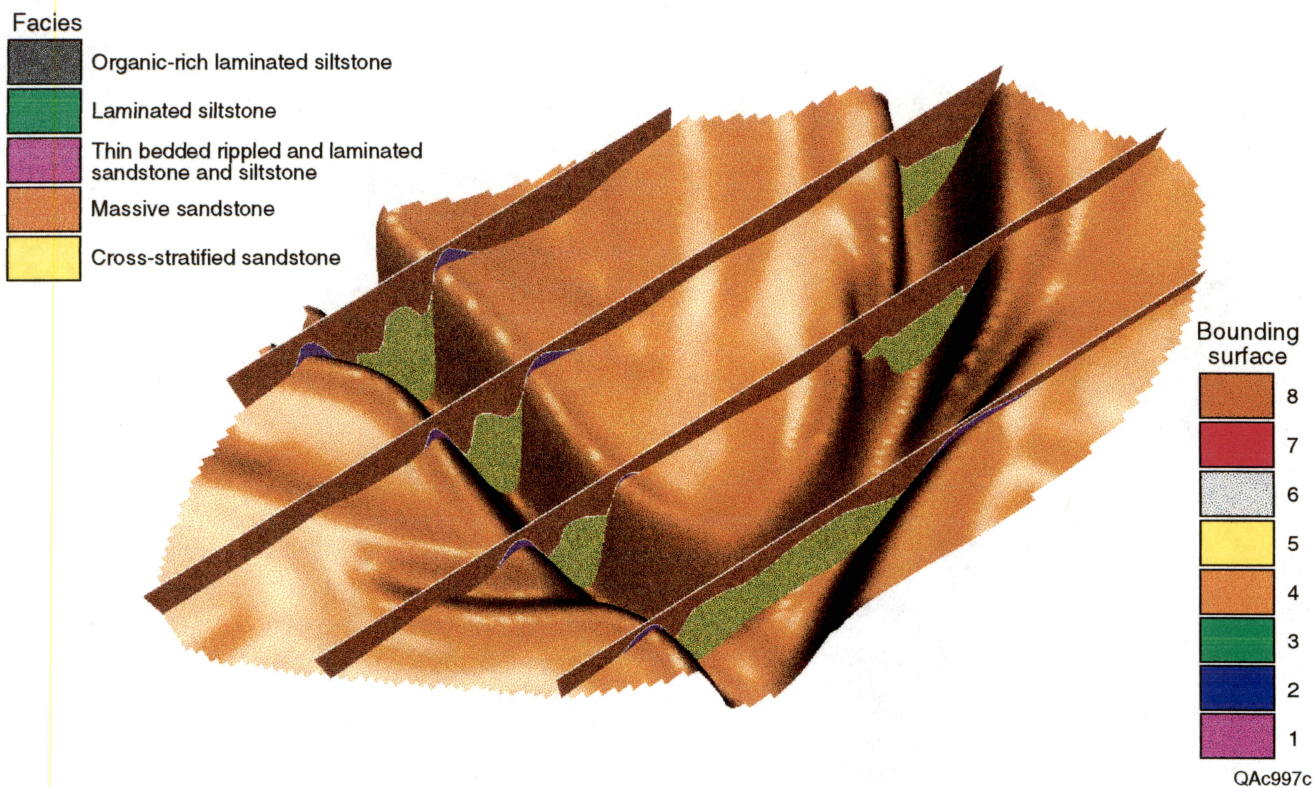
Figure B5. Facies distribution of Lithosome 5 on strike section on bounding surface 4 (orange).

Facies

- Organic-rich laminated siltstone
- Laminated siltstone
- Thin bedded rippled and laminated sandstone and siltstone
- Massive sandstone
- Cross-stratified sandstone

Bounding surface

	8
	7
	6
	5
	4
	3
	2
	1

QAc998c
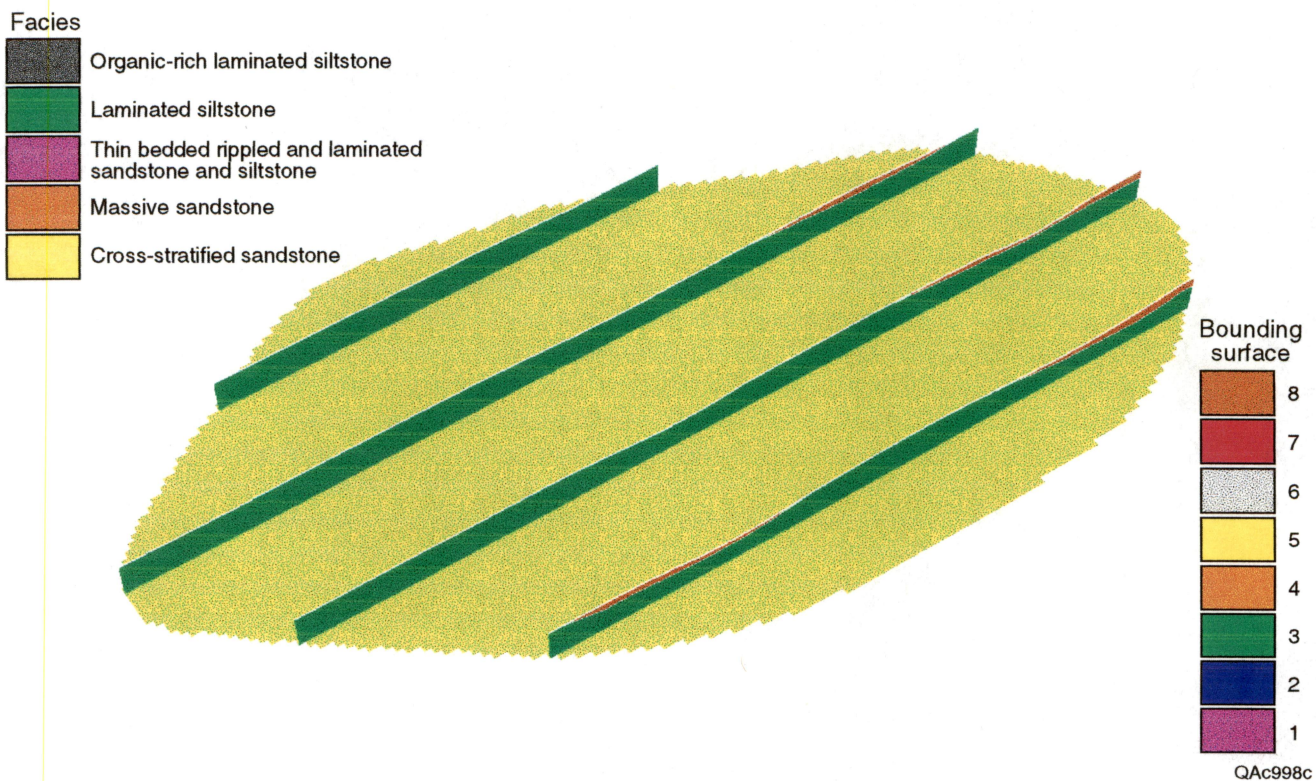
Figure B6. Facies distribution of Lithosome 6 on strike section on bounding surface 5 (yellow).

87

Facies

- ▓ Organic-rich laminated siltstone
- ▓ Laminated siltstone
- ▓ Thin bedded rippled and laminated sandstone and siltstone
- ▓ Massive sandstone
- ▓ Cross-stratified sandstone

Bounding surface

▓	8
▓	7
▓	6
▓	5
▓	4
▓	3
▓	2
▓	1

QAc999c
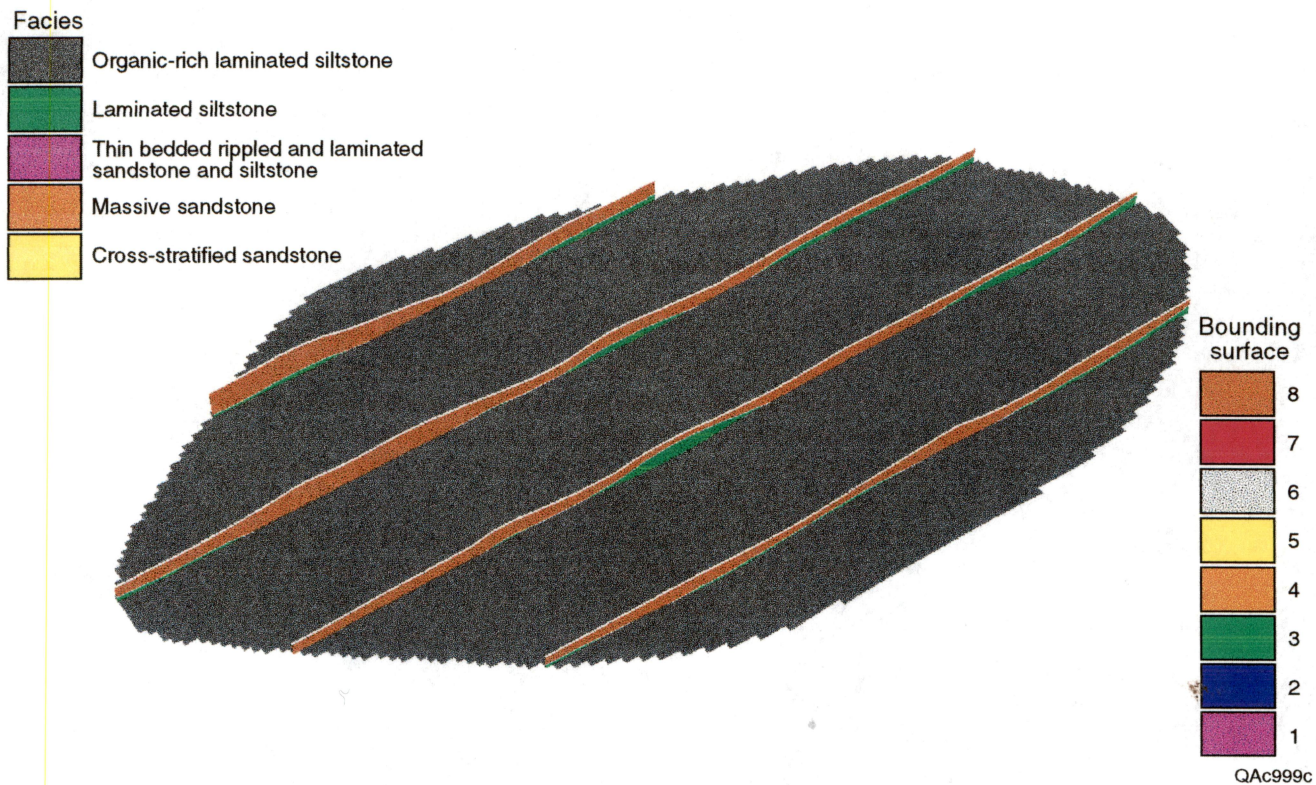
Figure B7. Facies distribution of Lithosome 7 on strike section on bounding surface 6 (gray).

Facies

- ▓ Organic-rich laminated siltstone
- ▓ Laminated siltstone
- ▓ Thin bedded rippled and laminated sandstone and siltstone
- ▓ Massive sandstone
- ▓ Cross-stratified sandstone

Bounding surface

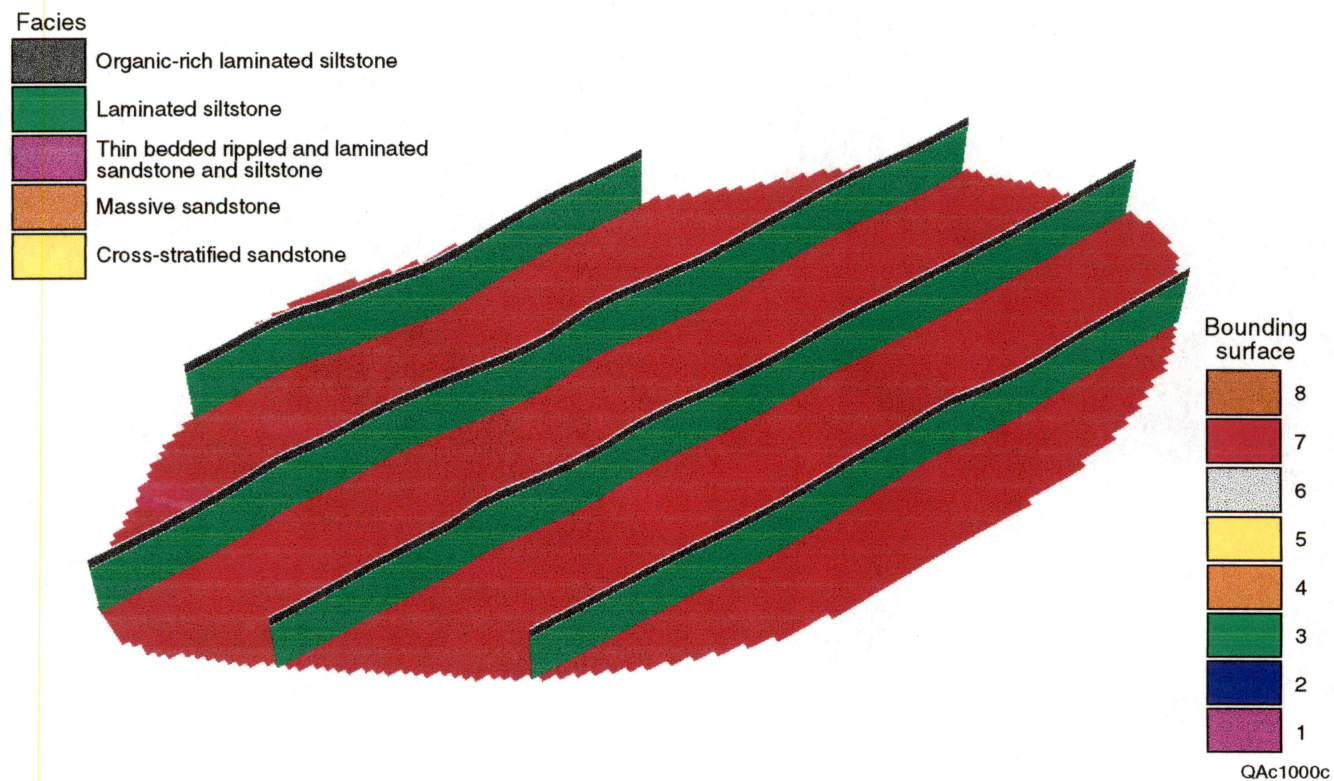|	
▓	8
▓	7
▓	6
▓	5
▓	4
▓	3
▓	2
▓	1

QAc1000c

Figure B8. Facies distribution of Lithosome 8 on strike section on bounding surface 7 (red).

Appendix C. Gridded Model.

Table C1. Petrophysical properties of Bell Canyon sandstone by facies.

Facies	Arithmetic mean porosity (%)	Mean permeability (md)	
		Geometric Mean	Arithmetic Mean
1 and 2	13.1	0.12	--
3	15.7	0.54	--
4	22.3	19	29
5	21.3	13	21
6	22.1	16	21

Notes:
1. All data from the Ford Geraldine Unit Ramsey Sandstone (Dutton and others, 1997).
2. Facies 4 values are for net sandstone within the heterolithic facies. The siltstone interbeds probably lower the facies average properties significantly.

Table C2. Summary of simulation layer properties.

Simulation layer	Stacking order	Lithosome	Facies	Fraction of area present	Average thickness (ft)
1	19	8	2	1.00	0.99
2	18		3	1.00	4.61
3	17	7	5	1.00	1.31
4	16		3	0.68	0.29
5	15	6	5	0.35	0.16
6	14		3	1.00	2.62
7	13	5	5	1.00	7.41
8	12		6	0.25	3.42
9	11		4	0.18	0.30
10	10	4	4	0.81	2.02
11	9		5	0.72	1.57
12	8		6	0.25	3.30
13	7	3	4	0.63	1.26
14	6		5	0.40	1.06
15	5		6	0.41	4.04
16	4	2	5	0.26	1.43
17	3		3	0.30	0.36
18	2	1	5	0.27	0.57
19	1		3	0.54	1.82

Notes
1. The fraction of area present is the area of the layer divided by the area of simulation layer 1, which extends over the entire simulation domain.
2. Other summary data can be found in the log and summary files produced by running the program "stackmaps."
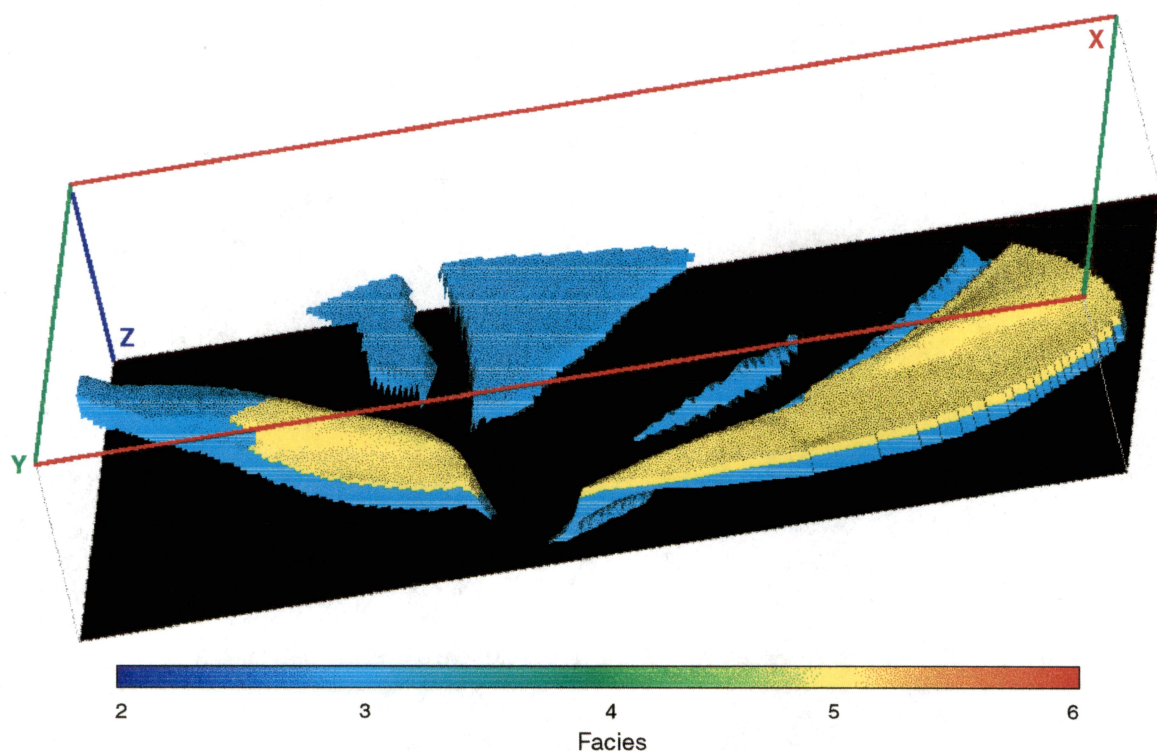
Figure C1. Perspective view of Lithosome 1. Color indicates facies. The vertical scale has been exaggerated by a factor of 20.
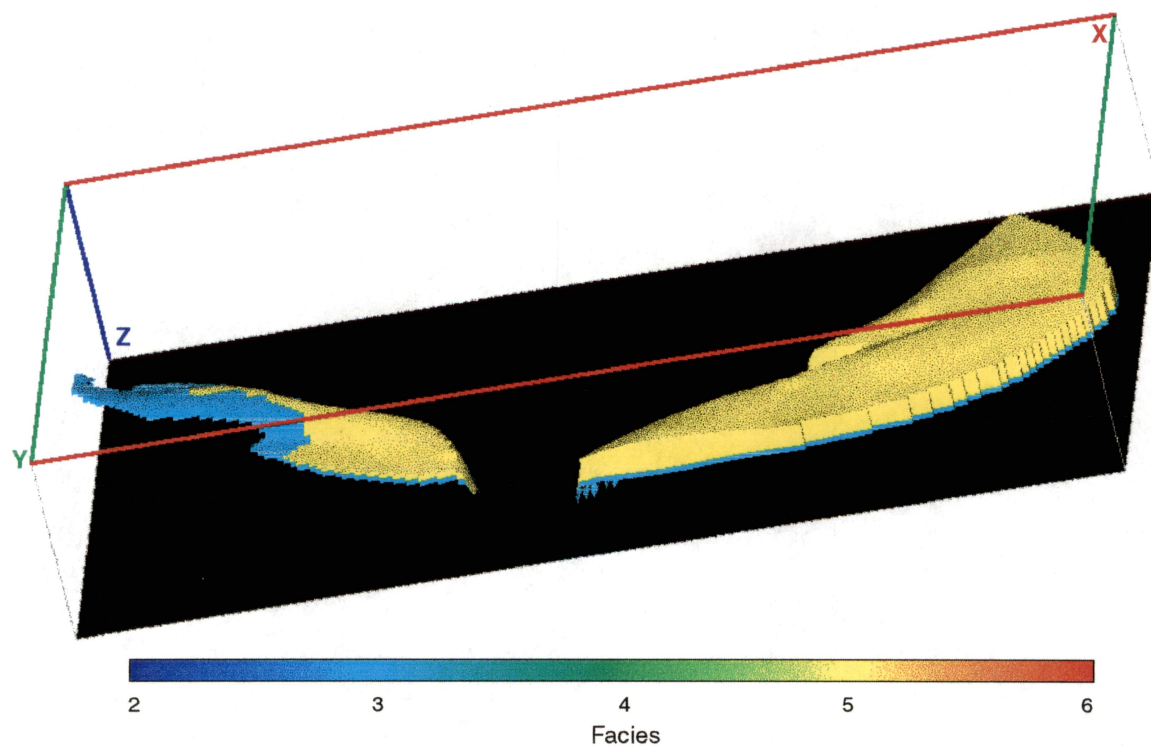
Figure C2. Perspective view of Lithosome 2. Color indicates facies. The vertical scale has been exaggerated by a factor of 20.

Figure C3. Perspective view of Lithosome 3. Color indicates facies. The vertical scale has been exaggerated by a factor of 20.

Figure C4. Perspective view of Lithosome 4. Color indicates facies. The vertical scale has been exaggerated by a factor of 20.

Figure C5. Perspective view of Lithosome 5. Color indicates facies. The vertical scale has been exaggerated by a factor of 20.

Figure C6. Perspective view of Lithosome 6. Color indicates facies. The vertical scale has been exaggerated by a factor of 20.
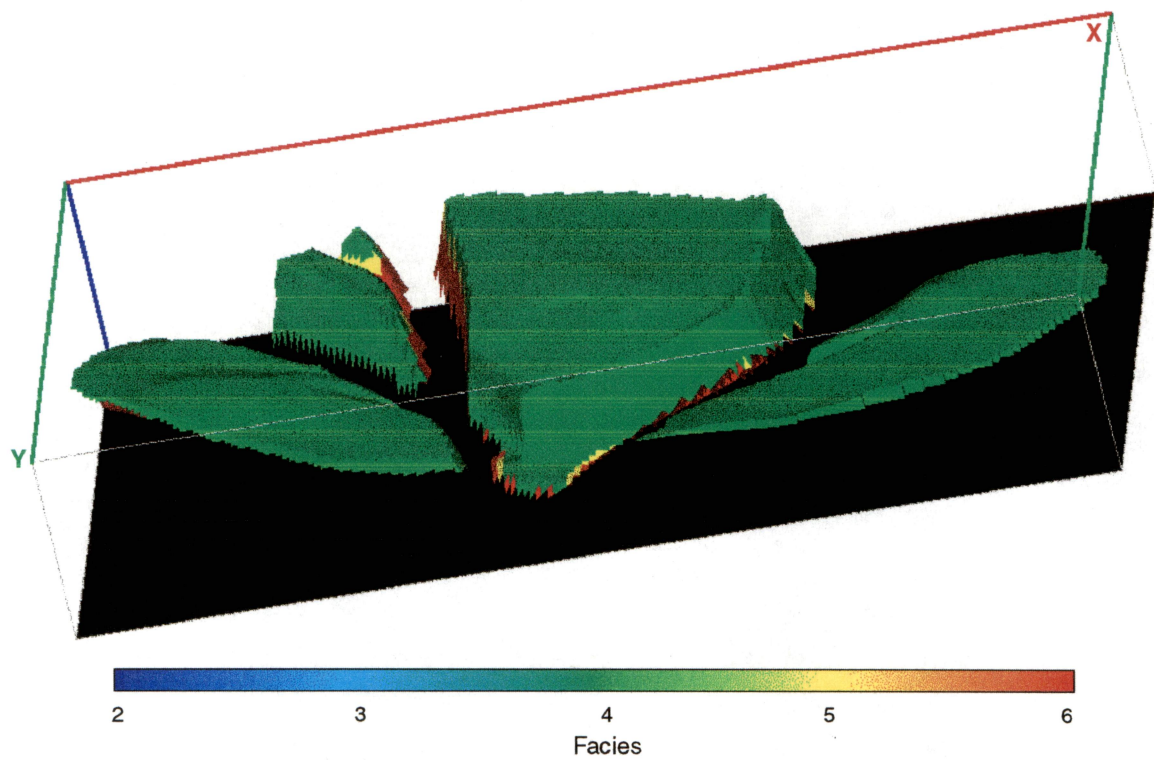
Figure C7. Perspective view of Lithosome 7. Color indicates facies. The vertical scale has been exaggerated by a factor of 20.
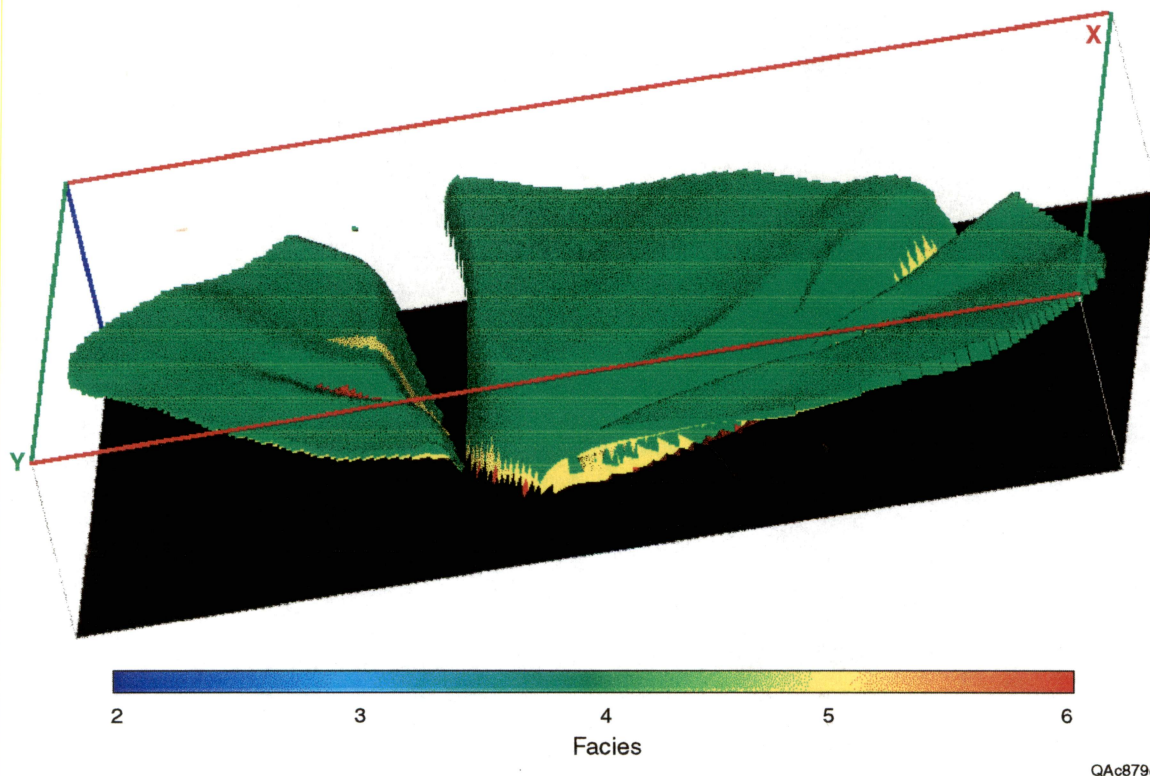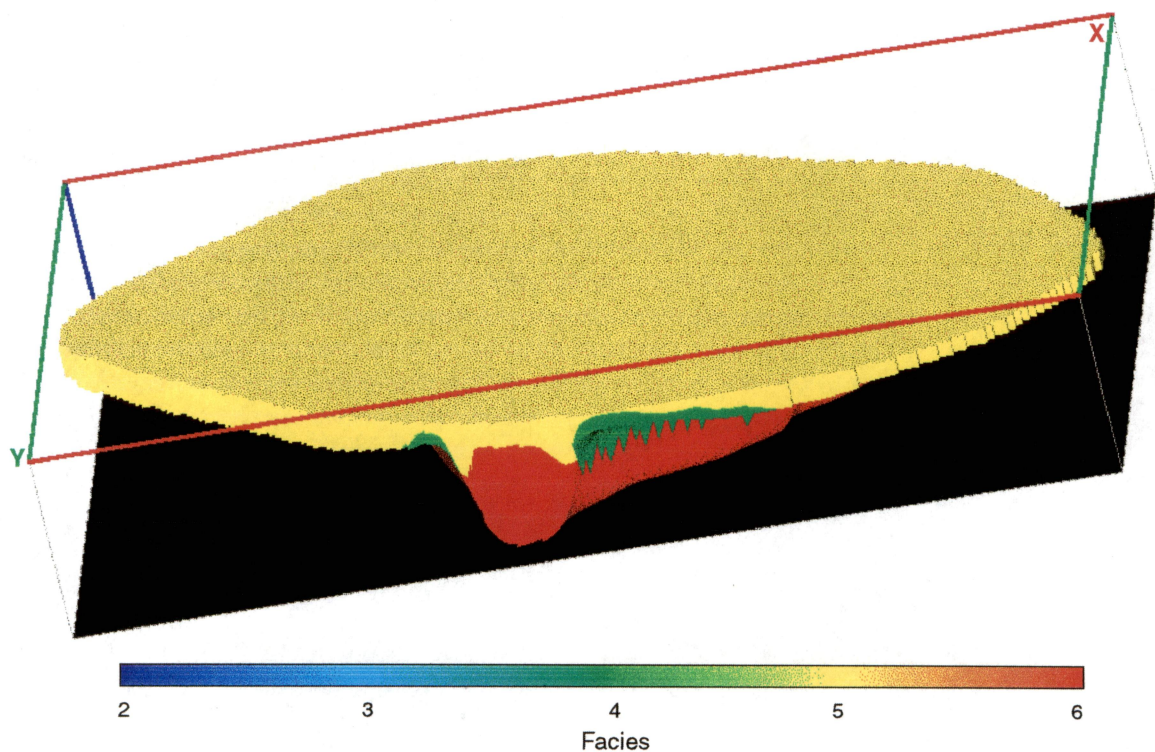

Figure C8. Perspective view of Lithosome 8. Color indicates facies. The vertical scale has been exaggerated by a factor of 20.

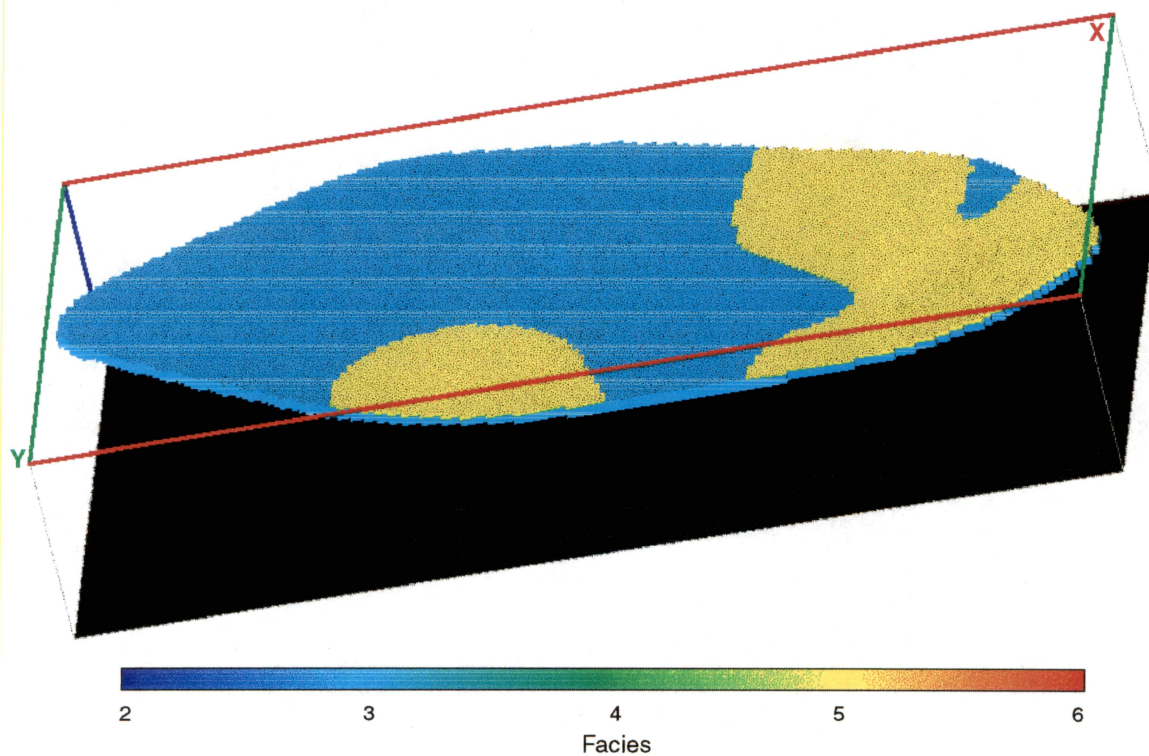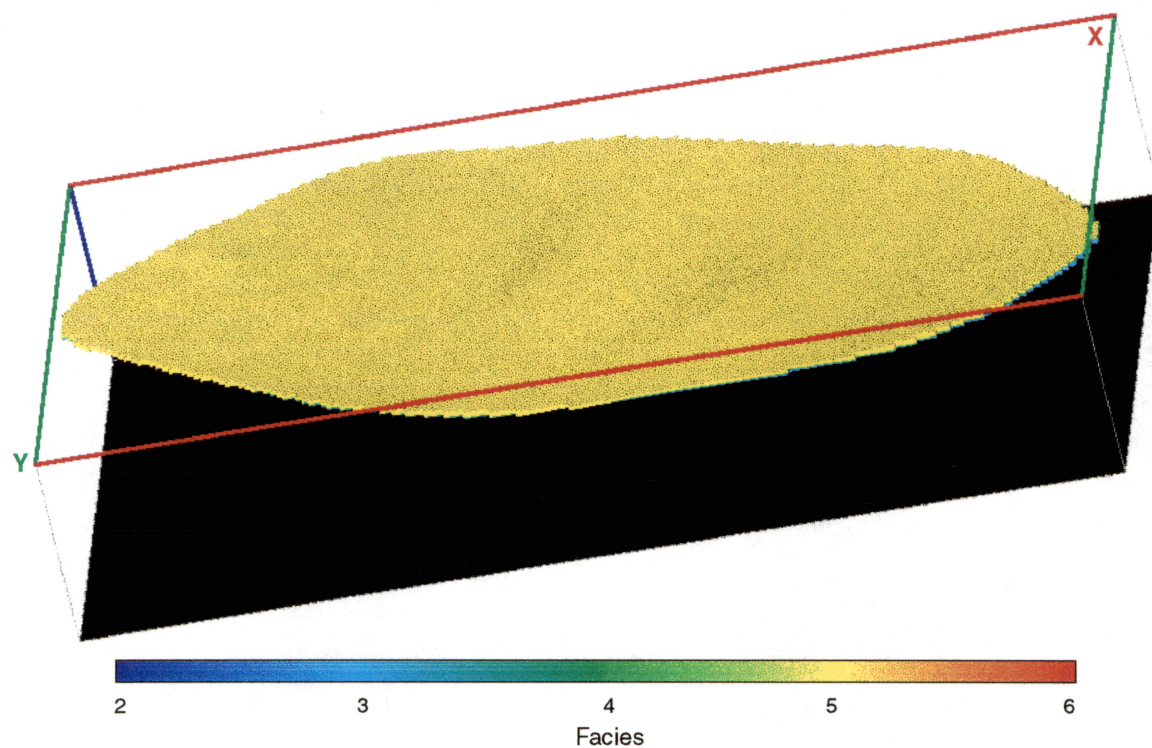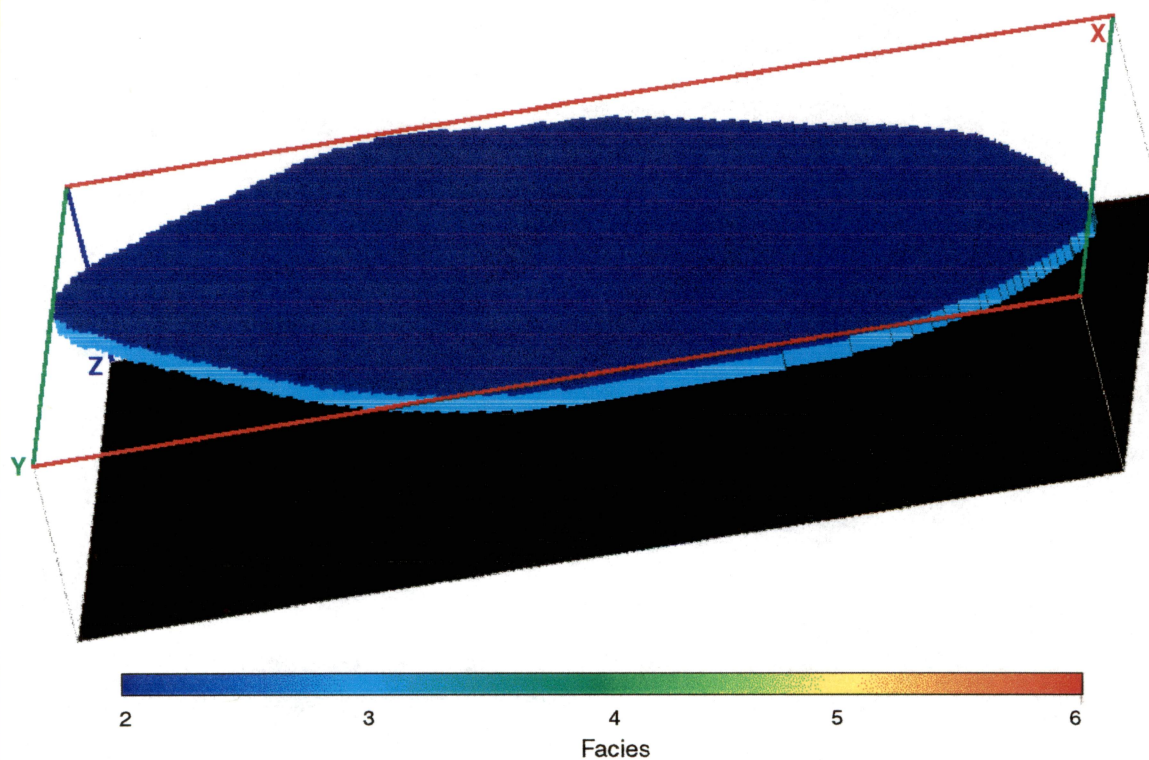## Appendix D. Contents of CD-ROM Set

Two read-only compact disks are transmitted with this report. The CD-ROM volumes contain maps, cross sections, posters, and views of the 3-D model, StrataModel input files, SGI showcase presentation files, files of gridded data, simulator input, and QuickTime animations.

Volume 1 contains maps and illustrations from section 1 of this report, and volume 2 contains data and illustrations from sections 2 and 3. The contents are summarized in table D1. More details can be found in the file "README.TXT," included in each directory of the CD-ROM volumes.

Table D1. Contents of compact disks.

Vol.	Directory	Category/Description
1		Section 1
	MAPS	Maps: 1. Map of study areas 2. Location of case studies 3. Wild Horse Draw 4. Willow Mountain
	SECTIONS	Cross Sections: 1. Regional 2. Wild Horse Draw 3. Willow Mountain A-A′ 4. Willow Mountain B-B′ 5. Willow Mountain C-C′ 6. Willow Mountain D-D′ 7. Willow Mountain E-E′

	PHOTOS	Photos & photomosaics:
		1. Wild Horse Draw
		    (a) with bedding traces
		    (b) without bedding traces
		2. Willow Mountain A
		    (a) with bedding traces
		    (b) without bedding traces
		3. Willow Mountain B
		    (a) with bedding traces
		    (b) without bedding traces
		4. Willow Mountain C
		    (a) with bedding traces
		    (b) without bedding traces

	POSTERS	Poster Panels 1. Dutton, 1997 AAPG(A) 2. Dutton, 1997 AAPG(B) 3. Dutton, 1997 AAPG(C) 4. Barton, 1997 AAPG(A) 5. Barton, 1997 AAPG(B) 6. Barton, 1997 AAPG(C) 7. Wild Horse Draw

Table D1 (cont.)

Vol.	Directory	Category/Description
2		Sections 2 and 3
	SGM*	Stratamodel files: (UNIX/Silicon Graphics)
		1. Control files
		2. Project files
		3. Model display files
		4. Input grids (lithosome / lithofacies boundary grids)
	CPS3*	CPS3 files: (UNIX/Silicon Graphics)
		1. Project files (binary)
		2. Input grids from PCMS
		3. Intermediate isopach, proportion grids
		4. Digitized contour maps
		5. Final CPS3 output grids (lithosome, lithofacies)
	PCMS*	PCMS files: (PC-DOS)
		1. Project files (binary)
		2. Digitized contour data input file
		3. PCMS output grid files
	SHOWCASE*	Views of geocellular model (SGI showcase file: bell.scs)
		1. Cover page (p. 1)
		2. Model displays of lithosome / lithofacies of outcrop cross section (p. 2-9)
		3. 3-D view of pre-stacking/pre-truncating lithosome bounding surface (1-5) (p. 10-14)
		4. Figure 27-32 (p. 15-20)
		5. Figure B1-B8 (p. 21-28)
		6. Legend (p. 29)
	CODE*	Program files:
		1. C routines
		2. Header files
		3. Makefile
		4. Stackmaps executable
	GRID*	Gridded arrays and simulator grid files:
		1. Gridded array
		2. Void indicators
		3. Z-cornerpoints
		4. Cornerpoint trajectories
		5. Gnuplot-formatted grid traces
		6. Stackmaps control, log, and summary files
		7. Include files to assign porosity, permeabilty, facies, and lithosome
	SIMULATE*	Simulator input and output:
		1. Eclipse input file
		2. Eclipse relative permeability and phase behavior files
		3. AVS visualization input file
	IMAGES	Images of gridded simulation model
		1. Figures 33 and 34, JPEG format
		2. Figures C1-C8, JPEG format
		3. Four animations showing lithosomes and layers from various perspectives, QuickTime format.

Table D1 (cont.)

*Files from these directories are stored in Unix tape archives. If restored with care, the extracted and uncompressed files will have the correct extended path and filenames, as required for compatability with applications like StrataModel, Eclipse, and Make.

1. Create hard disk directories for each of the TAR directories indicated above. If possible, use the names given in this table; otherwise, links may be broken.
2. Copy the TAR file from the CD to the hard disk directory.
3. Extract the files using "tar –xvf directory.TAR," where directory is a directory name such as GRID.
4. Compare the results of the Unix "ls" command to the tar listing "tar –tvf directory.TAR." If they compare properly, go ahead and delete directory.TAR from the hard disk.
5. Uncompress any files with an extension of "Z," thus: "uncompress file.ext.Z."